



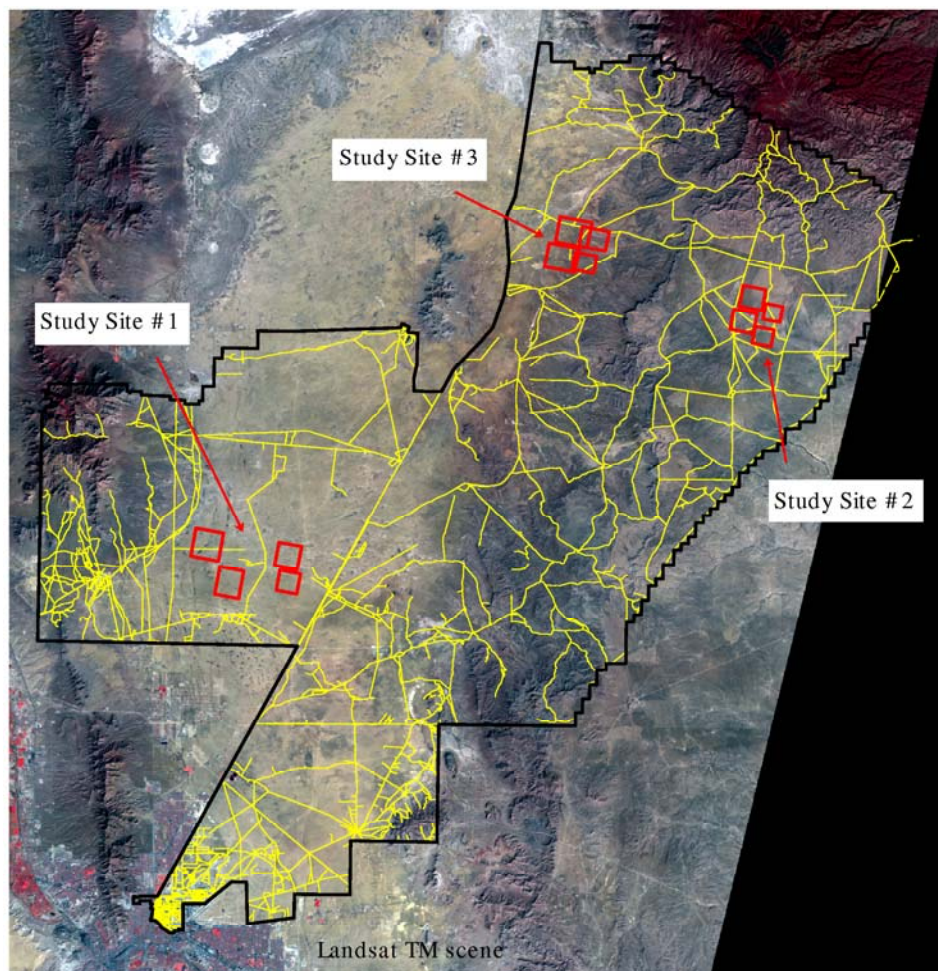
US Army Corps
of Engineers®

Engineer Research and
Development Center

Spectral Demixing and Spectral Index Correlations for Subpixel Quantification of Land-cover Components From Coarse Resolution Imagery at Fort Bliss, Texas

Scott Tweddale, William Jackson, and Paul Pope

December 2003



Spectral Demixing and Spectral Index Correlations for Subpixel Quantification of Land-cover Components From Coarse Resolution Imagery at Fort Bliss, Texas

Scott Tweddale and William Jackson

*Construction Engineering Research Laboratory
PO Box 9005
Champaign, IL 61826-9005*

Paul Pope

*University of Wisconsin
Environmental Remote Sensing Center
1225 W. Dayton Street
Madison, WI 53706-1612*

Final Report

Approved for public release; distribution is unlimited.

Prepared for U.S. Army Corps of Engineers
Washington, DC 20314-1000

ABSTRACT: Fort Bliss, Texas, is a Training and Doctrine Command (TRADOC) installation located in the northern Chihuahuan Desert of western Texas and south-central New Mexico. Encompassing approximately 445,170 hectares (1.1 million acres), it is the single largest TRADOC installation. Because Fort Bliss is located within an arid ecosystem characterized by slow vegetative growth, its land is more susceptible to long-term disturbance. Fort Bliss natural resource managers require a timely and cost-effective method for characterizing and monitoring land condition at various spatial scales and levels of detail.

This report documents evaluation of linear spectral demixing and spectral brightness and greenness index correlations with abundance of land-cover types as alternative methods for more detailed characterization and monitoring of land condition using coarse resolution satellite imagery. Detailed conclusions on the acceptability of various strategies and techniques are presented along with recommendations for related research.

DISCLAIMER: The contents of this report are not to be used for advertising, publication, or promotional purposes. Citation of trade names does not constitute an official endorsement or approval of the use of such commercial products. All product names and trademarks cited are the property of their respective owners. The findings of this report are not to be construed as an official Department of the Army position unless so designated by other authorized documents.

DESTROY THIS REPORT WHEN IT IS NO LONGER NEEDED. DO NOT RETURN IT TO THE ORIGINATOR.

Contents

List of Figures and Tables	vi
Preface.....	x
1 Introduction	1
Background.....	1
Objective.....	3
Approach	3
Mode of Technology Transfer	5
2 Background	6
Spectral Demixing.....	6
Spectral Brightness and Vegetation Indices	8
<i>Vegetation or Greenness Indices.....</i>	<i>8</i>
<i>Brightness Indices</i>	<i>10</i>
3 Study Area and Data	12
Study Area	12
Data	13
Study Site Selection.....	14
4 Methodology.....	18
Image Scanning.....	18
Image Preprocessing.....	21
<i>CIR Photography Exposure Falloff</i>	<i>21</i>
<i>Thematic Mapper Systematic Noise</i>	<i>21</i>
Classification of CIR Photographs.....	22
Geometric Registration.....	26
<i>Selection of Ground Control Points</i>	<i>26</i>
<i>Registration of CIR Photograph Classifications to TM Imagery.....</i>	<i>27</i>
<i>Accuracy Assessment of Geometric Registration.....</i>	<i>27</i>
<i>Subset TM Scene and Air Photo to Common Area.....</i>	<i>27</i>
Spectral Demixing.....	29
<i>Mathematics of Spectral Demixing</i>	<i>29</i>
<i>Example Implementation of Spectral Demixing</i>	<i>33</i>
<i>Demixing Evaluation and Accuracy Assessment.....</i>	<i>34</i>

<i>Spatial Extrapolation of Demixing Results</i>	35
Spectral Index Correlation Analysis	36
<i>Spectral Indices</i>	36
<i>Spectral Index Correlation Evaluation and Accuracy Assessment</i>	40
<i>Spatial Extrapolation of Spectral Index Correlation Results</i>	40
Summary of Methodology	41
5 Results	42
Spectral Demixing	42
<i>Five-class Results</i>	42
<i>Three-class Results</i>	47
<i>Two-class Results</i>	50
<i>Spatial Extrapolation</i>	61
Spectral Index Correlation Analysis	70
<i>Five-class Results</i>	71
<i>Three-class Results</i>	77
<i>Two-class Results</i>	81
<i>Spatial Extrapolation</i>	99
Summary of Results	114
<i>Study Site #1 - Coppice Dunes Maneuver Areas</i>	115
<i>Study Site #2 - Otero Mesa Grasslands</i>	116
<i>Study Site #3 - Controlled Burn Area/Otero Mesa Foothills</i>	117
6 Conclusions and Recommendations	118
Conclusions	118
<i>Vegetative Cover Estimation</i>	118
<i>Cover Estimation for Unique Land-cover/Vegetation Types</i>	119
<i>Spectral Demixing for Estimating Total Vegetation Cover</i>	119
<i>Spectral Index Correlations for Estimating Total Vegetative Cover</i>	120
<i>Spatial Extrapolation of Total Vegetative Cover Estimates</i>	121
Recommendations	122
References	125
Appendix A: Graphic Depiction of the Linear Spectral Demixing Process Flow	130
Appendix B: Summary of the Adjusted R² for all Correlations	133
Report Documentation Page	140

List of Figures and Tables

Figures

1	Location of Fort Bliss, Texas.....	2
2	Study site locations	4
3	CIR photographs analyzed for Study Site #1, overlaid on TM image.....	15
4	CIR photographs analyzed for Study Site #2, overlaid on TM image.....	16
5	CIR photographs analyzed for Study Site #3, overlaid on TM image.....	17
6	Example of exposure falloff corrections: (A) original image, (B) corrected image	22
7	Example of TM systematic Noise corrections: (A) original image, (B) corrected image.....	22
8	Original CIR photograph and examples of five-, three-, and two-class unsupervised classifications and four recodes of the five-class image for a subset of photo 381_158 in Study Site #1	25
9	Procedure for subsetting the common area between a TM image and a CIR photograph	29
10	Demixing results for five land-cover categories for photo 381_158 (left column is the demixing estimate of abundance for each category, right column is the reference abundance for each category)	43
11	Demixing results for three land-cover categories for photo 381_158 (left column is the demixing estimate of abundance for each category, right column is the reference abundance for each category)	48
12	Demixing results for two land-cover categories for photo 381-158 using recode 12_35	63
13	Demixing results for two land-cover categories for photo 381-158 using ISO2	64
14	Demixing results for two land-cover categories for photo 386-124 using recode 1_25	66
15	Demixing results for two land-cover categories for photo 386-124 using recode 14_5	67
16	Demixing results for two land-cover categories for photo 388-90 using recode 1_25	69
17	Demixing results for two land-cover categories for photo 388-90 using recode 14_5	70
18	Albedo correlation results for five land-cover categories for photo 381_158 (left column is the albedo-derived estimate of abundance for each category, right column is the reference abundance for each category).....	73
19	KTB correlation results for five land-cover categories for photo 381_158 (left column is the KTB-derived estimate of abundance for each category, right column is the reference abundance for each category).....	74

20	Albedo correlation results for three land cover categories for photo 381_158 (left column is the albedo-derived estimate of abundance for each category, right column is the reference abundance for each category).....	79
21	KTB correlation results for three land cover categories for photo 381_158 (left column is the KTB-derived estimate of abundance for each category, right column is the reference abundance for each category).....	80
22	Albedo correlation results for two land cover categories for photo 381_158 using recode 12_35	101
23	Albedo correlation results for two land cover categories for photo 381_158 using recode 12_35	102
24	KTB correlation results for two land cover categories for photo 381_158 using recode 12_35	103
25	KTB correlation results for two land cover categories for photo 381_158 using ISO2	104
26	Albedo correlation results for two land cover categories for photo 386_124 using recode 1_25	106
27	Albedo correlation results for two land cover categories for photo 386_124 using recode 14_5	107
28	KTB correlation results for two land cover categories for photo 386_124 using recode 1_25	108
29	KTB correlation results for two land cover categories for photo 386_124 using recode 14_5	109
30	Albedo correlation results for two land cover categories for photo 388_90 using recode 14_5	111
31	Albedo correlation results for two land cover categories for photo 388_90 using recode 1_25	112
32	KTB correlation results for two land cover categories for photo 388_90 using recode 14_5	113
33	KTB correlation results for two land cover categories for photo 388_90 using recode 1_25	114

Tables

1	Landsat-5 TM specifications	13
2	Summary of recodes of original five-class unsupervised classification of CIR photographs into two classes (Cover and Bare Ground)	24
3	Mean and standard deviation of abundance (percent cover) for five land-cover categories for photo 381-158, Study Site #1; estimated (demixing) versus reference	45
4	Descriptive and inferential statistics of difference image for five land-cover categories for photo 381_158, Study Site #1; estimated (demixing) minus reference	46
5	Mean and standard deviation of abundance for three land-cover categories for photo 381_158, Study Site #1; estimated (demixing) versus reference	49

6	Descriptive and inferential statistics of difference image for three land-cover categories for photo 381_158, Study Site #1; estimated (demixing) minus reference	49
7	Mean and standard deviation of cover abundance for photo 381_158, Study Site #1, derived from ISO2 and four recodes; estimated (demixing) versus reference	51
8	Descriptive and inferential statistics of difference image (estimated [demixing] minus reference) for two land-cover categories for photo 381_158, Study Site #1 using ISO2 and four recodes	51
9	Descriptive and inferential statistics of difference image (estimated [demixing] minus reference) for two land-cover categories for photos 380_18, 381_144, and 381_146, Study Site #1 using ISO2 and four recodes.....	52
10	Total sum of absolute differences for all four photographs for each recode tested for Study Site #1	54
11	Descriptive and inferential statistics of difference image (estimated [demixing] minus reference) for two land-cover categories for photos 386_122, 386_124, 386_16, and 386_18, Study Site #2 using ISO2 and four recodes.....	55
12	Total sum of absolute differences for all four photographs for each recode tested for Study Site #2	57
13	Descriptive and inferential statistics of difference image (estimated [demixing] minus reference) for two land-cover categories for photos 388_45, 388_47, 388_88, and 388_90, Study Site #3 using ISO2 and four recodes.....	58
14	Sums of absolute differences for all four photographs for each recode tested for Study Site #3	60
15	Descriptive and inferential statistics of difference image (estimated [extrapolated demixing] minus reference) for two land-cover categories for photo 381_158 for Study Site #1 using recode 12_35 and ISO2.....	61
16	Descriptive and inferential statistics of difference image (estimated [extrapolated demixing] minus reference) for two land-cover categories for photo 386_124 for Study Site #2 using recode 14_5 and 1_25	65
17	Descriptive and inferential statistics of difference image (estimated [extrapolated demixing] minus reference) for two land-cover categories for photo 388_90 for Study Site #3 using recodes 14_5 and 1_25	68
18	Mean and standard deviation of abundance for five land-cover categories for photo 381_158, Study Site #1; estimated (spectral index correlations) versus reference	75
19	Descriptive and inferential statistics of difference image (estimated [spectral index correlations] minus reference) for five land-cover categories for photo 381_158, Study Site #1	76
20	Mean and standard deviation of abundance for three land-cover categories for photo 381_158, Study Site #1; estimated (spectral index correlations) versus reference	81
21	Descriptive and inferential statistics of difference image (estimated [spectral index correlations] minus reference) for three land-cover categories for photo 381_158, Study Site #1	81

22	Mean and standard deviation of cover abundance for photo 381_158, Study Site #1 using ISO2 and four recodes: estimated (spectral index correlations) versus reference	82
23	Descriptive and inferential statistics of difference image (estimated [spectral index correlations] minus reference) for two land-cover categories for photo 381_158, Study Site #1 using ISO2 and four recodes.....	83
24	Descriptive and inferential statistics of difference image (estimated [spectral index correlations] minus reference) for two land-cover categories for photos 380_18, 381_144, and 381_146, Study Site #1 using ISO2 and four recodes.....	84
25	Total sum of absolute differences for all four photographs for each recode tested for Study Site #1	88
26	Descriptive and inferential statistics of difference image (estimated [spectral index correlations] minus reference) for two land-cover categories for photos 386_122, 386_124, 386_16, and 386_18, Study Site #2 using ISO2 and four recodes.....	89
27	Total sum of absolute differences for all four photographs for each recode tested for Study Site #2	93
28	Descriptive and inferential statistics of difference image (estimated [spectral index correlations] minus reference) for two land-cover categories for photos 388_45, 388_47, 388_88, and 388_90, Study Site #3 using ISO2 and four recodes.....	94
29	Total sum of absolute differences for all four photographs for each recode tested for Study Site #3	98
30	Descriptive and inferential statistics of difference image (estimated [extrapolated spectral index correlations] minus reference abundance) for two land-cover categories for photo 381_158 for Study Site #1 using recode 12_35 and ISO2.....	100
31	Descriptive and inferential statistics of difference image (estimated [extrapolated spectral index correlations] abundance minus reference abundance) for two land-cover categories for photo 386_124 for Study Site #2 using recode 14_5 and 1_25	105
32	Descriptive and inferential statistics of difference image (estimated [extrapolated spectral index correlations] abundance minus reference abundance) for two land-cover categories for photo 388_90 for Study Site #3 using recodes 14_5 and 1_25	110

Preface

This study was conducted for the Commander, U.S. Army Air Defense Artillery Center, Directorate of Environment, Fort Bliss, Texas, under Military Interdepartmental Purchase Request (MIPR) #95-63, Work Unit, “Fort Bliss Demixing and Vegetation Mapping on McGregor Range.” The technical monitors were Keith Landreth, Chief, Cultural and Natural Resources, Fort Bliss Directorate of Environment, and Kevin VonFinger, National Environmental Policy Act Ecologist, Fort Bliss Directorate of Environment.

The work was performed by Scott Tweddale, William Jackson, and Michael Shapiro of the Ecological Processes Branch (CN-N) of the Installations Division (CN), Construction Engineering Research Laboratory (CERL), and Paul Pope of the University of Wisconsin—Environmental Remote Sensing Center. The CERL Principal Investigator was Scott Tweddale. The technical editor was Gloria J. Wienke, Information Technology Laboratory — Champaign. Stephen Hodapp is Chief, CN-N, and Dr. John T. Bandy is Chief, CN. The associated Technical Director was Dr. William D. Severinghaus, CV-T. The Director of CERL is Dr. Alan W. Moore.

Initial scoping resources for the project were provided by the U.S. Army Environmental Center (technical monitor: Steve Sekscienski). The authors acknowledge all participants in the 1994-1995 Environmental Monitoring Practicum Course at the University of Wisconsin, Institute for Environmental Studies (instructor: Professor Frank Scarpace) for their initial research on spectral demixing at Fort Bliss. The authors also acknowledge Brett Russell, Dallas Bash, Doug Chamlee, and Kevin von Finger, Fort Bliss Directorate of Environment, for their assistance with collecting field data.

CERL is an element of the U.S. Army Engineer Research and Development Center (ERDC), U.S. Army Corps of Engineers. The Commander and Executive Director of ERDC is COL James R. Rowan, EN, and the Director of ERDC is Dr. James R. Houston.

1 Introduction

Background

Fort Bliss, Texas, is a U.S. Army Training and Doctrine Command (TRADOC) installation located in the northern Chihuahuan Desert of western Texas and south-central New Mexico. Encompassing approximately 445,170 hectares (1.1 million acres), it is the single largest TRADOC installation (Figure 1). Because Fort Bliss is located within an arid ecosystem characterized by slow vegetative growth, its land is more susceptible to long-term disturbance. Typically, land degradation in arid environments is associated with a decrease in vegetative cover and abundance, and an increase in soil erosion potential. Such degradation can result from either anthropogenic (resulting from human activity) disturbances or allogenic (successional change caused by nonliving environmental conditions) disturbances, including impacts from training, and can occur at many different scales. The Fort Bliss Directorate of Environment (DOE) is responsible for managing Fort Bliss training lands in a sustainable manner to support the current and future training mission. Vegetation abundance, condition, and species composition are important indicators of training land condition. Therefore, Fort Bliss natural resource managers require a timely and cost-effective method for characterizing and monitoring land condition at various spatial scales and levels of detail. Proactive land management requires detailed, large-scale characterization and monitoring tools. These tools can help resource managers monitor changes in vegetative cover, which will allow them to evaluate the susceptibility of the landscape to soil erosion using wind and water soil erosion models. Resource managers also need a method to monitor percent vegetative cover of specific plant species or plant communities that may be sensitive habitats or indicative of disturbance. Detailed resource characterization and monitoring also provides improved input into land-based carrying capacity and other ecological models, thereby improving the ability to evaluate land management scenarios and predict future land condition. The ability to detect subtle effects of both anthropogenic and allogenic disturbances across training lands may allow time for land rehabilitation or temporary reallocation of training so the carrying capacity of training lands is not exceeded.

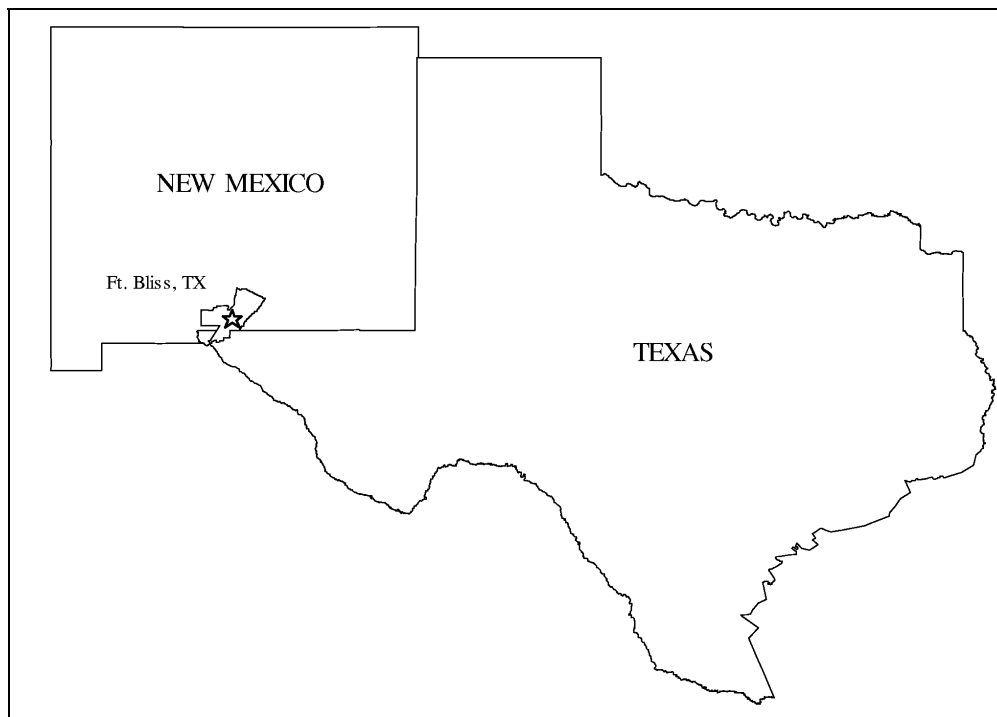


Figure 1. Location of Fort Bliss, Texas.

In response to these requirements, many Department of Defense (DoD) training and testing installations, including Fort Bliss, have implemented the Land Condition Trend Analysis (LCTA) program, which is part of the Army's Integrated Training Area Management (ITAM) plan (Tazik et al. 1992). The LCTA program provides a standard method for inventory and monitoring of vegetation and wildlife on military lands. Under the LCTA program, permanent plots are established and visited annually to conduct a detailed census of vegetation and wildlife. However, field surveys are costly; therefore, a complete survey of large installations is not possible and a detailed vegetation map is often lacking. Long-term trends in the vegetation condition can be monitored by evaluating all the aggregated information collected for individual LCTA field surveys, but it is impossible to assess vegetation condition at any one time over a large area based solely on field surveys. To assess a large area, information collected at LCTA field survey point locations must be spatially extrapolated to those areas that are not sampled. This is especially true of large installations like Fort Bliss.

Satellite imagery provides a good supplement to field surveys because of its large geographic coverage and relatively high temporal frequency. However, the spatial resolution (20 to 30 m) of contemporary satellite imagery is not suitable for large-scale characterization and monitoring. Variability of land cover and disturbance patterns may occur at subpixel spatial scales in arid environments. At this spatial resolution, each pixel represents a mixture of the spectral responses of all surface components located within that pixel. At Fort Bliss, such pixels

represent a mixture of perennial desert shrubs; perennial and annual grasses and forbs, both vigorous and dormant; senesced litter; soils; and shadows. In addition, vegetation is typically sparse, and the mixed spectral signature is usually dominated by the spectral signature of background soil. It is necessary to determine the contribution of each land-cover component to the overall spectral response in a pixel to be able to use this scale of imagery to monitor vegetation amount and condition.

Emerging technologies and methods generate satellite imagery and photography with high spatial and spectral resolution. These images are much more likely to contain pixels that represent a single homogenous land-cover type. However, high-resolution spectral imagery is costly in terms of collection, processing, and interpretation, and typically provides unmanageable data volumes for large installations such as Fort Bliss. Therefore, complete coverage of high spatial resolution imagery is not acquired regularly for installation monitoring.

Given these limitations, training managers and natural resource managers need an alternative method to estimate, extrapolate, and monitor more detailed percent vegetative cover from coarse resolution imagery across arid landscapes.

Objective

The primary objective of this investigation was to evaluate linear spectral demixing and spectral brightness and greenness index correlations with abundance of land-cover types as alternative methods for more detailed characterization and monitoring of land condition using coarse resolution satellite imagery.

Approach

Three study areas were chosen to represent the three primary vegetation/land form areas of Fort Bliss. Study Site #1 was an area of mesquite-covered coppice dunes in the Tularosa Basin, primarily located within Maneuver Areas #4 and #5. Study Site #2 was a grassland-dominated site on Otero Mesa. Study Site #3 was a mixed desert shrub/grassland area in the foothill transition zone between the Tularosa Basin and Otero Mesa (Figure 2). At each site, four digital 1:16,000 Color Infrared (CIR) images were acquired as samples. Classifications of the CIR photographs provided a ground reference of abundance or percent cover of individual land-cover types. A Landsat Thematic Mapper (TM) image of Fort Bliss was also acquired with approximately the same acquisition date as the CIR photographs.

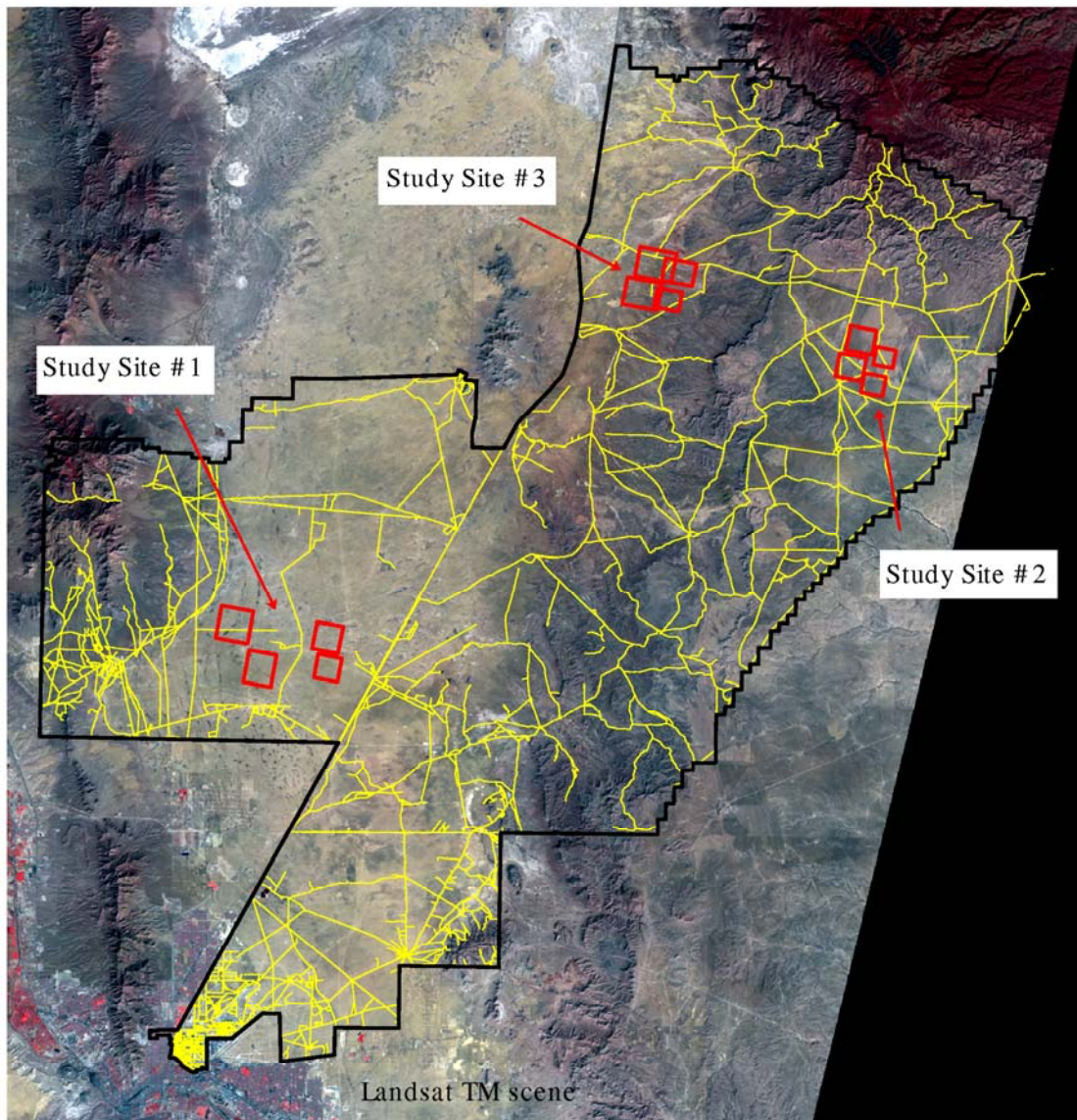


Figure 2. Study site locations

Using spectral demixing, the percent cover of individual land-cover components (as derived from CIR photograph classifications) and TM spectral response in six spectral wavelengths were used to determine the spectral contribution of each land-cover component to the mixed spectral response recorded in a single TM pixel. The equations used to determine the spectral contribution of each land-cover component were then inverted so that given the known spectral contribution of individual land-cover components and the known spectral response recorded in an individual TM pixel, other TM pixels were OR could be demixed to estimate percent cover of individual land-cover components.

A second method of characterization and monitoring land condition was also evaluated. This method involved using correlations between percent cover of individual land-cover components and spectral brightness and greenness indices. Again, percent cover of individual land-cover components was derived from classifications of the CIR imagery. Spectral brightness and greenness indices were derived from spatially and temporally coincident Landsat TM imagery. Correlations between greenness and brightness indices and abundance were then used to extrapolate estimates of percent cover over a large geographic region.

Mode of Technology Transfer

This report will be made accessible through the World Wide Web (WWW) at URL:

<http://www.cecer.army.mil>

2 Background

The literature describes many applications of spectral demixing analysis and spectral brightness correlations using spectral imagery for assessing land-cover types and vegetation abundance. A review of literature is provided below. These approaches have been applied successfully and validated statistically. Researchers have applied spectral demixing analysis and spectral brightness correlations to resource characterization and monitoring in arid and semiarid environments similar to Fort Bliss.

Spectral Demixing

Various studies have shown that spectral demixing of multiband satellite imagery can provide estimates of the aerial percentage of various land-cover types (Marsh et al. 1980; Foody and Cox 1994; Foschi 1994; Smith et al. 1990). The technique of linear spectral demixing, as it relates to multispectral imagery, is an attempt to extract the amounts of various land-cover types within an area imaged by a single pixel (Adams et al. 1985; Smith et al. 1990; Marsh et al. 1980; Roberts et al. 1991). The key assumption of linear spectral demixing is that the mixed spectra associated with each pixel of a multiband satellite image are assumed to be linear combinations of weighted pure spectrums. Each pure spectrum, or spectral endmember, is assumed to be unique and representative of a particular type of land cover. The weight associated with each pure spectrum is assumed to be equal to the fractional area of the pixel occupied by the types associated with that pure spectrum. These weights are called “percent covers.” Nonlinear spectral demixing is similar in principle to linear demixing, except that nonlinear demixing accounts for multiple interactions of reflected light with several groundcover or endmember components (Borel and Gerstl 1994; Roberts et al. 1993; Smith et al. 1990; Ray and Murray 1996). However, nonlinear demixing was not tested in this research. Demixing techniques offer a method of land-cover classification that differs from statistical classification schemes in two important ways. First, the method is deterministic. It attempts to physically model the reflection of light from various land covers that make up the terrain. Second, unlike statistical classifiers, it does not assume a homogenous classification for each individual pixel in an image. Therefore, the surface area imaged by each pixel element can have several different land-cover classes, which is more

realistic classification output since almost all pixels in a scene will contain a mixture of land-cover types (Foschi 1994). Therefore, the resulting output from demixing analysis provides an individual abundance image for each endmember or land-cover type used to develop the demixing model. This abundance image depicts the spatial distribution and abundance of that respective land-cover type (Bateson and Curtiss 1996). This demixing method can greatly improve the accuracy of vegetative cover and abundance estimates, especially in arid and semi-arid environments with incomplete or sparse canopy covers. In such environments, the ratio of vegetation to bare ground can change rapidly over distances that are smaller than the spatial resolution of coarse resolution satellite imagery (Smith et al. 1990; Huete 1986; Tueller 1987).

Spectral demixing; can be categorized into one of two methods. The first method assumes that the percent cover of each of the land-cover types of interest within several pixels is known. The pure spectrum of each land-cover type can then be determined by inverting the model (Huete 1986; Puyou-Lascassies et al. 1994; Adams et al. 1995; Marsh et al. 1980). The model is developed by correlating known percent cover values of land-cover types with the spectral values for a sample of pixels from the coarse resolution imagery using regression techniques. The known percent cover estimates used to parameterize the model are typically derived from field measurements or corresponding high spatial resolution imagery or photography. This is the method applied in this research. A more detailed description of the method used is summarized in Chapter 4, Methodology (page 18). Conversely, the algorithm can also be applied in reverse. If the pure spectrum of land-cover types or spectral endmembers is known, then the percent cover of each type within a single mixed pixel can be determined (Ray and Murray 1996; Farrand et al. 1994; Asrar et al. 1986; Smith et al. 1990; Smith et al. 1994). In either case, this image processing technique is referred to as spectral demixing or spectral unmixing.

Spectral demixing has been evaluated as a technique for estimating vegetative cover and abundance in arid environments using multispectral imagery with mixed results. Typically, spectral demixing is capable of providing estimates of green leaf vegetative matter, gray matter and litter, and bare ground with some degree of success (Sohn and McCoy 1997; Smith et al. 1990; Marsh et al. 1980). However, there are still recognized problems with demixing analysis in arid environments, including difficulties in identifying spectrally unique endmembers and accounting for shadowing effects within sparse canopy desert shrubs (Ray and Murray 1996; Pech et al. 1986; Ustin et al. 1986). Appendix A contains a graphic depiction of the linear spectral demixing process flow.

Spectral Brightness and Vegetation Indices

Correlations between spectral index values derived from multispectral imagery and ground observations of vegetative cover have also been used to spatially extrapolate estimates of vegetative cover and abundance. Spectral indices have been developed to reduce multispectral scanner data observed by satellites to a single number or index that attempts to quantify the amount of vegetative cover or bare ground in an individual pixel. Direct empirical relationships between these indices and ground measurements of vegetative cover are then used to spatially extrapolate cover estimates. This method differs from spectral demixing, where cover is estimated by determining the unique spectral contribution of each land-cover type or spectral endmember existing within a single pixel. A review of literature is provided below.

Vegetation or Greenness Indices

Common commercial satellite sensors record reflectance from the Earth's surface in several regions of the electromagnetic spectrum. Depending on the intended application, different wavelengths are better suited for analyzing different aspects of the Earth-atmosphere system. For assessing vegetation, the red and near infrared regions of the spectrum are most commonly analyzed. Within each portion of the spectrum, different properties of vegetation control the amount of electromagnetic energy that is absorbed, transmitted, or reflected. In general, healthy vegetation has been characterized by low reflectance in the visible wavelengths (400 to 700 μm) and high reflectance in the near infrared wavelengths (Kauth et al. 1978; Tucker 1979; Curran 1980). Therefore, high reflectance in the near infrared wavelengths is directly proportional to plant biomass. In general, an inverse relationship exists between reflectance in the visible region, particularly in the red wavelengths, and biomass production of a plant (Jensen 1986).

Several vegetation indices have been developed to reduce multispectral scanner data observed by satellites to a single number or index, to be used to qualitatively and quantitatively assess vegetation conditions (Tucker 1979; Price 1987). Almost all vegetation indices are transformations based on the near infrared and red portions of the electromagnetic spectrum. Most vegetation indices can be characterized as either ratio or orthogonal. Ratio indices exploit the contrasting low red reflectance and high near infrared reflectance of vegetation by simple ratios of these two bands. Orthogonal indices are based on the Tasseled Cap transformation, which is a characteristic plot of red reflectance (x-axis) vs. near infrared reflectance (y-axis) that is useful for extracting the relative greenness of vegetation and soil brightness (Kauth et al. 1978). Within the Tasseled Cap dis-

tribution, Kauth determined that the distribution of the soil reflectance variation was confined to a “line of soils” extending from the plot origin at approximately 45 degrees from the x-axis (red) with soil brightness increasing with distance from the origin. Reflectance variation of vegetation is then measured perpendicularly from this line of soils in the direction of the y-axis (near infrared). This distribution was aptly named because if viewed in three dimensions, it resembles a cap with a tassel extending from the top. Although the original Tasseled Cap transformation was based on Landsat Multispectral Scanner (MSS) data, the same transformations have been applied to Landsat TM data (Crist and Ciccone 1984). Variations of the Tasseled Cap have been customized for arid environments (Graetz and Gentle 1982; Pickup et al. 1993). Regardless of the sensor, greenness and soil brightness indices derived from this characteristic plot are commonly referred to as Kauth-Thomas or Tasseled Cap Soil Brightness and Greenness Indices.

Other derivations of ratio and orthogonal vegetation indices are beyond the scope of this report. However, all indices are similar in that they provide dimensionless values that represent relative ranges of vegetation amount or condition. In general, vegetation indices have been correlated with a number of vegetative characteristics such as biomass (Tucker 1979), percent cover (Senseman et al. 1996), and leaf area index (Richardson and Wiegand 1977).

The Normalized Difference Vegetation Index (NDVI) is probably the most commonly applied vegetation index for assessing vegetative amount and condition (Rouse et al. 1974). In the first comprehensive study of correlation between NDVI and vegetative parameters, high coefficients of determination for a simple linear regression were found between NDVI and total wet biomass, total dry biomass, leaf water content, dry green biomass, and total chlorophyll for clipped blue grama prairie grass plots (Tucker 1979). Several vegetation indices have also been correlated with measurements of shrub and grass cover in various rangelands, including southern Australia (Graetz and Gentle 1982; Pickup et al. 1993), north-eastern Colorado (Anderson et al. 1993), central Washington (Senseman et al. 1996), north-central Texas (McDaniel and Haas 1982; Boyd 1986), and specifically in the Chihuahuan Desert (Duncan et al. 1993; Franklin et al. 1993; Peters et al. 1997; Yool et al. 1997).

However, one limitation of using the NDVI in arid environments is that the spectral response of the exposed soils often dominates the spectral response of any extant vegetation. This domination is due to the sparse vegetation cover and the high near infrared reflectance of arid soils. Therefore, several indices have been developed that attempt to correct for this factor, including the Weighted Difference Vegetation Index (WDVI; Richardson and Wiegand 1977), the Soil Adjusted

Vegetation Index (SAVI; Huete 1988), and the Modified Soil Adjusted Vegetation Index (MSAVI; Qi et al. 1994). These indices are designed to maximize the influence of vegetation and minimize the effect of background soil. The SAVI index requires a user-defined soil correction factor “L” as input into the indices. The constant “L” represents an estimate of percent vegetative cover, and therefore is often unknown. Typically, different “L” factors are tested and a final value is selected based on agreement with ground estimates, or an “L” factor is assigned based on user knowledge of the study site. In general, the “L” factor is difficult to objectively quantify. An MSAVI has since been developed that calculates a self-adjustable “L” factor directly from spectral information. MSAVI also increases the sensitivity to vegetation and minimizes soil influences (Qi et al. 1994). The MSAVI accounts for possible variations of soil reflectance through an inductive method based on opposite trends of NDVI and WdVI, thus eliminating subjective assignment of the soil correction “L” factor. In the original field test in cotton fields, density of cotton canopy was predicted more accurately by MSAVI than other derivations of SAVI using remotely sensed imagery. Not only does MSAVI eliminate the requirement to estimate “L,” but for arid lands, MSAVI has been promoted as the best predictor of shrub cover measurements among the indices that attempt to mitigate the influence of soil reflectance (Rondeux et al. 1996; Senseman et al. 1996).

Brightness Indices

Albedo (or reflectance) and soil brightness indices have also been calculated and can be used to estimate percent vegetative cover from satellite imagery. Whereas vegetation or greenness indices attempt to measure the reflectance of vegetation directly while minimizing the effects of bare soil, brightness indices measure the total brightness or reflectance of the Earth’s surface, and therefore are more sensitive to soil background reflectance. Vegetation tends to mask the reflectance of soils, particularly in sparsely vegetated arid environments with highly reflective background soils. Therefore, an inverse relationship between brightness indices and vegetative cover has been used to estimate vegetative cover (Robinson et al. 1981; Sanden et al. 1996; Satterwhite 1984; Frank 1985; Musick 1986).

Albedo is defined as the ratio of all shortwave radiation reflected by the Earth’s surface to solar irradiance incident on the surface. Albedo has been correlated with measurements of vegetative cover in several arid and semiarid environments (Price et al. 1992; Robinson et al. 1981; Frank 1984). Planetary albedo, or planetary reflectance, is a measure of reflectance of the entire Earth-atmosphere system, and is calculated directly from observations (data) recorded at the satellite. Surface reflectance, or surface albedo, is a measure of reflectance of the

Earth's surface. To calculate surface albedo using remotely sensed observations, radiometric and atmospheric corrections must be applied to correct for atmosphere, topography, and solar geometry variations. Many times, reflectance is calculated across all of the visible and near infrared wavelengths available. Other times, reflectance of a single spectral band, or in-band albedo, often correlates well with vegetative cover in arid environments. In all cases, vegetative cover is measured indirectly by the relative decrease in brightness of the background soils due to vegetative cover or shadowing.

Other soil brightness indices have also been developed to assess soil brightness, and indirectly, vegetation cover. One common index is the Kauth-Thomas Soil Brightness Index (SBI; Kauth et al. 1978). The SBI is also calculated based on the Tasseled Cap transformation described earlier. Similar to the Greenness Index, the SBI is derived from the characteristic plot of red vs. near infrared reflectance in spectral space. Soil brightness indices have been correlated with arid shrub cover in several studies at the Jornada Long-Term Ecological Research (LTER) site, which is near Fort Bliss (Duncan et al. 1993; Musick 1984).

Like spectral demixing, spectral brightness and greenness indices have been used to estimate vegetative cover with mixed results. There are unique challenges associated with applying these methods to arid environments. In the case of vegetation or greenness indices, the challenge is to isolate the contribution of vegetation cover to the spectral response while reducing the contribution of all other land-cover components, including the dominant background soil. The opposite is true for brightness indices, where the influence of vegetation cover is measured indirectly.

3 Study Area and Data

Study Area

Fort Bliss is in western Texas and south-central New Mexico on the northern edge of the Chihuahuan Desert (Figure 1). The installation is approximately 445,170 ha (1.1 million acres) and is located within Otero and Dona Ana Counties in New Mexico and El Paso and Hudspeth Counties in Texas. White Sands Missile Range is located along the western boundary, and the Lincoln National Forest and Bureau of Land Management (BLM) lands are located along the northeastern and western boundaries. The installation is surrounded by four mountain ranges: the southern Sacramento Mountains to the northeast, the Hueco Mountains to the southeast, the Organ Mountains to the west, and the Franklin Mountains to the southwest. Otero Mesa is a gently tilted plateau along the eastern boundary of the installation. Two basins, the Tularosa and Hueco, are located in the central region of the installation. Elevations range from 1350 m in the Tularosa Basin floor to over 3100 m at the top of the Organ Mountains (Budd et al. 1979; Mehlop et al. 1996; Boykin et al. 1997).

Average annual precipitation is between 21 and 28 cm in the Tularosa Valley to 31 to 46 cm on the Otero Mesa. The mean annual precipitation is 22.5 cm. Most of the annual rainfall occurs between July and October. Snow may fall from November through March and ranges from 8 to 26 cm annually. The mean annual temperature ranges between 14 and 17 °C. Relative humidity is low, and severe dust storms are frequent under prolonged dry conditions. Soils within the study area range from loamy sand with many exposed rocks on the steep slopes of the foothills to more well-drained soils on the Otero Mesa (USDA 1980; U.S. Army 1978).

Vegetation at Fort Bliss is diverse, ranging from Chihuahuan Desert grassland and shrublands to Rocky Mountain conifer forest in the highest elevations. The basin floors are characterized by shrublands dominated by honey mesquite (*Prosopis glandulosa*), creosote bush (*Larrea tridentata*), sandsage (*Artemisia filifolia*), saltbush (*Atriplex canescens*), with isolated patches of grasslands dominated by dropseed (*Sporobolus* spp.), and tobosa grass (*Hilaria mutica*). The alluvial fans and piedmonts are dominated by a mixture of shrubs and grasslands, including honey mesquite, creosote bush, tarbush (*Florencia cernua*) and acacia

(*Acacia* spp.), along with grama grasses (*Bouteloua* spp.), and bush muhly (*Muhlenbergia porteri*). Otero Mesa is dominated by grama grasses, burrograss (*Scleropogon brevifolius*), vine mesquite (*Panicum obtusum*), and yucca (*Yucca* spp.). Higher mountain elevations support wavy leaf oak (*Quercus undulata*), mountain mahogany (*Cercocarpus montanum*), sotol (*Dasylirion wheeleri*), sumac (*Rhus* spp.), juniper (*Juniperus* spp.), pinyon pine (*Pinus edulis*), ponderosa pine (*Pinus ponderosa*), and Douglas-fir (*Pseudotsuga menziesii*) (Mehlop et al. 1996; Boykin et al. 1997). All study sites in this research were located within the basins, alluvial fans, and piedmonts, and on Otero Mesa.

Data

A Landsat TM satellite image and Kodak color infrared aerial photographs were acquired to evaluate spectral demixing and spectral index correlations as alternative methods for estimating and extrapolating abundance of vegetative cover at Fort Bliss.

A single Landsat-5 TM image of Fort Bliss was acquired on 9 November 1994 (Scene ID: 94313). This acquisition date was the nearest available date to the acquisition date of existing Kodak CIR photography. TM is a space-borne scanning sensor that records reflected and emitted energy in the blue, green, red, near infrared, middle infrared, and thermal regions of the electromagnetic spectrum. Landsat-5, the satellite that carries the TM sensor, is in a sun-synchronous orbit approximately 705 km above the Earth's surface. TM has a temporal revisit time of 16 days and a spatial resolution of approximately 30 m. The spectral characteristics of the Landsat-5 TM are summarized in Table 1.

Table 1. Landsat-5 TM specifications.

Channel #	Band Width (μm)	Ground IFOV (m)
1	0.45 - 0.52	30
2	0.53 - 0.60	30
3	0.63 - 0.69	30
4	0.76 - 0.90	30
5	1.55 - 1.75	30
6	10.42 - 12.50	120
7	2.08 - 2.35	30
Adapted from Table 2-4 of Jensen (1986).		

Kodak CIR aerial photography was acquired for this project from the Fort Bliss DOE. The DOE contracted the National Aeronautics and Space Administration (NASA, John C. Stennis Space Center) to acquire Airborne Terrestrial Applications Sensor (ATLAS) data for Fort Bliss. The ATLAS scanner is a 15-channel multispectral scanning system with direct digital recording capabilities. ATLAS was developed by the Advanced Sensor Development Laboratory Sverdrup Technology Inc. at the Stennis Space Center. An ATLAS scanner records pixel information with a nominal resolution of 5 meters. The CIR photography was collected at the same time as the ATLAS data. The ATLAS mission was flown at an elevation at 8200 ft (2732 m) above mean terrain level. With a 6-inch (3.46-cm) focal length on the scanner lens, the resulting Kodak CIR photographs had a nominal scale of 1:16000 (1 inch = 1333 feet; 2.54 cm = 443 m). The overflights were acquired over an 8-day period beginning October 29, 1994 and ending November 5, 1994.

Study Site Selection

Three general study areas were chosen to represent the three primary vegetation/landform areas of Fort Bliss (Figure 2). Study Site #1 represents the Honey Mesquite/Coppice Dunes area of the Tularosa Valley, primarily located within Maneuver Areas #4 and #5. Study Site #2 represents a grassland-dominated site on Otero Mesa. Study Site #3 represents a mixed desert shrub/grassland area in the foothill transition zone between the Tularosa Valley and Otero Mesa. Not only were these sites chosen to represent the primary vegetation and landform areas of the installation, but they also correspond to locations of other related field studies ongoing at Fort Bliss. Study Site #2 was located near the Wheeled Vehicle Carrying Capacity Controlled Impact Sites on Otero Mesa. Study Site #3 was located near the Controlled Burn Study Sites directly south of Highway 506. Therefore, maps of estimated total vegetative cover resulting from this research can be incorporated into those research efforts.

NASA provided the Kodak CIR photographs to Fort Bliss DOE on color-positive transparencies on drum type reels. No photograph index was supplied. CIR transparencies were visually inspected and several CIR photographs were identified for each general study site. Four digital 1:16,000 CIR images were ultimately selected as samples for each of the three general study areas (Figures 3 through 5). These photographs were selected based on their suitability for testing spectral demixing and spectral index correlations. Photographs that contained some diversity in land cover and vegetation types and had minimal urban features were optimal.

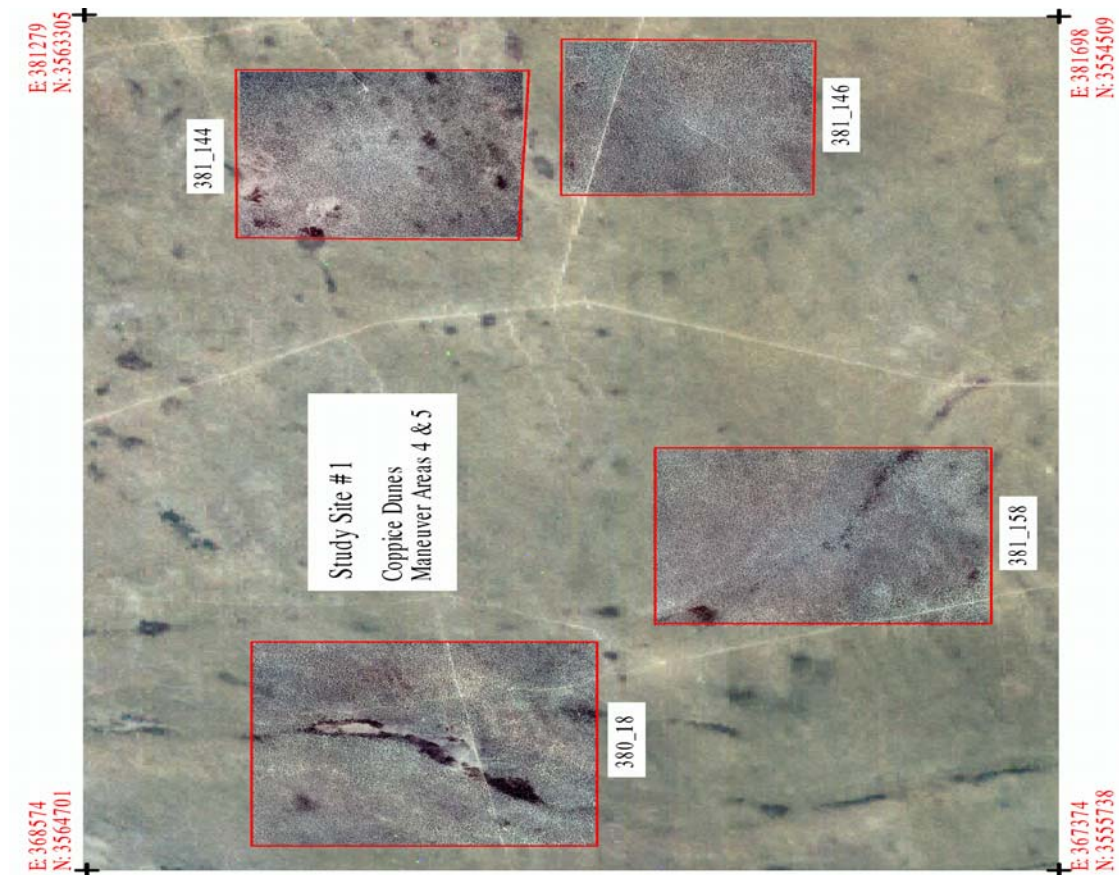


Figure 3. CIR photographs analyzed for Study Site #1, overlaid on TM image.

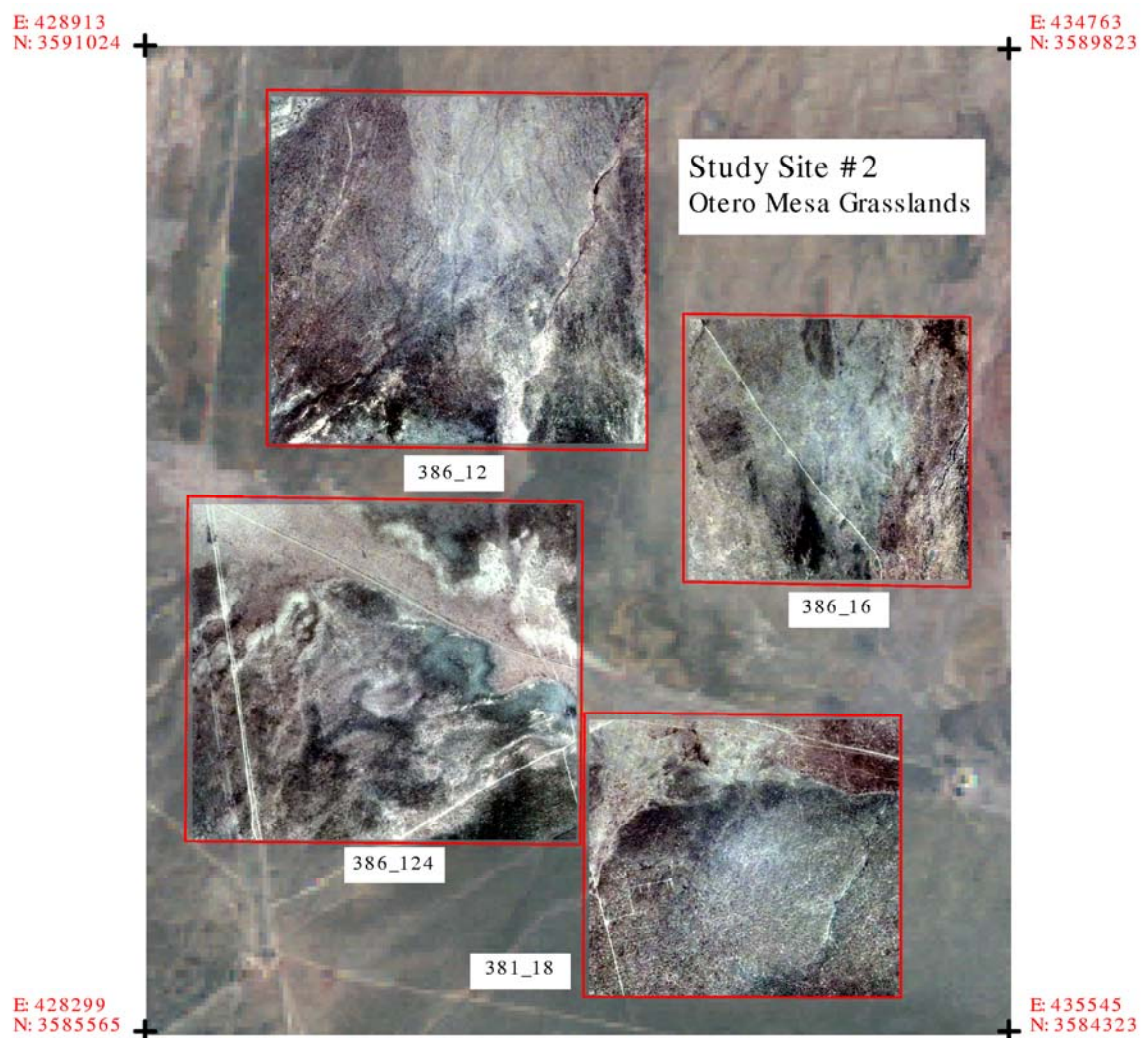


Figure 4. CIR photographs analyzed for Study Site #2, overlaid on TM image.

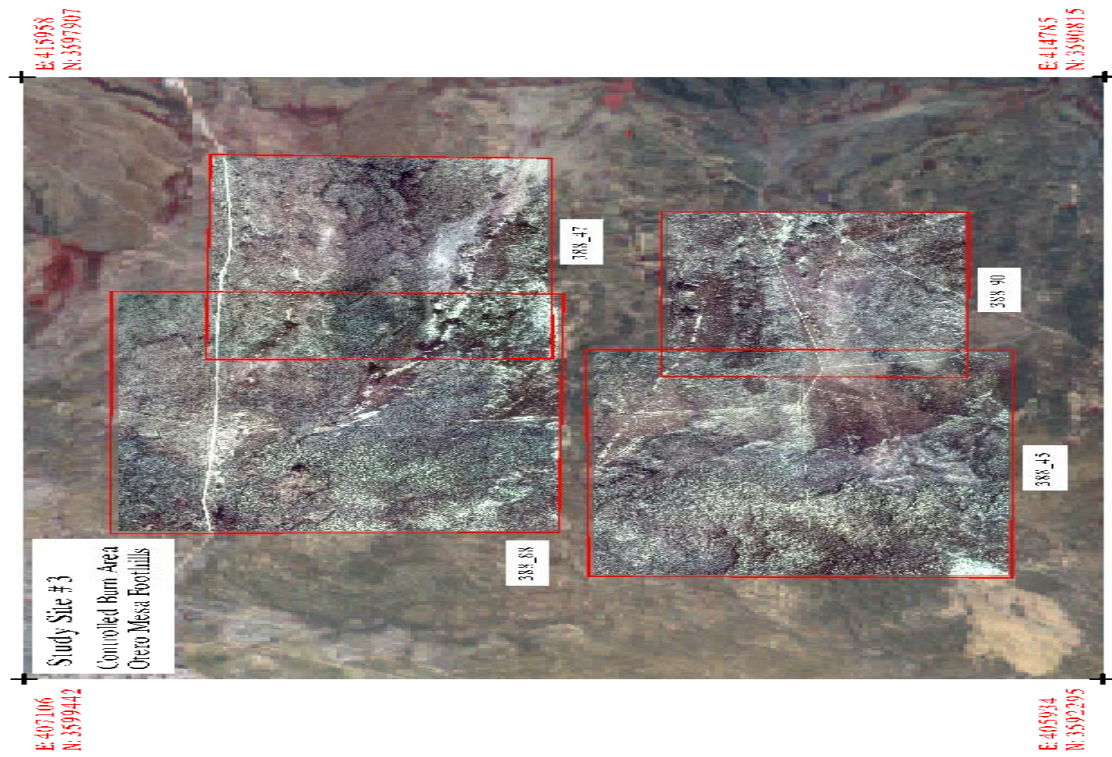


Figure 5. CIR photographs analyzed for Study Site #3, overlaid on TM image.

4 Methodology

Image Scanning

Digital copies of the CIR photographs were required to conduct demixing and spectral index correlation analysis. Spectral demixing also required accurate radiometric scanning. Therefore, project researchers contracted scanning services to Image Scans, Inc. of Denver, Colorado. Image Scans used a professional quality Leica/Helava DSW200 scanner with a maximum scan rate of 5 microns (μ). During discussions to determine the appropriate scanning resolution, Image Scans offered to scan one photograph at several different resolutions, at no cost, for testing. One photograph was arbitrarily selected for test scanning from Study Site #1, which contains primarily mesquite-covered coppice dunes in Maneuver Areas #4 and #5. The same digital image was scanned at 12.5 μ , 25 μ , and 50 μ and provided as an Leica Geosystems ERDAS Imagine* .lan[†] files. These scan rates corresponded to effective ground pixel sizes of 0.2 m, 0.4 m, and 0.8 m, respectively. Effective ground pixel sizes were calculated as follows. The nominal average scale of the CIR photography was 1:16,000. The photographs were 23 cm x 23 cm. Using the scale, 1 μ on the photograph equaled 16,000 μ on the ground.

$$1 \mu = 10^{-6} \text{ m}$$

or

$$1 \text{ m} = 10^6 \mu$$

$$16,000 \mu \times (1 \text{ m} / 10^6 \mu) = 16 \times 10^{-3} \text{ m} = 0.016 \text{ m}.$$

Therefore:

$$1 \mu \text{ on the photo} = 0.016 \text{ m on the ground,}$$

$$12.5 \mu \text{ on the photo} = 0.2 \text{ m on the ground,}$$

$$25 \mu \text{ on the photo} = 0.4 \text{ m on the ground,}$$

$$50 \mu \text{ on the photo} = 0.8 \text{ m on the ground.}$$

* ERDAS Imagine is a product of Leica Geosystems GIS & Mapping, LLC, 2801 Buford Highway, N.E., Atlanta, GA 30329-2137, telephone: 404-248-9000.

[†] A .lan file is a multiband continuous image file; the name is derived from the Landsat satellite.

Preliminary classifications were applied to the 12.5- μ (0.2-m), 25- μ (0.4-m) and 50- μ (0.8-m) images to determine if the scanning rates and resulting spatial resolution affected the image classification results. Before any preliminary comparison of the multiresolution photographs could be conducted, it was necessary to coregister the imagery. The 50- μ and 25- μ images were registered to the 12.5- μ image using a first-order linear transformation by selecting four control points at the image tic marks (retaining the original pixel size). It was also necessary to subset an area common to each resolution image.

Three classification methods were used to test the variable scanning rates: (1) Iterative Self Organizing Data Analysis Technique (ISODATA) in ERDAS Imagine, (2) maximum-likelihood discriminant analysis classifier (MAXLIK) in ERDAS Imagine, and (3) sequential maximum a posteriori (SMAP) estimation in the Geographical Resources Analysis Support System (GRASS). The primary test was to determine if classification results varied significantly when derived from either different spatial resolution imagery or from different classification algorithms. Variations on the number of spectral classes requested and the use of ancillary data such as texture were also tested.

Initial classifications were conducted requesting a range of three to seven categories for the test photograph. Visual comparisons between the original CIR photograph and several classifications with a varying number of categories were used to determine the appropriate number of categories to request for analysis. Through visual observations and consultation with Fort Bliss DOE staff, a decision was made to request five land-cover categories for analysis. Increasing the number of requested categories to six or seven seemed to introduce the added complexity of land-cover categories that were not apparent in the original CIR photographs and were not identifiable in the field. Decreasing the number of requested categories to three or four tended to eliminate land-cover categories that were of potential interest for characterization and monitoring.

Classification of the image into five spectral classes appeared to clearly separate individual honey mesquite plants and bare unvegetated sandy soils. Two additional categories occurred primarily in the interdunal areas, and appeared to correspond to interdunal grasses, small shrubs, or variations in soil material. A fifth spectral category appeared to correspond to the edges of mesquite-covered dunes and was generally one to three pixels wide (1 to 3 m). This spectral category was originally thought to be due to an edge effect around the coppice dunes that could be a combination of shadows, litter, and solar geometry due to the sloping effect of the dunes. However, this spectral category did not seem to occur at any particular spatial orientation to the dune, and in some isolated cases, it occurred in interdunal areas not associated with any dune formation. Therefore,

it was assumed to be a combination of litter; grasses; decreased mesquite foliar, stem, and branch densities; and some shadowing, but not purely shadow.

Statistical comparison between ISODATA, MAXLIK, and SMAP results showed no significant difference in classifications for the same spatial resolutions and for different spatial resolutions. Therefore, ISODATA, the default unsupervised classification tool in ERDAS Imagine, was used for all classifications in this research project.

An ERDAS Imagine spatial enhancement tool that uses texture was explored in an attempt to determine the optimal scanning resolution, and also to assist in assigning information classes to the five spectral classes identified. Texture can be defined as the frequency of tonal change in an image. The Texture image enhancement tool within the ERDAS Imagine Image Interpreter Module's Spatial Enhancement suite was applied to images at all three spatial resolutions. This tool uses either Variance (2nd order) or Skewness (3rd order) filters, and was applied using roving window sizes of 3 x 3, 5 x 5, and 7 x 7 pixels. Every filter and window size option was tested, with each test producing three texture output bands that corresponded to the original three spectral bands. The three texture output bands were "layer stacked" with the three base image bands and classifications were generated for five classes. A comparison between the original five-class ISODATA classification and the five-class ISODATA classification augmented with image texture revealed no significant difference between the images.

Evaluation of all test results for the three different scan rates, revealed that there was no significant difference in classification of land-cover types at the different spatial resolutions. Therefore, the remaining photographs were scanned at 25 microns, or 0.4-m spatial resolution, and were supplied in an ERDAS Imagine .lan file format. This scan rate appeared to be a good compromise that retained significant detail from the original photographs while addressing the practical concerns of electronic file size and disk storage space. At this resolution, a single digital three-band CIR image was 255 MB; two images could be placed on a single 650 MB CD. However, after initial processing of several images, the images were resampled to 1-m spatial resolution before analysis. To test the effect of resampling on classifications, additional classifications were performed using ISODATA by requesting five classes for the 0.4-meter pixel images and for the same photographs resampled to 1 meter. The resulting classifications were compared using differencing. The results indicated that resampling did not significantly affect the classification results.

Image Preprocessing

CIR Photography Exposure Falloff

After the individual .lan files were imported into ERDAS Imagine, further image processing was required to correct a geometric effect called exposure falloff, which was evident in all of the photographs. This effect appears as maximum exposure at the center of the film with gradual dimming at increased radial distance from the center (Lillesand and Keifer 1987). The effect was corrected with a detrend function using TNTmips* software. Figure 6 illustrates the process. The image on the left is an example of exposure falloff. The image on the right illustrates the removal of exposure falloff using TNTmips software.

Thematic Mapper Systematic Noise

Variations in the response of individual detectors used for each spectral wavelength recorded by the TM sensor sometimes causes systematic striping or banding to occur. It is desirable to correct these anomalies and restore the image as much as possible to resemble the original scene. This type of systematic noise was evident in the TM image acquired for this research. A common technique used to correct striping problems in satellite imagery is Fourier Transform. This process converts a raster image from a spatial domain to a frequency domain. In ERDAS Imagine, the Fast Fourier Transform (FFT) tool was used to convert the TM image into a series of two-dimensional sine waves of various frequencies. An image was created through this process and viewed in a graphical editor. Through trial and error, the Fourier image was edited to remove periodic striping. After the Fourier image was edited, it was then transformed back into the spatial domain by using an inverse FFT. The result is an enhanced version of the original image with periodic noise or striping reduced or removed (ERDAS Field Guide 1997). Figure 7 illustrates systematic noise removal. The image on the left is an example of periodic striping that occurred in the November 1994 Landsat TM image. The image on the right illustrates the removal of systematic banding in the TM image using Fourier Transform.

* TNTmips is a product of MicrolImages, 11th Floor - Sharp Tower, 206 South 13th Street, Lincoln NE 68508-2010 , telephone; 402-477-9554.



Figure 6. Example of exposure falloff corrections: (A) original image, (B) corrected image.

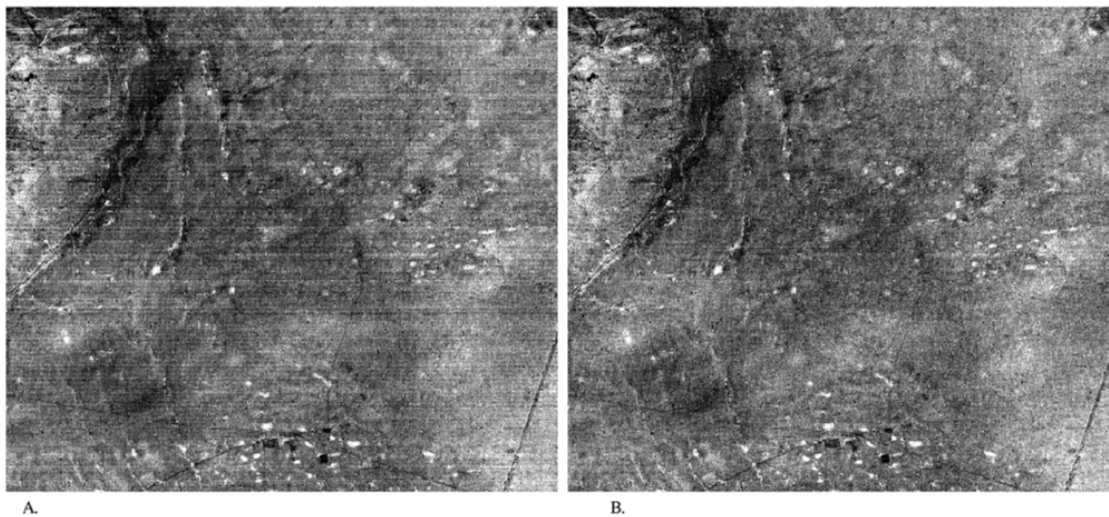


Figure 7. Example of TM systematic noise corrections: (A) original image, (B) corrected image.

Classification of CIR Photographs

Critical to both the spectral demixing and correlation analysis was the accurate classification of the CIR photographs. All reference or “ground truth” information on percent coverage of each land-cover component was extracted from these classifications. All CIR photographs were classified before coregistration to the TM imagery.

The CIR photographs and TM imagery used in this study were archival; therefore, there was no opportunity to collect the temporally coincident field data necessary to perform a supervised classification. As a result, the default unsupervised classification routine (ISODATA) in ERDAS Imagine was used to classify the CIR photographs, specifying 10 iterations and 0.95 convergence.

Determining the number of classes to request for the unsupervised classification was also critical. The number of classes requested was equivalent to identifying the number of unique land-cover types (e.g., plant species, litter, bare ground) to be characterized in terms of abundance or percent cover using demixing and spectral index correlation analysis.

Initial classifications were conducted requesting a range of three to seven categories per photograph. Visual comparisons between the original CIR photographs and several classifications with a varying number of categories were used to determine the appropriate number of categories to request for analysis. Through visual field observations and in consultation with Fort Bliss DOE staff, a decision was made to request five land-cover categories for all classification of CIR photographs. Increasing the number of requested categories to six or seven seemed to introduce the added complexity of landscape types that were not apparent in the original CIR photographs. Decreasing the number of requested categories to three or four tended to eliminate land-cover types that were of potential interest for characterization and monitoring. As an example, Figure 8 shows a subset of CIR photo 381_158 and the resulting five-category unsupervised classification.

In this example, category 1 (green) is clearly mesquite and category 5 (white) is clearly bare ground. Category 2 (yellow) appears to be an edge effect around mesquite-covered dunes that could be a combination of shadows, litter, and solar geometry due to sloping effect of the dunes. Categories 3 (red) and 4 (blue) appear to be a combination of different interdunal vegetation types, litter, and exposed surface materials of different source material.

Similar classifications were conducted for all 12 photographs. Although analysis was conducted approximately 2 to 3 years after the acquisition date of the CIR imagery (October 1994), several photograph locations were visited in the field with Fort Bliss DOE personnel to evaluate the classifications. Classification for all photographs at Study Site #1 (Coppice Dunes Maneuver Areas) resulted in a breakout of land-cover types similar to the example above for photo 381_158. However, observations at photograph locations for Study Site #2 (Otero Mesa Grasslands) and Study Site #3 (Controlled Burn/Otero Mesa Foothills) revealed that land-cover categories were not necessarily delineating individual land-cover

types, but rather represented a gradient of decreasing aerial cover, crown density, and canopy closure moving from land-cover categories 1 through 5. For example, category 1 typically delineated desert shrubs with dense canopies and the highest amount of total vegetative cover. Categories 2 thru 4 delineated a gradual decrease in canopy cover or shift from a shrub to a grass or forb with less canopy cover. Category 5 consistently delineated bare ground.

Due to the ambiguities in assigning information classes to the spectral classes resulting from unsupervised classification of the photographs, the five-class unsupervised results were recoded or aggregated in a number of different ways in an attempt to simply distinguish between cover (independent of vegetation type, and including standing dead biomass and litter) and bare ground. For each recode possibility, the end product was a two-category map where category 1 = Cover and category 2 = Bare Ground. Table 2 contains a summary of the different recodes. A simple two-class unsupervised classification using ISODATA was also conducted for each photograph in an attempt to distinguish between cover and bare ground. Figure 8 also shows examples of each of these recoded maps for a subset of photo 381_158. The subset shows enough detail to identify individual shrubs.

Table 2. Summary of recodes of original five-class unsupervised classification of CIR photographs into two classes (Cover and Bare Ground).

Recode ID	Class Recode Combinations		Recode Classes
1_25	class 1	=	Cover
	class 2, class 3, class 4, and class 5	=	Bare Ground
12_35	class 1, class 2	=	Cover
	class 3, class 4, and class 5	=	Bare Ground
13_45	class 1, class 2, class 3	=	Cover
	class 4, class 5	=	Bare Ground
14_5	class 1, class 2, class 3, and class 4	=	Cover
	class 5	=	Bare Ground

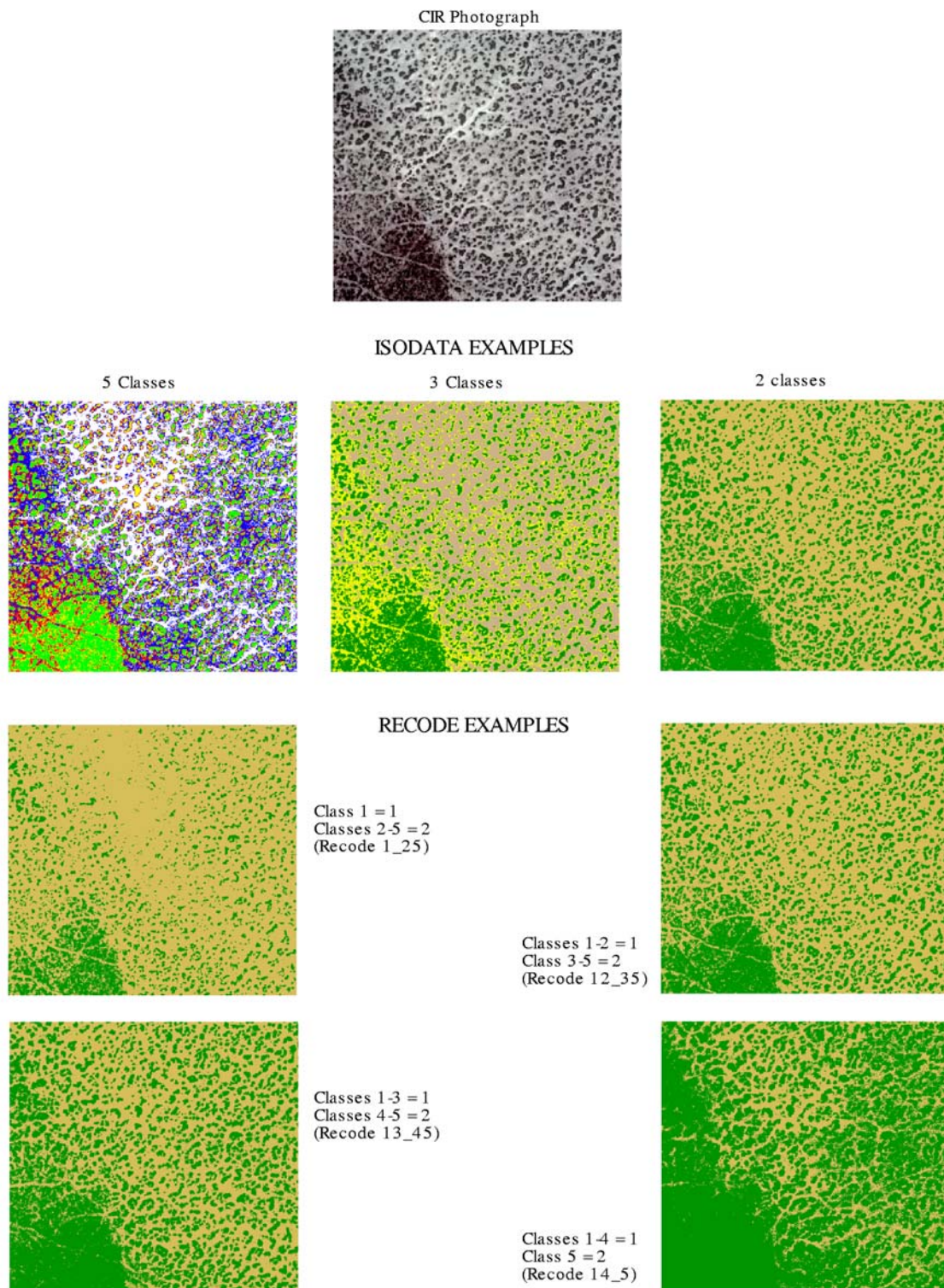


Figure 8. Original CIR photograph, examples of five-, three-, and two-class unsupervised classifications, and four recodes of the five-class image for a subset of photo 381_158 in Study Site #1.

The difficulty in identifying individual land-cover types in some photographs was indicative of the difficulties associated with spectral inseparability or spectral crossover of many desert vegetation types and bare ground. Spectral inseparability also indicated that it would be difficult to use spectral demixing and correlation analysis to quantify cover by individual land-cover type. Demixing and correlation results later confirmed this problem and are discussed in Chapter 5, Results, page 42. Consequently, binary maps of cover versus bare ground, as derived from either the above recodes of an original five-class classification or from a two-class unsupervised classification, were ultimately used in a majority of the demixing and correlation analysis.

Geometric Registration

Selection of Ground Control Points

Spectral demixing requires accurate spectral information for each pixel in the image. Therefore, to avoid resampling the Landsat TM image and effectively changing the TM pixel values, the photographs were instead coregistered to the TM image. The high spatial resolution (1 m) of the photographs compared to relatively coarse spatial resolution of the TM image (30 m) made the georeferencing process difficult. To facilitate identification of common features for the placement of control points, the photographs were degraded to 30 m using the ERDAS Imagine Degrade function and were saved in separate files. Several ERDAS Imagine tools were used during the coregistration process.

Initially, four or five ground control points were identified and evenly distributed across both the aerial photograph and TM image using well-defined manmade features visible in both images. A Transformation Matrix was calculated and the points were adjusted at the subpixel level to minimize the Root Mean Square Error (RMSE) while retaining apparent visual correctness. In many cases, however, it was difficult to locate well-defined features to select as control points. ERDAS Imagine's Ground Control Point (GCP) Matching Function, which is contained within the Geometric Correction tool, was designed for such cases where control points are difficult to select. The GCP Matching Function uses the spectral characteristics of a single band of the raster data (in this case, Band 2 of the aerial CIR photograph [Red] and Band 3 of the TM image [Red]), in conjunction with a transformation matrix to automatically digitize corresponding GCPs. Correlation threshold parameters were set and points having a correlation coefficient value within the threshold were retained; other points were discarded. Also, a maximum search radius, usually a distance of three pixels (the minimum), and a search window size parameter were defined. Using this GCP

matching utility, additional GCP points were identified throughout the image, preferably on manmade features common to both images. Points that did not meet the defined minimum correlation coefficient value were removed automatically. The analyst also removed any points that did not appear as suitable GCPs. This method proved very effective, yielding apparent accuracy within $\frac{1}{2}$ pixel (15 m). A transformation matrix file (.cff) was saved and later used to transform unsupervised classifications of the CIR photographs rather than the original CIR photographs.

Registration of CIR Photograph Classifications to TM Imagery

To limit undesirable pixel resampling during the transformation process, an Affine Transformation (Transformation Order = 1) was used to coregister the classified and recoded CIR photographs to the TM image. For some photographs, this still resulted in a misalignment of pixels that was identified through visual examination. Therefore, a second order transformation was used. The second order transformation was necessary because of terrain effects and aircraft yaw, pitch, and roll, which affected some images more than others. Ideally, the aerial photographs would have been photogrammetrically corrected using camera data defining the elevation, lens focal length, nadir position, tilt, swing, and azimuth. The transformation used the transformation matrix file (.cff) that was created as described earlier.

Accuracy Assessment of Geometric Registration

Rectification results were checked visually with ERDAS Imagine's Blend/Fade utility, which is a very effective visualization tool whereby the images are overlaid one on top of another in a single viewer. The analyst is able to fade the newly rectified image interactively into the underlying source image to check overlap by toggling between the two images at any desired toggle rate. The rectification process involved considerable trial and error. Usually rectification was done several times before achieving a satisfactory correction. Accurate geometric registration between the high-resolution CIR photography and coarse-resolution satellite imagery was critical to both spectral demixing and spectral index correlation analysis.

Subset TM Scene and Air Photo to Common Area

Common areas between the TM image and the georeferenced aerial photograph classification were defined. Because the CIR photographs were aligned along the flight path of the aircraft and not in a true north-south orientation, the maximum square area of TM imagery that fell within the footprint of the CIR photo-

graph had to be identified. This was accomplished using ERDAS Imagine by displaying the TM and the aerial photograph images in separate viewers, side by side, linking the viewers together, then running an “inquire box” in the TM viewer and roughly defining the common area with the box, taking care not to expand the box beyond the photograph image area (Figure 9). File coordinates returned from the inquire box tool were rounded by increasing smaller numbers and decreasing larger numbers (to integers) to ensure that the TM subset was clearly within the footprint of the CIR photograph. These file coordinates were used to subset the six-band TM image.

Secondly, the CIR photograph was subsetted by using “imageinfo” on the subsetted TM scene to get map coordinates and pixel sizes. Map coordinates for the upper left pixel and lower right pixel of the photograph were computed based on map coordinates for the TM subset as follows.

Notation:

TM_ULX	Upper Left X Map Coordinate for the TM subset
TM_ULY	Upper Left Y Map Coordinate for the TM subset
TM_LRX	Lower Right X Map Coordinate for the TM subset
TM_LRY	Lower Right Y Map Coordinate for the TM subset
TM_XSZ	X Pixel size (in Map Coordinates) the TM subset
TM_YSZ	Y Pixel size (in Map Coordinates) the TM subset

and similarly for the photograph:

P_ULX	Upper Left X Map Coordinate for the photo subset
P_ULY	Upper Left Y Map Coordinate for the photo subset
P_LRX	Lower Right Map Coordinate for the photo subset
P_LRY	Lower Right Map Coordinate for the photo subset
P_XSZ	X Pixel size (in Map Coordinates) the photo subset
P_YSZ	Y Pixel size (in Map Coordinates) the photo subset

$$\begin{aligned}
 P_ULX &= TM_ULX - TM_XSZ/2 + P_XSZ/2 \\
 P_ULY &= TM_ULY + TM_YSZ/2 - P_YSZ/2 \\
 P_LRX &= TM_LRX + TM_XSZ/2 - P_XSZ/2 \\
 P_LRY &= TM_LRY - TM_YSZ/2 + P_YSZ/2
 \end{aligned}$$

Common data sets were used to evaluate both demixing and spectral index correlation analysis. Therefore, it was necessary to complete the above image and photograph preprocessing and classification steps only once to compile a data set of CIR photography and TM imagery subsets that was suitable for both demixing and spectral index correlation analysis.

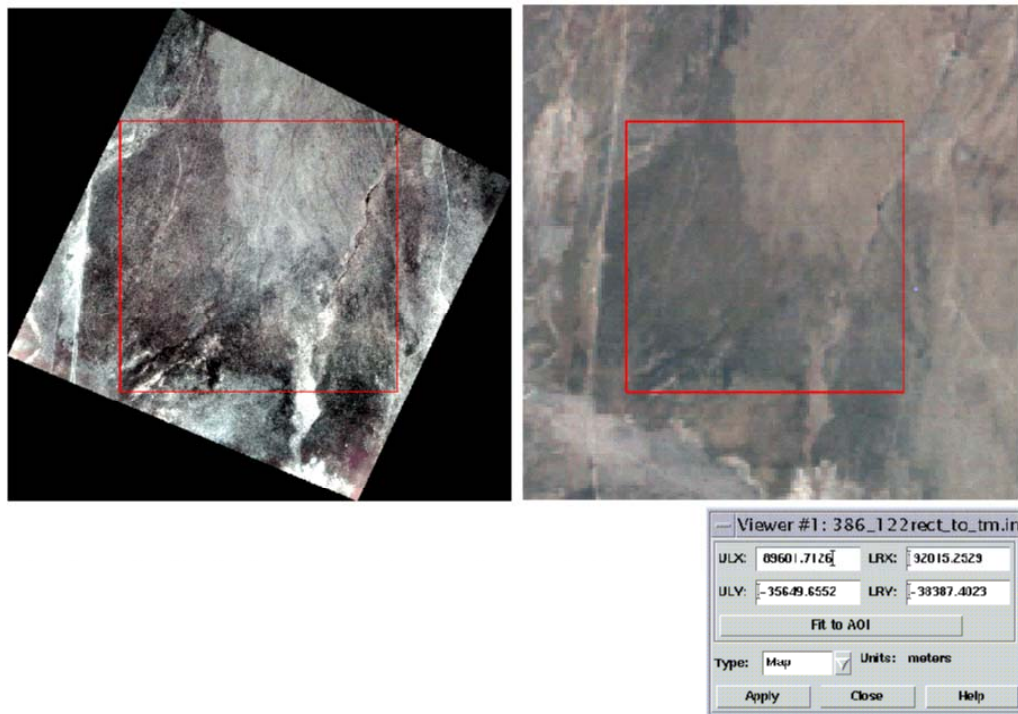


Figure 9. Procedure for subsetting the common area between a TM image and a CIR photograph.

Spectral Demixing

Spectral demixing used 12 1:16,000 CIR photographs resampled to 1-m spatial resolution and a temporal coincident Landsat TM image at 30-m resolution. For each CIR footprint, a subset of the TM scene that matched the geographic extent of the CIR footprint was extracted from the TM scene, resulting in 12 pairs of CIR photographs and matching TM subsets. Band 6 of TM was not used in this analysis. Only Bands 1 through 5 and 7, or a total of 6 bands, were used. Thus, any reference to Band 6 in this report actually refers to Band 7 of the TM sensor. Therefore, there were six pixel values associated with spatial position of any given pixel, the values corresponding to TM Bands 1 through 5 and 7.

Mathematics of Spectral Demixing

Within Landsat TM data, a single pixel images approximately 30 m by 30 m on the ground, or 900 m². Since a pixel represents a 900-m² area on the Earth's surface, there may be many different land-cover types present, yet all land-cover

types are represented by a single spectral signature for that pixel. The contribution from any particular cover type is assumed to be proportional to the amount of area that it takes up within the total area represented by that pixel. The assumption is made that each of the various land-cover types has a unique, or “pure,” spectral signature. Therefore, the spectral signature associated with a pixel is a mixture of these pure spectra, or a “mixed signature” or “mixed pixel.” A second assumption is that the mixing can be modeled by the sum of the pure spectra, each weighted by the fractional area it covers within the total area represented by the pixel. For a single band, b , this can be summarized as shown in Equation 1.

$$M_b = P_1 S_{b1} + P_2 S_{b2} + \dots P_n S_{bn} = \sum_{j=1}^n P_j S_{bj} \quad \text{Equation 1}$$

Where:

M_b = the mixed pixel value for that band,

P_j = the fractional area (percentage) of the j^{th} land-cover type (in this case, derived from classified aerial photographs),

S_{bj} = the pure signature value of the particular land-cover type for that band, and

$j = 1$ to n is the number of land-cover types.

The user must decide how many land-cover types are necessary to represent the terrain. In this research, the number of land-cover types was five. Once air photo classifications were recoded to binary maps of cover vs. bare ground, the number of land-cover types was reduced to two. The values of both M_b and S_{bj} depend on the band being analyzed. However, P_j does not depend on the band because it is a spatial quantity, not a spectral quantity. The fractional areas (percentages) should sum to unity, or 100 percent coverage (Equation 2).

$$P_1 + P_2 + \dots + P_n = \sum_{j=1}^n P_j = 1 \quad \text{Equation 2}$$

The mixed pixel value for band b , M_b , is always known from the TM image. The unknowns are the percentage covers and the pure signature values for each band and for each land-cover type. To use Equation 1, either the cover percentages must be known or the pure spectra must be known (or combinations thereof). Using a hypothetical example below, an assumption is made that the terrain can be represented by three land-cover types (i.e., $n = 3$). First, assume that the percentages, P_j , of each of the three land-cover types are known for the area covered by a single pixel. In this research, the percentages were obtained from aerial

photography. For each band there are three unknowns in Equation 1: S_{b1} , S_{b2} , and S_{b3} (the pure signature values for band b). Thus, a unique solution is not attainable. However, if the percentages are known for at least three pixels A, B, and C (i.e., three different areas on the ground), a solution can be obtained. The equations to be solved, for each spectral band are:

$$M_{bA} = P_{1A} S_{b1} + P_{2A} S_{b2} + P_{3A} S_{b3} \quad \text{Equation 3}$$

$$M_{bB} = P_{1B} S_{b1} + P_{2B} S_{b2} + P_{3B} S_{b3}$$

$$M_{bC} = P_{1C} S_{b1} + P_{2C} S_{b2} + P_{3C} S_{b3}$$

Where:

M_{bA} = the pixel value for band b at point A,

P_{jA} = the fractional area (percentage) of the jth land-cover type at point A,
and

S_{bj} = the pure signature value of the jth land-cover type for band b.

If the percentages for more than three pixels are known, the pure signature values for band b can be solved using the method of least squares. This can be performed for each of the six bands in the image to calculate the pure signatures of the three land-cover types. Alternatively, pure spectrum signature data are also available for various materials from data reference libraries provided by the U.S. Geological Survey (USGS) and other agencies. However, a spectral library of all plant species and soil types at Fort Bliss was not available.

Next, by solving Equation 3 by sampling a number of TM pixels, the pure signatures for the three land-cover types are known. What is unknown is the percentage cover, P_j , of each of the three land-cover types for every remaining pixel in the image, or for each remaining pixel that you wish to extrapolate cover estimates. For each remaining pixel in the image, Equation 1 is written for each of the six bands. This provides six equations to solve for the three unknowns; P_1 , P_2 and P_3 for each pixel. The equations are:

$$M_1 = P_1 S_{11} + P_2 S_{12} + P_3 S_{13} \quad \text{Equation 4}$$

$$M_2 = P_1 S_{21} + P_2 S_{22} + P_3 S_{23}$$

$$M_3 = P_1 S_{31} + P_2 S_{32} + P_3 S_{33}$$

$$M_4 = P_1 S_{41} + P_2 S_{42} + P_3 S_{43}$$

$$M_5 = P_1 S_{51} + P_2 S_{52} + P_3 S_{53}$$

$$M_6 = P_1 S_{61} + P_2 S_{62} + P_3 S_{63}$$

Where:

M_i = the pixel value for the i^{th} band,

P_j = the fractional area (percentage) for the j^{th} land-cover type, and

S_{ij} = the pure signature value of the j^{th} land-cover type for the i^{th} band.

The solution can be performed by the method of least squares. These equations can be written more compactly in matrix form as shown in Equation 5.

$$\mathbf{M} = \mathbf{S} \mathbf{P}$$

Equation 5

Where:

\mathbf{M} = the vector of mixed pixels,

\mathbf{S} = the matrix of pure spectra where the j^{th} column is the pure spectrum of the j^{th} land-cover type, and

\mathbf{P} = the vector of unknown fractional areas (percentages).

This is the mathematical model of linear spectral demixing. Solving for the vector \mathbf{P} is the “demixing” calculation implied by the method’s name.

Finally, note that the row dimension of \mathbf{S} is equal to the number of bands and the column dimension is equal to the number of land-cover types (the number of pure spectra). Thus, the number of bands sets the upper limit on the number of land-cover types that can be modeled with this method. Attempting to model the terrain with more pure signatures would lead to an undetermined set of equations. Of course, this assumes that the pure spectra are unique. Nonuniqueness of the pure spectra would also reduce the dimensionality of the system of equations, making a solution difficult to obtain.

For each pixel of the input image, Equation 5 can be solved for percent cover for each of the three land-cover types, thereby creating an image of percent cover or abundance. Each band of this imagery is a percent coverage classification of a particular land-cover type. Since the percentages range from 0 to 100, an 8-bit per pixel grayscale image can be used to store the results. As one moves the cursor across the image, the pixel value at each point represents the percentage cover or abundance of the land type associated with that image. Also, the images can be summed to see if Equation 2 holds as an indication of the accuracy of the linear mixing of pure spectra used to model the terrain.

The algorithm used to find a least squares solution in this research was Singular Value Decomposition (Press et al. 1992). Singular Value Decomposition is very stable and was appropriate for finding a least squares solution to an overdetermined set of linear equations. This algorithm is not necessarily the fastest, but it can handle both overdetermined and underdetermined systems of equations with equal ease. The singular values calculated by the algorithm indicate whether or not the system of equations has a full rank. In the case of linear spectral demixing it indicates that one of the spectra in matrix *S* of Equation 5 is not unique.

Example Implementation of Spectral Demixing

An example of the complete spectral demixing process was accomplished using photo 381_158 of Study Site #1 (Coppice Dunes Maneuver Areas). In this example, five land-cover types were classified from the CIR photograph and used to model the landscape: honey mesquite, mesquite/dune edge/shadow/litter, two interdunal vegetation cover types, and bare soil.

A 30-m by 30-m grid was superimposed on top of the five-class map derived from the unsupervised classification of the photograph. Each grid element represented the spatial extent of a single TM pixel (30 m by 30 m = 900 m²). At 1-m resolution in the CIR photographs, 900 CIR photo pixels cover the same area as 1 TM pixel. A simple geographic information system (GIS) program (AIRCOVER) was written to summarize the percent cover of each land-cover component in the CIR photo map that falls within each individual TM pixel. The resulting output from this program is a five-band GIS data file, with each band representing the fractional percentage of a single land-cover type. As one moves the cursor across a single band of the image, the pixel value at each point represents the percentage cover or abundance of the specific land-cover type associated with that band of the image. The abundance or percent cover value of the pixel represents the percent cover of that particular land-cover type that exists within the footprint of a single TM pixel, which in this case is 30 m by 30 m. If only two land-cover types were classified, as was the case for most of the demixing analysis in this investigation, then a two-band output image was created. The pixel values in the resulting output image are the fractional area or percentages, *P* in Equation 1. This output image is hereafter referred to as the AIRCOVER image. The AIRCOVER images served as the reference or ground truth of percent covers for both spectral demixing and spectral index correlation analysis.

Next, both the AIRCOVER output (in this example, five bands) and the matching TM subset (six bands) were input into a sampling program called TRAINDAT.

Approximately 500 pixels were randomly sampled from each photograph. The analyst can specify the number of samples. For each band of TM imagery, 500 paired observations of the mixed TM signature (M in Equation 3) were extracted from the TM image, and the fractional percent covers for each land-cover component (P in Equation 3) were extracted from the AIRCOVER file. This sampling was repeated for each spectral band of TM imagery resulting in six sets of equations like Equation 3, with each equation set containing 500 equations—1 for each pixel sampled. The TRAINDAT program outputs tabular ASCII data. Tabular data for each of the six sets of equations was then formatted for input into the MINITAB statistical package. Using 500 samples for each set of equations or spectral band, a singular value decomposition method of least squares was used to solve for the pure signature values (P in Equation 3) for each land-cover type. Each set of equations solves for the respective pure signature values for each land-cover type in a different spectral band.

Finally, for each remaining pixel in the image, the mixed pixel response for each of six TM bands and the pure spectrum for each land-cover type were input into a DEMIX program. DEMIX solves Equation 4 for P , thus providing an estimate of the fractional percent cover of each individual land-cover type within each TM pixel. DEMIX outputs a separate band corresponding to fractional percent covers of each land-cover type. In this example, DEMIX produced five bands corresponding to the five land-cover types.

The above procedure was repeated for each individual CIR photo-TM image pair. In addition, the above procedure was repeated for each recode of the original five-class unsupervised classification for each photograph.

Demixing Evaluation and Accuracy Assessment

An evaluation of demixing performance was conducted on a photo-by-photo basis, including all possible recode combinations tested. Performance was evaluated based on how closely the demixing estimates of fractional cover by land-cover type matched the reference fractional cover estimates derived directly from the classified aerial photography. This was accomplished by subtracting each band of the reference AIRCOVER image from each corresponding band of the demixing output on a pixel-by-pixel basis.

Descriptive statistics such as mean and standard deviation (SD) of each difference image were used to evaluate demixing performance. A mean difference of 0 between the estimated and reference cover would indicate that the demixing procedures accurately predicted the fractional percent covers of land-cover categories. The standard deviation provided some indication of the variance in these

estimates. However, it was recognized that these descriptive statistics may not have provided a suitable method for evaluating accuracy, because demixing could potentially overestimate cover in some areas, while underestimating cover in other areas. These types of errors may have canceled each other out; therefore, the mean difference may still have been relatively low.

An additional descriptive statistic used to compare the estimated versus the reference fractional percent land-cover values for each photograph was the sum of absolute difference between estimated and reference cover values on a pixel-by-pixel basis. By computing absolute differences, the possibility of a mean difference equaling 0 resulting from an equal number of overestimations and underestimations of cover was eliminated. By tabulating the absolute difference the amount by which estimates of cover overestimate or underestimate reference cover values are summed, providing a more robust evaluation of demixing accuracy.

Inferential statistics were also calculated to compare estimated vegetative cover amounts derived from demixing with reference vegetative cover amounts. These statistics included a paired Students T-test (t-value), probability value (P), and a 95% confidence interval for the mean difference between the estimated and the reference abundance amounts. The t-value and P were used to evaluate the null hypothesis that the mean difference between the estimated percent covers from demixing analysis and the reference percent cover values from air photo classifications was equal to 0 at $\alpha = .05$, or 95% confidence. The 95% confidence interval indicates that for any paired sample for any given pixel, the mean difference between the demixing estimates of cover and the reference cover values will fall within this interval with 95% confidence. Again, the reference image was always subtracted from the estimated image. Therefore, positive confidence intervals indicated that demixing consistently overestimated cover, intervals straddling zero indicated that differences were close to zero, and negative intervals indicated that demixing consistently underestimated cover. The same null hypothesis was tested to evaluate all demixing and spectral index correlation estimates of cover in this research.

Spatial Extrapolation of Demixing Results

A final evaluation of demixing results was to evaluate demixing capabilities for spatially extrapolating the fractional land-cover percentage estimate to areas beyond the photo footprint locations that were used to parameterize the demixing model. Extrapolation capabilities were tested at each study site. For each site, three of the four photographs were randomly chosen to parameterize the demixing model. The remaining TM subset, which matched the fourth CIR foot-

print, was then demixed from the other three photo/TM subset pairs. Demixing procedures using three photographs were conducted in the same manner as demixing of a single TM/photograph pair described above. The only variation was that paired samples of mixed TM pixel values and fractional land-cover percent coverages from the classified CIR photograph were taken from three photographs instead of one. Instead of random sampling 500 pixels in one photograph, 1500 random samples were collected across three photographs. These 1500 samples were then used to solve for pure spectra values, P in Equation 3. These same P values, along with TM mixed spectra values (M) for the remaining TM subset to be demixed were input to Equation 4 to solve for the fractional percent coverage of each land-cover component, whether it be two cover types or five, within each TM pixel.

Spectral Index Correlation Analysis

Correlations between various spectral brightness and greenness indices and percent cover were evaluated using exploratory regression analysis as an alternative for estimating and extrapolating groundcover estimates using coarse resolution TM imagery. The same CIR photo/TM subset pairs that were used for demixing analysis were also used for correlation analysis. The same 5 class unsupervised classifications of the CIR photographs were used, including the various recodes of the classifications, resulting in a number of 2 class images depicting cover versus bare ground (See Table 2, page 24).

In addition, the same fractional land-cover percent coverages from classified CIR photographs that fall within a single TM pixel were also used as reference cover amounts. These values were extracted from the classified CIR photographs using AIRCOVER, as described earlier. However, rather than using fractional covers and mixed TM pixel values as input into Equation 3 to conduct demixing, the TM subsets were first processed to produce a number of spectral brightness/greenness indices. These indices were then used as independent variables and correlated with fractional cover percentages (the dependent variable) using least squares linear regression.

Spectral Indices

A total of seven greenness or vegetation indices, and two brightness indices were calculated for each of the 12 TM subsets and evaluated as dependent variables for predicting fractional covers. In addition, each of the TM spectral bands, with the exception of Band 6, was also evaluated as a dependent variable.

As described earlier, greenness indices are designed to measure the amount of photosynthetically active vegetation. They are not well suited for arid environments such as Fort Bliss where vegetation is sparse and background soil dominates the spectral response. Brightness indices are better suited for arid environments, as they are designed to measure the total reflectivity of the Earth's surface. Therefore, the amount of vegetation present, which acts to mask the reflectivity of background soils, is usually inversely related to brightness index values. Although brightness indices were expected to provide better estimations of cover, the process of evaluating a number of different greenness and brightness indices did not require substantial additional effort. Therefore, all nine indices (seven greenness and two brightness) were evaluated as potential surrogate measures of vegetative cover. The vegetation or greenness indices calculated were: NIR/Red, SQRT (NIR/Red), the Vegetation Index (IR-R), the Normalized Difference Vegetation Index, the Transformed Normalized Vegetation Index (TNDVI), the Modified Soil Adjusted Vegetation Index, and the Kauth-Thomas or Tassled Cap Greenness Index (KTG). The brightness indices calculated were albedo or reflectance over all visible and near infrared bands, in-band albedo or reflectance of individual TM bands, and the Kauth-Thomas or Tassled Cap Soil Brightness Index (KTB). All processing was done using ERDAS Imagine. A graphical model in Imagine was used to calculate the indices as described below. A more complete explanation of these indices is included in Chapter 2 Background, page 6.

Greenness Indices

- NIR/Red

$$\frac{NIR}{Red}$$

Equation 6

- SQRT (NIR/Red)

$$\sqrt{\frac{NIR}{Red}}$$

Equation 7

- NIR-Red

$$NIR - Red$$

Equation 8

- NDVI

$$\frac{NIR - Red}{NIR + Red}$$

Equation 9

- TNDVI

$$\sqrt{\frac{NIR - Red}{NIR + Red} + 0.05}$$

Equation 10

- MSAVI

$$\frac{2NIR + 1 - \sqrt{(2NIR + 1)^2 - 8(NIR - RED)}}{2}$$

Equation 11

- Kauth-Thomas Tasseled Cap Greenness Vegetation Index

$$KTG = (-0.273)(TM1) - (.217)(TM2) - (.551)(TM3) + (.722)(TM4) + (.073)(TM5) - (0.165)(TM7)$$

Equation 12

Brightness Indices

- Kauth-Thomas “Tassled Cap” Brightness Index (KTB)

$$KTB = (.291)(TM1) + (.249)(TM2) + (.481)(TM3) + (.557)(TM4) + (.444)(TM5) + (.171)(TM7)$$

Equation 13

- Albedo

Prior to calculation of albedo or reflectance, digital numbers were converted to spectral band radiance for TM imagery using (Markham and Barker 1986):

$$L_{\lambda} = \frac{L_{\min \lambda} + [L_{\max \lambda} - L_{\min \lambda}] DN}{D_{\max}}$$

Equation 14

Where:

L_{\min} = spectral radiance of each band at DN = 0 in $mWcm^{-2}Sr^{-1}:m^{-1}$,

L_{\max} = spectral radiance of each band at DN=255 in $\text{mWcm}^{-2}\text{Sr}^{-1}:\text{m}^{-1}$,
 D_{\max} = range of rescaled radiance in DN, and
 DN = input digital number.

Once spectral radiance was calculated according to Equation 14, albedo was calculated as the ratio of reflected solar radiation to incoming solar irradiance:

$$\rho = \frac{\pi L_{\lambda} d^2}{E_{\lambda} \cos \theta} \quad \text{Equation 15}$$

Where:

L_{λ} = spectral radiance in $\text{mWcm}^{-2}\text{Sr}^{-1}:\text{m}^{-1}$ (from Equation 14)
 d = earth-sun distance in astronomical units,
 E_{λ} = exoatmospheric spectral irradiance at the top of the atmosphere in $\text{mWcm}^{-2}:\text{m}^{-1}$, and
 θ = solar zenith angle.

Radiance is derived from Equation 14. Exoatmospheric spectral irradiances at the top of the atmosphere are estimates derived from Markham and Barker (1986). Correcting exoatmospheric solar irradiance in the denominator by $\cos \theta$ normalizes the scene to an overhead or nadir sun angle and accounts for differences in solar irradiance for the time of day and day of the year (Robinove 1982; Hughes and Henderson-Sellers 1982).

Total reflectance or planetary albedo was calculated by integrating spectral radiance and irradiances across all of the visible and near and middle infrared bands. Planetary albedo for TM imagery was integrated across Bands 1 through 5 and 7. In-band planetary albedo or reflectance for individual bands was calculated in the same manner as total reflectance or planetary albedo (Equation 15). However, reflectances were calculated using only radiance and irradiances in each respective wavelength of that particular TM band.

For each TM subset that matched a CIR photo footprint, a separate GIS data layer was created for each of the nine indices calculated and each of the six individual TM bands, for a total of 15 GIS layers. These 15 layers were stacked into a single GIS data layer for sampling. Similar to the demixing analysis, the TRAINDAT program was used to randomly sample paired observations of a spectral index value from 1 band of the 15-band stack and spatially corresponding fractional covers of each land-cover component as extracted from the classified CIR photographs using AIRCOVER. For each photograph in each study

site, 500 paired observations were sampled for each of the 15 possible independent variables to be tested.

The paired observations were then input into the MINITAB statistical package. A least squares linear regression was performed between each individual index or TM band (independent variable) and each land-cover category, including recodes of the original five-class unsupervised classifications. For classifications involving only two classes (cover and bare ground), only the cover class was evaluated as a dependent variable because the bare ground class was equal to $[100 - \text{cover}]$ and would simply have an inverse correlation.

Spectral Index Correlation Evaluation and Accuracy Assessment

The linear relationship between each independent variable and each fractional land-cover was evaluated based on adjusted R^2 values, or coefficients of determination. All possible correlations between indices or individual TM spectral bands and fractional land-cover percent cover values were evaluated for each photograph at all three study sites.

The regression formula produced by MINITAB for each correlation between the TM/spectral indices and cover estimates was then applied to each pixel in the respective spectral index image or individual TM band to derive a fractional percent cover estimate for each pixel in the image. The process was repeated for each land-cover component, resulting in a separate estimated cover image for each land-cover type present.

Similar to the evaluation of demixing performance, each reference image of fractional covers extracted from the classified CIR photographs was subtracted from the corresponding estimated fractional cover derived from the regression equations. Mean and SD of the difference images, as well as statistical T-tests and absolute differences were tabulated in the same manner as they were for evaluations of demixing performance.

Spatial Extrapolation of Spectral Index Correlation Results

Similar to the demixing analysis, the final evaluation of spectral index correlation analysis results was to evaluate the capability of the correlation to extrapolate fractional percent cover estimates to geographic areas beyond the photo footprints that were sampled to develop the regression equations.

Rather than sampling paired observations of the index values and corresponding fractional covers on a photo-by-photo basis, paired samples were taken from

three of the four photographs for each study site. These samples were then used to develop a regression formula for estimating fractional percent covers for the fourth photograph using the respective index or spectral band for the TM subset that matched the fourth photograph. Again, similar to photo-by-photo evaluations, the mean, SD, T-test, and absolute differences were compiled by differencing the reference cover values derived from the classification of the fourth CIR photograph from the extrapolated cover estimates for the area of the fourth photograph.

Summary of Methodology

Descriptive statistics such as mean difference, standard deviation of mean difference, and sum of absolute difference between estimates of abundance and reference abundance were used to evaluate the accuracy of vegetation abundance estimates. Reference abundance amounts were derived from high-resolution CIR photographs. Estimates of abundance were either extracted from coarse resolution TM imagery using spectral demixing or were derived from spectral index correlation models. Inferential statistics were also used to evaluate the predictive ability of these models to estimate and extrapolate cover estimates derived from coarse resolution satellite imagery.

Inferential statistics were based on random samples of results. However, because remotely sensed imagery provides a complete census of a population, sampling and inferential statistics were not necessary; automated analysis of imagery offers the ability to rapidly compile descriptive statistics of entire populations of image pixels in a rapid and cost effective manner. Inferential statistics such as the Student's T-test were useful for understanding the predictive capabilities of demixing and spectral index correlation analysis for estimating and extrapolating percent groundcover estimates. However, the sums of absolute differences between estimated and reference cover percentages were ultimately used to identify the best performing models. The same descriptive statistics were also useful for identifying the reclassification or recode of spectral categories into cover vs. bare ground, which resulted in the most accurate estimates of abundance of cover and bare ground.

The same statistics were compiled for four CIR photographs and matching TM subsets for each of the three sites, resulting in a total of 12 photograph samples. The sum of absolute differences was evaluated for each individual photograph, for all four photographs for an individual site, and for extrapolated estimated derived from sampling three of four photographs for a site.

5 Results

Spectral Demixing

Demixing analysis produced a separate GIS data layer for each land-cover component that was demixed from TM pixels. The pixel values in each individual data layer represented abundance or percent cover estimates for that respective land-cover type. Therefore, demixing results were evaluated in two ways. First, individual GIS data layers of predicted abundance were visually compared with reference images of abundance for each land-cover type to assess similarity in the spatial distribution of abundance. Second, because the pixel values in the demixing and reference images were actual estimates of percent cover, inferential and descriptive statistics were also used to quantify and evaluate the accuracy of percent cover estimates derived from spectral demixing analysis.

Five-class Results

Using photo 381_158 from Site #1 (Coppice Dunes Maneuver Areas) as an example, the resulting images created from demixing five separate land-cover classes and their corresponding reference images are displayed in Figure 10.

Images in Figure 10 represent increasing vegetative cover with increasing pixel brightness for each respective land-cover type. For example, a bright pixel in Category #1 (Honey Mesquite) indicates a large abundance of mesquite cover, while a dark pixel in this same category represents a low abundance of mesquite. The column of images on the left depicts abundance estimates derived from spectral demixing for five land-cover types. The column of images on the right depicts reference abundance values derived from unsupervised classifications of CIR photographs for the same land-cover types. Ideally, the spatial patterns of estimated abundance from spectral demixing should appear similar to the corresponding reference images of abundance for each respective land-cover type. However, visual inspection of the photographs indicates that spectral demixing was not able to predict fractional land-cover percentages for five land-cover types, as there was very little similarity between estimates of abundance and reference images of abundance. For land-cover Category #1 (Honey Mesquite), the only slight similarity in abundance patterns was for circular area of

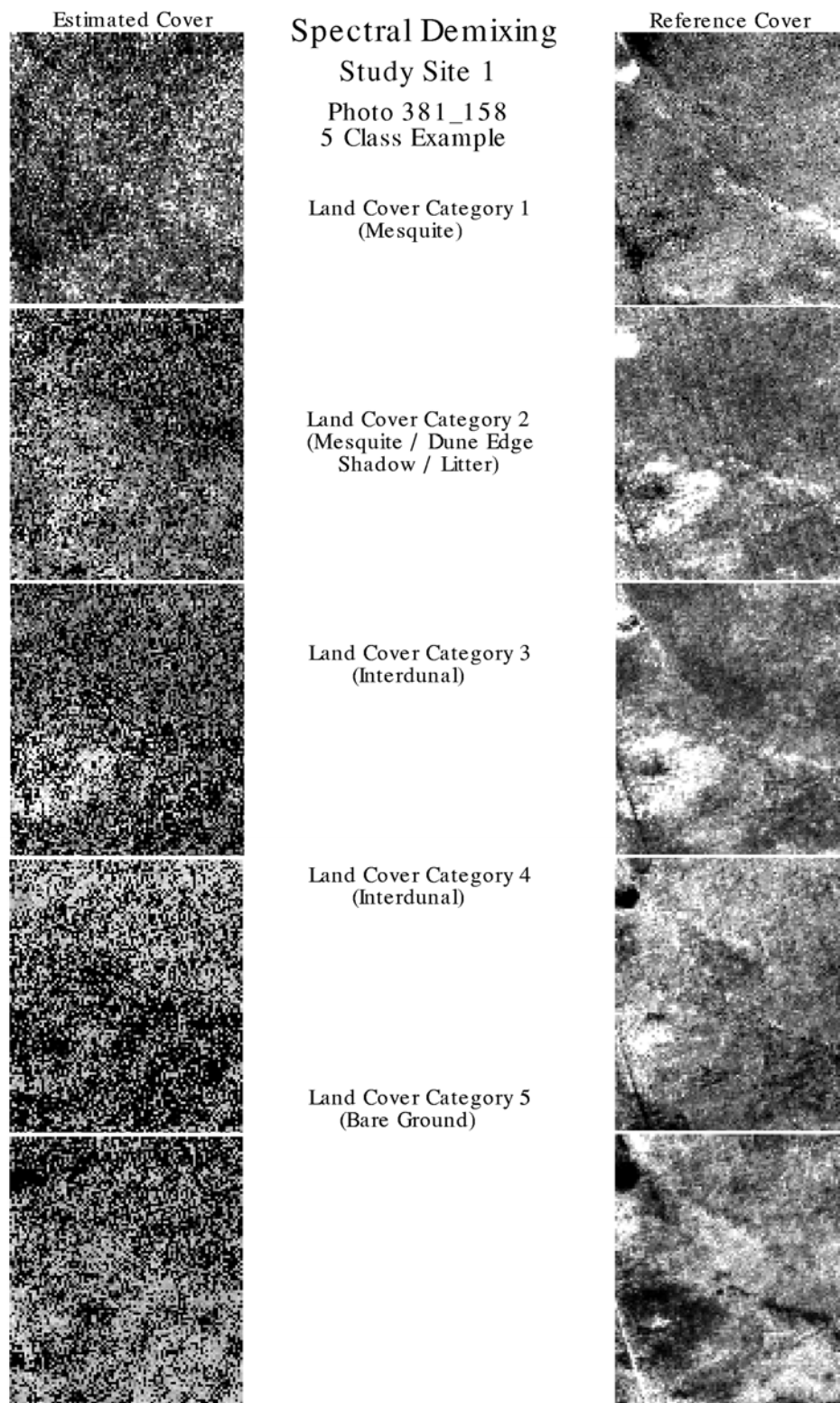


Figure 10. Demixing results for five land-cover categories for photo 381_158 (left column is the demixing estimate of abundance for each category, right column is the reference abundance for each category).

relatively low abundance of honey mesquite in the lower southwest quadrant of the image. The demixing image did not capture the high amount of honey mesquite cover in the extreme northwest corner of the image and along a linear feature extending from approximately the center of the image to the southeast. The reference image of Category #2 (Mesquite/Dune Edge/Shadow/Litter) indicated a relatively high amount of cover in the southwest quadrant and in an isolated area in the extreme northwestern corner of the image. Demixing estimates for the same land-cover class indicated only a slightly higher abundance in the southwest quadrant and no increase in abundance in the northwest corner. In addition, the distinct patterns of high cover in the reference image were not evident in the estimated image. Estimates of land-cover Category #3 (Interdunal Cover) appeared to detect a higher abundance in the southwest quadrant of the image, but again, the distinct patterns found in the reference image were not discernable in the estimated image. Estimates of land-cover Category #4 (Interdunal Cover) did appear to estimate a slightly higher abundance in the northern half of the image, but none of the observed patterns in the reference image appear in the estimated image. Estimates of land-cover Category #5 (Bare Ground) did not depict a road in the southwestern corner of the image, which was clearly evident in the reference image, and did not appear to capture of the patterns that were evident in the reference image.

In addition to visual inspection, a number of metrics, including results from statistical analysis, also were used to evaluate performance of spectral demixing. The mean and standard deviation of abundance of land-cover types derived from reference classifications of the CIR photographs were compared to mean and standard deviations of estimated abundance of land-cover types resulting from spectral demixing for each land-cover category.

Table 3 summarizes mean abundance for each land-cover category in both the reference image and the estimate image derived from demixing analysis. Estimated mean abundances derived from demixing analysis were similar to means derived from reference images for land-cover Categories 2 and 3, but differences were considerably higher for Categories 1, 4, and 5. The largest difference for any land-cover type was approximately 10 percent for Honey Mesquite, Category #1. The estimated proportional cover for each land-cover type was similar to the proportional cover in the reference image. Demixing overestimated abundance for Categories 4 and 5 and underestimated cover for Categories 1, 2, and 3. Reference cover amounts indicated 24.31 percent cover of Category #1 (Honey Mesquite) and 26.41 percent cover of Category #5 (Bare Ground), while demixing estimated 14.12 percent Honey Mesquite cover and 35.32 percent bare ground. Standard deviations for demixing estimates of abundance were considerably higher than standard deviations in the reference image.

Table 3. Mean and standard deviation of abundance (percent cover) for five land-cover categories for photo 381-158, Study Site #1; estimated (demixing) versus reference.

Photo 381_158	ESTIMATED		REFERENCE	
CATEGORY	Mean	SD	Mean	SD
Mesquite	14.118	11.483	24.307	7.530
Mesquite/ Dune Edge/ Shadow/Litter	8.832	7.806	11.482	4.192
Interdunal	9.938	10.345	13.393	5.488
Interdunal	30.206	33.052	24.403	8.255
Bare Ground	35.322	32.787	26.412	12.927
Totals	98.416		99.997	

Statistical comparisons between the estimated vegetative cover amounts derived from demixing and the reference vegetative cover amounts are presented in Table 4 and include a paired Student's T-test statistic (t-value), probability value (P), and a 95% confidence interval (CI) for the mean difference between estimated and reference abundance amounts. The t-value and P were used to evaluate the null hypothesis that the mean difference between the estimated percent covers from demixing analysis and the reference percent cover values from air photo classifications were equal to zero at $\alpha = .05$, or 95% confidence. The 95% confidence interval indicates that for any paired sample for any given pixel, the mean difference between the demixing estimates of cover and the reference cover values will fall within this interval with 95% confidence. Again, the reference image was always subtracted from the estimated image. Therefore, positive confidence intervals would indicate that demixing consistently overestimated cover, intervals straddling zero would indicate that differences were close to zero, and negative intervals would indicate that demixing consistently underestimated cover. The same null hypothesis was tested for assessing all demixing spectral index correlation estimates of cover in this research.

Table 4. Descriptive and inferential statistics of difference image for five land-cover categories for photo 381_158, Study Site #1; estimated (demixing) minus reference.

Photo 381_158	t-value	P	CI	abs. diff.	Mean	SD
Mesquite (1)	-88.04	0.0000	-10.416, -9.962	138156	-10.189	11.885
mesquite/ dune edge/ shadow/litter (2)	-32.60	0.0000	-2.8100, -2.4911	76106	-2.6505	8.3490
interdunal (3)	-33.24	0.0000	-3.658, -3.251	100835	-3.454	10.673
interdunal (4)	17.81	0.0000	5.164, 6.441	321597	5.803	33.448
bare ground (5)	27.46	0.0000	8.274, 9.546	322962	8.910	5.803

The null hypothesis was rejected for all five cover types for photo 381_158 at a 95% level of confidence ($P < .05$). In addition, the mean difference and the standard deviation of the difference between paired samples of estimated percent cover, as derived from demixing, and the reference percent cover derived from air photo classifications were calculated for each pixel in the image and are also included in Table 4. Mean differences between estimated (demixing) and reference cover amounts ranged from -10.189 for Category #1 (Honey Mesquite) to 8.910 for Category #5 (Bare Ground). Similar to the calculation of confidence intervals, reference cover amounts were always subtracted from predicted cover amounts throughout this research. Therefore, positive mean differences indicated that the estimated cover amounts overestimated cover, while negative mean differences indicated that the estimated cover amounts underestimated cover. For photo 381_158, demixing underestimated cover for Category #1 (Honey Mesquite), Category #2 (Honey Mesquite/Dune Edge/Litter/Shadow), and Category #3 (Interdunal Cover), and overestimated cover for Category #4 (Interdunal Cover) and Category #5 (Bare Ground). The variance in mean difference was also quite high for all cover classes.

Again, although these differences provide a relative measure of demixing performance, they do not account for the cancellation effect of both overestimation and underestimation of vegetative cover. For example, demixing may have overestimated cover for a number of pixels, and also underestimated cover for a number of pixels. If the amounts of overestimation and underestimation were relatively equal for a relatively equal number of pixels, the resulting mean difference may be close to zero. Because demixing results were evaluated based on how well they predicted reference groundcover estimates, a mean difference close to zero for a specific land-cover category may have lead to a misleading interpretation of performance. In this example, because demixing significantly underestimated and overestimated cover for a number of pixels, the predictive capability of the demixing model may not have been as great as the mean difference would have indicated. Therefore, a sum of absolute differences between the estimates of cover from demixing and the reference cover values was also

compiled for comparison. Based on the sum of absolute differences, demixing performed best for Category #2 and Category #3 in photo 381_158, as indicated by their lower sums of absolute difference.

Both a visual inspection of demixing results and a quantitative analysis confirmed the relatively poor results when demixing five land-cover classes. The same analysis was performed for all photographs using five land-cover classes with similar results. Demixing appeared to estimate abundance accurately for individual land-cover categories in different sample photographs, but was not able to accurately estimate abundance of five land-cover types within any single photograph.

Three-class Results

Due to the inability to accurately estimate abundance of the five separate land-cover types, a number of different recodes of the original five classes were also analyzed. Specific to the Coppice Dunes Maneuver Areas of Study Site #1, one of the primary goals of this research was to quantify the abundance of interdunal vegetation, which would be a good indicator of impacts due to military training. Therefore, a three-class unsupervised classification was applied to identify three land-cover types: Honey Mesquite, Interdunal Vegetation, and Bare Ground. Spectral demixing was then used to estimate abundance of these three cover types.

Again, using photo 381_158 as an example, Figure 11 contrasts the results of demixing estimates of abundance with reference images of abundance for three land-cover types. In contrast to the five-class results, visual inspection of three-class demixing results indicated considerable improvement. For land-cover Category #1 (Honey Mesquite), abundance patterns were similar in the estimated and reference images, including a circular area of relatively high abundance of honey mesquite in the upper northwest corner of the image and also extending from approximately the center of the image to the southeast. The estimated image also captured the road in the southwest corner of the image. The reference image of Category #2 (Interdunal) indicated a relatively high amount of cover in the southwest quadrant and in an isolated area in the extreme northwestern corner of the image. Demixing estimates for the same land-cover class did capture a higher abundance in the southwest quadrant, although the patterns were slightly different, and failed to delineate the area of high abundance in the northwest corner. Estimates of land-cover Category #3 (Bare Ground) appeared to correspond well with the reference image, as both indicate a relatively low abundance of bare ground in the northwest corner and southwest quadrant of the image, as well as a high abundance of bare ground along a road in the southwest corner of the image.

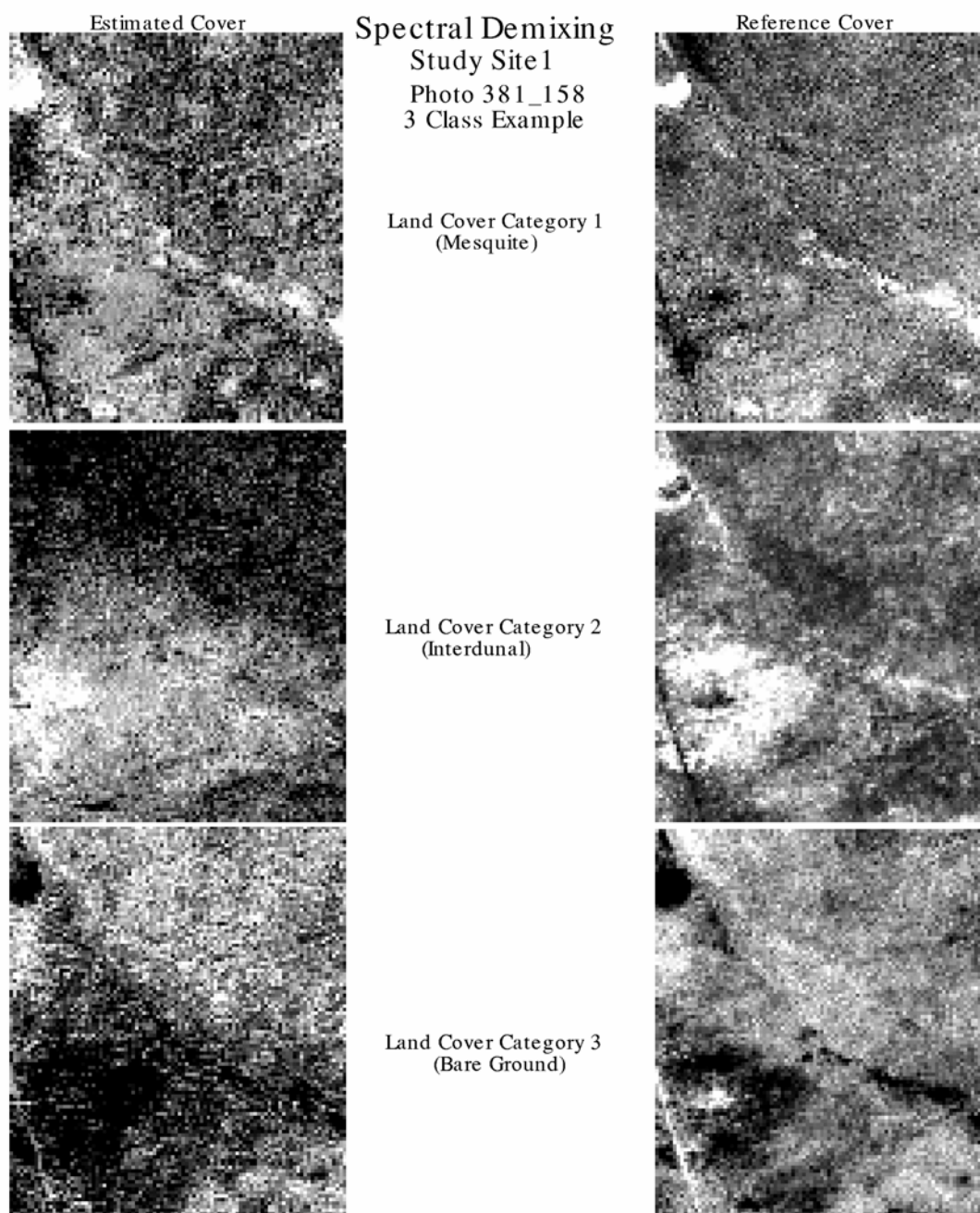


Figure 11. Demixing results for three land-cover categories for photo 381_158 (left column is the demixing estimate of abundance for each category, right column is the reference abundance for each category).

Table 5 lists the mean and standard deviation for both the reference images and demixing estimates for three land-cover types. Similar to the five-class breakout, demixing estimates of mean abundance were similar to mean reference amounts. Demixing appeared to slightly overestimate Category #1 (Honey Mesquite) and slightly underestimate Category #2 (Interdunal Cover) and Category #3 (Bare Ground). In general, the estimated abundance was much closer to the reference abundance for the three land-cover classes as opposed to five, with the

largest difference between estimated and reference cover being 4 percent for Category #1 (Honey Mesquite). However, standard deviations for estimates derived from demixing were still much higher than standard deviations of abundance in the reference images.

Table 5. Mean and standard deviation of abundance for three land-cover categories for photo 381_158, Study Site #1; estimated (demixing) versus reference.

CATEGORY	ESTIMATED		REFERENCE	
	Mean	SD	Mean	SD
mesquite (1)	34.535	20.388	30.590	8.162
interdunal (2)	24.528	20.133	26.594	9.653
bare ground (3)	39.780	29.614	42.818	12.879
Totals	98.843		100.002	

Table 6 summarizes the inferential and descriptive statistics for the difference between estimated and reference cover for three land-cover classes for photo 381_158. Although the null hypothesis that differences were equal to zero was rejected for each land-cover type, the relatively low mean differences and smaller confidence intervals indicated that demixing estimates improved when only three land-cover classes were identified, as opposed to five. Visual inspections of the spatial patterns for three-class estimates confirmed these results. However, variance in estimated cover derived from demixing was still considerably higher than what was found in the reference images.

After evaluating all five-class and three-class recodes for all photographs at each of the three sites, it was determined that spectral demixing was not able to accurately predict fractional land-cover percentages of specific land-cover types identified through field observations at Fort Bliss. Therefore, five-class and three-class recodes were eliminated from further analysis. Demixing analysis was focused on estimating the abundance of cover and bare ground by analyzing only those classifications and recodes containing two classes (Cover and Bare Ground).

Table 6. Descriptive and inferential statistics of difference image for three land-cover categories for photo 381_158, Study Site #1; estimated (demixing) minus reference.

Category	t-value	P	CI	abs. diff.	Mean	SD
mesquite (1)	21.76	0.0000	3.588, 4.299	165442	3.943	18.610
interdunal (2)	-10.84	0.0000	-2.439, -1.692	170479	-2.066	19.570
bare ground (3)	-12.29	0.0000	-3.521, -2.552	224513	-3.036	25.371

Two-class Results

Study Site #1 - Coppice Dunes Maneuver Areas

Four different recodes of an original five-class unsupervised classification were evaluated for the power to distinguish between cover and bare ground using demixing analysis. Each recode represented a slightly different grouping of categories (see Table 2, page 24). Field verification of land-cover categories for each spectral class was not possible because archival CIR photography from October and November 1994 was used. However, field reconnaissance was able to clearly identify Category #1 as Honey Mesquite and Category #5 as Bare Ground. Spectral categories 2 through 4 could not be associated with a specific and unique cover type. Therefore, different recodes were tested by grouping these uncertain categories into both Cover and Bare Ground categories. A fifth grouping of land-cover types based on a two-class unsupervised classification was also evaluated. A total of five slightly different binary maps depicting Cover vs. Bare Ground were tested for each photograph in this analysis.

Table 7 lists the mean percentage or abundance of the Cover category resulting from each of the different recodes and the two-class unsupervised classification (ISO2). The mean percentage or abundance of Bare Ground is not included Table 7, but is equal to $100\% - \text{Cover}\%$. As expected, as additional land-cover categories are placed in the Cover category, the mean for both the estimated and the reference cover also increase. In all cases, estimates of cover are very similar to reference amounts, with the largest difference occurring for Recode 14_5, at approximately 3 percent. However, the variance in cover estimates was significantly higher than the variance found in the reference images.

Table 8 lists the inferential and descriptive statistics for the differences between demixing-derived estimates and reference abundance for these five recodes for photo 381_158. The null hypothesis was rejected for all five of the recode/classifications. However, all recodes appeared to estimate the abundance of vegetative cover with some degree of accuracy, as indicated by the relatively low mean differences. Both the ISO2 classification and the 12_35 recode underestimated bare ground by less than 1 percent, on average. The largest mean difference resulted from the 14_5 recode, at -2.82 percent. The two-class unsupervised classification (ISO2) appeared to be the best performer, with absolute differences of 141003 (Cover) and 140716 (Bare Ground). On average, this classification underestimated Cover by 1.5 percent and overestimated Bare Ground by 0.71 percent. These results were considerably better than the five-class and three-class break-outs evaluated earlier. This indicates that a simple two-class unsupervised classification would provide the most accurate estimates of Cover versus Bare Ground for photo 381_158.

Table 7. Mean and standard deviation of cover abundance for photo 381_158, Study Site #1, derived from ISO2 and four recodes; estimated (demixing) versus reference.

	Estimated		Reference	
Recode	Mean	SD	Mean	SD
ISO2	36.974	19.347	38.480	9.751
1_25	25.589	22.036	24.307	7.530
12_35	34.458	21.130	35.716	9.158
13_45	47.261	21.372	49.178	11.874
14_5	70.772	20.338	73.588	12.927

Table 8. Descriptive and inferential statistics of difference image (estimated [demixing] minus reference) for two land-cover categories for photo 381_158, Study Site #1 using ISO2 and four recodes.

381_158	Recode	t-value	P	CI	abs. diff.	Mean	SD
Cover	ISO2	-9.39	0.0000	-1.857, -1.215	141003	-1.536	16.97
Bare Ground	ISO2	4.16	0.0000	0.374, 1.042	140716	0.708	17.490
Cover	1_25	6.27	0.0000	0.861, 1.643	175986	1.252	20.500
Bare Ground	1_25	-9.28	0.0000	-2.325, -1.514	177742	-1.920	21.240
Cover	12_35	-7.00	0.0000	-1.687, -0.949	164568	-1.318	19.326
Bare Ground	12_35	2.47	0.014	0.096, 0.837	164338	0.466	19.401
Cover	13_45	-10.92	0.0000	-2.263, -1.574	151545	-1.918	18.040
Bare Ground	13_45	5.97	0.0000	0.704, 1.393	150816	1.049	18.042
Cover	14_5	-15.34	0.0000	-3.175, -2.456	158866	-2.815	18.841
Bare Ground	14_5	11.22	0.0000	1.689, 2.404	157418	2.047	18.731

Table 9 summarizes the same recode/classifications for three additional photographs for Study Site #1 (Coppice Dune Maneuver Areas). The top performing recode was not consistent for each photograph in Study Site #1. For example, Recode 12_35 appeared to be the best performer for photo 381_144, as indicated by the lowest absolute differences for Cover (123226) and Bare Ground (123806). The mean difference between estimated and reference cover was also relatively low. The ISO2 also performed well, as indicated by the relatively low mean differences for Cover and Bare Ground, although the absolute differences were significantly higher than Recode 12_35. The null hypothesis that the difference between estimated cover and reference cover was equal to zero was accepted at the 95% confidence level for Cover for ISO2 and Bare Ground for Recode 13_45.

Table 9. Descriptive and inferential statistics of difference image (estimated [demixing] minus reference) for two land-cover categories for photos 380_18, 381_144, and 381_146, Study Site #1 using ISO2 and four recodes.

380_18	Recode	t-value	P	CI	abs. diff.	Mean	SD
Cover	ISO2	-5.09	0.0000	-0.816, -0.362	123514	-0.589	12.898
Bare Ground	ISO2	-1.74	0.0819	-0.457, 0.027	123511	-0.215	13.766
Cover	1_25	4.03	0.0000	1.350, 1.788	120637	1.569	12.468
Bare Ground	1_25	-19.68	0.0000	-2.602, -2.131	122212	-2.366	3.409
Cover	12_35	-9.07	0.0000	-1.361, -0.877	132662	-1.119	13.751
Bare Ground	12_35	2.12	0.0340	0.019, 0.503	132386	0.261	13.768
Cover	13_45	-17.94	0.0000	-2.566, -2.060	140113	-2.313	14.377
Bare Ground	13_45	11.19	0.0000	1.250, 1.781	138971	1.516	15.100
Cover	14_5	-43.10	0.0000	-7.886, -7.200	198716	-7.543	19.512
Bare Ground	14_5	37.96	0.0000	6.452, 7.155	195455	6.803	19.986

381_144	Recode	t-value	P	CI	abs. diff.	Mean	SD
Cover	ISO2	1.69	0.0900	-0.071, 0.969	164843	0.449	24.271
Bare Ground	ISO2	-4.29	0.0000	-1.706, -0.635	165630	-1.170	24.988
Cover	1_25	25.27	0.0000	6.377, 7.450	163195	6.913	25.031
Bare Ground	1_25	-26.38	0.0000	-8.004, -6.896	165674	-7.450	25.841
Cover	12_35	2.66	0.0080	0.142, 0.943	123226	0.542	18.687
Bare Ground	12_35	-6.25	0.0000	-1.748, -0.914	123806	-1.331	19.474
Cover	13_45	-2.22	0.0260	-1.384, -0.086	209687	-0.735	30.278
Bare Ground	13_45	0.20	0.8400	-0.591, 0.728	209982	0.069	30.790
Cover	14_5	-22.36	0.0000	-10.487, -8.796	269441	-9.642	39.466
Bare Ground	14_5	21.42	0.0000	8.451, 10.154	268329	9.302	39.737

381_146	Recode	<i>t</i> -value	<i>P</i>	<i>CI</i>	abs. diff.	Mean	SD
Cover	ISO2	-1.38	0.1700	-0.769, 0.134	100336	-0.318	18.772
Bare Ground	ISO2	-1.76	0.0780	-0.906, 0.048	100997	-0.429	19.832
Cover	1_25	2.20	0.0280	0.047, 0.802	83802	0.424	15.697
Bare Ground	1_25	-5.53	0.0000	-1.560, -0.744	84692	-1.152	16.968
Cover	12_35	-8.72	0.0000	-2.131, -1.349	85866	-1.740	16.260
Bare Ground	12_35	4.53	0.0000	0.548, 1.383	85936	0.965	17.358
Cover	13_45	-1.19	0.2300	-0.689, 0.169	720932	-0.260	17.825
Bare Ground	13_45	-2.27	0.0230	-0.976, -0.072	774613	-0.524	18.796
Cover	14_5	-13.77	0.0000	-4.578, -3.437	123979	-4.008	23.721
Bare Ground	14_5	11.31	0.0000	2.790, 3.960	123158	3.375	24.321

In photo 380_18, Recode 1_25 had the lowest absolute difference, although ISO2 also performed relatively well, and actually had lower mean differences for Cover and Bare Ground. The only apparent difference was that ISO2 slightly underestimated Cover and Recode 1_25 slightly overestimated Cover. The null hypothesis was accepted for Bare Ground using ISO2. In photo 381_146, Recode 1_25 resulted in the lowest absolute difference, although Recode 12_35 and ISO2 also performed relatively well. The null hypothesis was accepted for both Cover and Bare Ground for ISO2, and for Cover for Recode 13_45.

Table 10 summarizes the total sum of absolute differences for all four photographs for each recode tested for Study Site #1. Although Recode 12_35 was the top performer for only one of the four photographs in Study Site #1, it did perform relatively well for each photograph, and therefore was the top overall performer for Study Site #1, based on the lowest sum of absolute differences for all four photographs. This recode grouped Honey Mesquite and Mesquite/Dune Edge/Litter/Shadow in the Cover category and grouped all remaining classes into the Bare Ground category. Recode 1_25 and ISO2 also performed well, with Recode 1_25 being the top performer in two of the four photographs for Study Site #1. Recode 12_35 slightly underestimated Cover in three of the four photographs.

Table 10. Total sum of absolute differences for all four photographs for each recode tested for Study Site #1.

Category	Recode	380_18	381_144	381_146	381_158	TOTALS
Cover	ISO2	123514	164843	100336	141003	529696
Bare Ground	ISO2	123511	165630	100997	140716	530854
Cover	1_25	120637	163195	83802	175986	543620
Bare Ground	1_25	122212	165674	84692	177742	550320
Cover	12_35	132662	123226	85866	164568	506322
Bare Ground	12_35	132386	123806	85936	164338	506466
Cover	13_45	140113	209687	720932	151545	1222277
Bare Ground	13_45	138971	209982	774613	150816	1274382
Cover	14_5	198716	269441	123979	158866	751002
Bare Ground	14_5	195455	268329	123158	157418	744360
TOTALS		1428177	1863813	2284311	1582998	7159299

Study Site #2 - Otero Mesa Grasslands

The same four recodes of a five-class unsupervised classification, as well as a two-class unsupervised classification were evaluated for Study Site #2. Field reconnaissance was also conducted in an attempt to identify specific plant species or plant communities associated with each of the five unsupervised spectral classes. Study Site #2 was dominated by *Bouteloua gracilis* (blue grama), *Muhlenbergia arenicola* (sand muhly), *Panicum obtusum* (vine mesquite), *Scleropogon brevifolius* (burrograss), and *Sporobolus cryptandrus* (sand dropseed) grassland communities ranging between 40 and 60 percent cover. The remaining vegetative cover was predominantly *Gutierrezia sarothrae* (snakeweed), *Yucca elata* (soaptree yucca) and *Croton pottsii* (leatherweed), and a mixture of annuals, including *Salsola australis* (Russian thistle) and *Amaranthus palmeri* (sarelessweed) ranging between 20 and 30 percent cover, with approximately 25 percent bare ground, on average. However, it was determined that the five spectral classes identified did not correspond to any specific plant species, but rather depicted a gradient of aerial cover, crown density, and canopy closure in decreasing order moving from Category #1 through #5. For example, Category #1 consistently corresponded to dense grass or shrub cover, while Category #5 consistently corresponded to bare ground. Therefore, the same five recodes of spectral categories were evaluated for all four photographs in Study Site #2. Table 11 presents the inferential and descriptive statistics for these four photographs.

Table 11. Descriptive and inferential statistics of difference image (estimated [demixing] minus reference) for two land-cover categories for photos 386_122, 386_124, 386_16, and 386_18, Study Site #2 using ISO2 and four recodes.

386_122	Recode	t-value	P	CI	abs. diff.	Mean	SD
Cover	ISO2	2.65	0.0082	0.195, 1.309	139829	0.752	24.853
Bare Ground	ISO2	-4.43	0.0000	-1.871, -0.722	140485	-1.296	25.604
Cover	1_25	39.59	0.0000	6.598, 7.285	88269	6.942	15.329
Bare Ground	1_25	-42.35	0.0000	-7.867, -7.171	91078	-7.519	15.524
Cover	12_35	18.58	0.0000	4.517, 5.582	136845	5.049	23.755
Bare Ground	12_35	-20.68	0.0000	-6.178, -5.108	138441	-5.643	23.857
Cover	13_45	-16.71	0.0000	-5.802, -4.584	148745	-5.193	27.166
Bare Ground	13_45	14.94	0.0000	4.032, 5.250	148075	4.641	27.156
Cover	14_5	-51.91	0.0000	-17.504, -16230	148128	-16.867	28.410
Bare Ground	14_5	51.00	0.0000	15.793, 17.056	145325	16.425	28.155

386_124	Recode	t-value	P	CI	abs. diff.	Mean	SD
Cover	ISO2	11.65	0.0000	3.655, 5.134	180242	4.394	32.733
Bare Ground	ISO2	-13.21	0.0000	-5.734, -4.251	180807	-4.992	32.810
Cover	1_25	61.74	0.0000	15.994, 17.043	150804	16.518	23.220
Bare Ground	1_25	-63.40	0.0000	-17.677, -16.616	154533	-17.146	23.474
Cover	12_35	37.64	0.0000	12.998, 14.426	190318	13.712	31.622
Bare Ground	12_35	-39.25	0.0000	12.998, 14.426	192460	-14.355	31.742
Cover	13_45	2.83	0.0047	0.323, 1.781	172912	1.052	32.270
Bare Ground	13_45	-4.31	0.0000	-2.334, -0.875	172800	-1.604	32.306
Cover	14_5	-30.92	0.0000	-8.293, -7.304	109984	-7.798	21.892
Bare Ground	14_5	28.88	0.0000	6.752, 7.736	107589	7.244	21.771

386_16	Recode	t-value	P	CI	abs. diff.	Mean	SD
Cover	ISO2	-0.96	0.3400	-1.571, 0.539	118109	-0.516	35.221
Bare Ground	ISO2	0.29	0.7700	-0.922, 1.245	118082	0.161	36.176
Cover	1_25	-6.40	0.0000	-2.277, -1.209	43283	-1.743	17.832
Bare Ground	1_25	4.24	0.0000	0.629, 1.710	44953	1.169	18.039
Cover	12_35	1.58	0.1100	-0.189, 1.772	102510	0.792	32.722
Bare Ground	12_35	-2.60	0.0092	-2.289, -0.323	103029	-1.306	32.819
Cover	13_45	-23.02	0.0000	-14.570, -12.282	140913	-13.426	38.177
Bare Ground	13_45	22.21	0.0000	11.786, 14.070	140048	12.928	38.107
Cover	14_5	-30.97	0.0000	-12.052, -10.616	72669	-11.334	23.953
Bare Ground	14_5	29.89	0.0000	10.114, 11.534	71019	10.824	23.705

386_18	Recode	t-value	P	CI	abs. diff.	Mean	SD
Cover	ISO2	1.71	0.2300	-0.116, 1.727	128851	0.806	33.306
Bare Ground	ISO2	-2.86	0.0450	-2.268, -0.423	129090	-1.346	33.341
Cover	1_25	26.06	0.0000	5.179, 6.022	51296	5.60	15.234
Bare Ground	1_25	-27.90	0.0000	-6.518, -5.662	52929	-6.090	15.470
Cover	12_35	11.49	0.0000	3.932, 5.551	112754	4.741	29.263
Bare Ground	12_35	-12.90	0.0000	-6.158, -4.533	113696	-5.346	29.378
Cover	13_45	-8.07	0.0000	-4.643, -2.827	127216	-3.735	32.825
Bare Ground	13_45	6.92	0.0000	2.290, 4.103	126797	3.197	32.764
Cover	14_5	-29.38	0.0000	-7.864, -6.880	59585	-7.372	17.787
Bare Ground	14_5	27.9	0.0000	6.412, 7.382	57880	6.897	17.527

Unlike Study Site #1, where different recodes performed best for different photographs, Recode 1_25 had the lowest absolute difference for photos 386_122 (179347), 386_16 (88236), and 386_18 (104225), and had the second lowest absolute difference for photo 386_124 (305337), where Recode 14_5 had the lowest absolute difference. In general, mean differences and standard deviations of mean differences were considerably higher than for Study Site #1. The null hy-

pothesis was rejected for all recode combinations for photos 386_122 and 386_124. The null hypothesis was accepted for Cover and Bare Ground using ISO2 and for Cover using Recode 12_35 in photo 386_16, as well as for Cover using ISO2 in photo 386_18.

Table 12 summarizes the total sum of absolute differences for all four photographs for each recode tested for Study Site #2. Recode 1_25 was identified as the best performer for Study Site #2 based on the lowest sum of absolute differences for all photographs for Cover (543620) and Bare Ground (550320).

Table 12. Total sum of absolute differences for all four photographs for each recode tested for Study Site #2.

Category	Recode	386_122	386_124	386_16	386_18	TOTALS
Cover	ISO2	139829	180242	118109	128851	567031
Bare Ground	ISO2	140485	180807	118082	129090	568464
Cover	1_25	88269	150804	43283	51296	333652
Bare Ground	1_25	91078	154533	44953	52929	343493
Cover	12_35	136845	190318	102510	112754	542427
Bare Ground	12_35	138441	192460	103029	113696	547626
Cover	13_45	148745	172912	140913	127216	589786
Bare Ground	13_45	148075	172800	140048	126797	587720
Cover	14_5	148128	109984	72669	59585	390366
Bare Ground	14_5	145325	107589	71019	57880	381813
TOTALS		1325220	1612449	954615	960094	4852378

Study Site #3 - Controlled Burn Area/Otero Mesa Foothills

The same field reconnaissance and analysis were conducted for four photographs in Study Site #3. Study Site #3 was a mixed shrubland/grassland site. Dominant shrubs were *Larrea tridentata* (creosote bush), *Florencia cernua* (American tarbush), and *Prosopis glandulosa* (honey mesquite), which typically accounted

for approximately 50 percent of the total cover. Grass cover ranged from 25 to 50 percent and was dominated by *Sclerapogon brevifolius* (burrograss), but also included *Muhlenbergia porteri* (bush muhly), *Bouteloua eriopoda* (black grama), *Hilaria mutica* (tobosagrass), and *Panicum halli* (Hall's panicgrass). Bare ground was typically 25 to 30 percent. Similar to Study Site #2, it was determined that the spectral categories represented a gradient of decreasing vegetation density and crown cover moving from Categories 1 thru 5. For example, Category #1 was usually associated with a dense mixture of shrubs and grasses with complete canopy cover. Increasing category values were associated with decreasing plant density and canopy closure. Category #5 was associated with bare ground.

Table 13 summarizes the results from Study Site #3. Recode 14_5 was clearly the best performer for all four photographs based on the lowest absolute difference for each photograph. The null hypothesis was rejected for all recodes for all photographs evaluated. In general, mean differences between estimated and reference cover were slightly higher than Study Site #1, but lower than Study Site #2. Recode 14_5 slightly underestimated cover and slightly overestimated bare ground for all four photographs. Table 14 summarizes the total sum of absolute differences for all photographs for Study Site #3, confirming that recode 14_5 was the best performer for Study Site #3.

Table 13. Descriptive and inferential statistics of difference image (estimated [demixing] minus reference) for two land-cover categories for photos 388_45, 388_47, 388_88, and 388_90, Study Site #3 using ISO2 and four recodes.

388_45	Recode	t-value	P	CI	abs. diff.	Mean	SD
Cover	ISO2	-7.01	0.0000	-2.302, -1.296	246550	-1.799	27.410
Bare Ground	ISO2	4.22	0.0029	0.581, 1.589	246306	1.085	27.432
Cover	1_25	27.28	0.0000	5.440, 6.283	209003	5.861	22.939
Bare Ground	1_25	-30.26	0.0000	-6.979, -6.130	212144	-6.554	23.128
Cover	12_35	10.88	0.0000	2.374, 3.417	259318	2.895	28.40
Bare Ground	12_35	-13.61	0.0000	-4.152, -3.106	260613	-3.629	28.482
Cover	13_45	-12.48	0.0000	-3.275, -2.386	211676	-2.830	24.204
Bare Ground	13_45	9.26	0.0000	1.653, 2.540	210519	2.097	24.165
Cover	14_5	-25.29	0.0000	-3.437, -2.942	110184	-3.190	13.466
Bare Ground	14_5	20.23	0.0000	2.281, 2.770	107777	2.525	13.326

388_47	Recode	t-value	P	CI	abs. diff.	Mean	SD
Cover	ISO2	-14.93	0.0000	-3.895, -2.991	268068	-3.443	26.111
Bare Ground	ISO2	11.56	0.0000	2.216, 3.121	267693	2.668	26.137
Cover	1_25	25.90	0.0000	5.110, 5.946	241420	5.528	24.169
Bare Ground	1_25	-28.70	0.0000	-6.597, -5.753	245018	-6.175	24.371
Cover	12_35	9.02	0.0000	1.658, 2.579	273912	2.119	26.601
Bare Ground	12_35	-12.31	0.0000	-3.366, -2.441	276189	2.903	26.709
Cover	13_45	-7.56	0.0000	-2.046, -1.203	242798	-1.624	24.350
Bare Ground	13_45	3.88	0.0046	0.411, 1.254	242833	0.833	24.326
Cover	14_5	-33.01	0.0000	-5.541, -4.920	168701	-5.230	17.943
Bare Ground	14_5	29.11	0.0000	4.264, 4.880	165536	4.572	17.788

388_88	Recode	t-value	P	CI	abs. diff.	Mean	SD
Cover	ISO2	-14.93	0.0000	-3.895, -2.991	168920	-3.443	26.111
Bare Ground	ISO2	11.56	0.0000	2.216, 3.121	169166	2.668	26.137
Cover	1_25	20.40	0.0000	4.761, 5.774	146619	5.268	23.442
Bare Ground	1_25	-21.64	0.0000	-6.341, -5.288	148918	-5.815	24.392
Cover	12_35	14.73	0.0000	4.097, 5.355	195069	4.726	29.127
Bare Ground	12_35	-16.76	0.0000	-6.028, -4.765	196749	-5.396	29.233
Cover	13_45	-13.01	0.0000	-4.208, -3.106	163202	-3.657	25.512
Bare Ground	13_45	10.37	0.0000	2.422, 3.552	162842	2.987	26.152
Cover	14_5	-13.88	0.0000	-2.799, -2.106	90035	-2.453	16.040
Bare Ground	14_5	10.5	0.0000	1.497, 2.185	88538	1.841	15.916

388_90	Recode	t-value	P	CI	abs. diff.	Mean	SD
Cover	ISO2	-5.89	0.0001	-2.734, -1.369	127168	-2.051	26.944
Bare Ground	ISO2	3.83	0.0092	0.651, 2.018	127168	1.335	27.022
Cover	1_25	15.90	0.0000	3.758, 4.816	94535	4.287	20.748
Bare Ground	1_25	-16.86	0.0000	-5.403, -4.278	95991	-4.841	22.089
Cover	12_35	5.15	0.0005	1.098, 2.446	126412	1.722	26.448
Bare Ground	12_35	-7.22	0.0000	-3.169, -1.815	127148	-2.492	26.553
Cover	13_45	-6.17	0.0000	-2.360, -1.222	102826	-1.791	22.332
Bare Ground	13_45	3.73	0.0002	0.535, 1.723	102599	1.129	23.292
Cover	14_5	-18.47	0.0000	-3.725, -3.010	59396	-3.367	14.022
Bare Ground	14_5	14.88	0.0000	2.332, 3.040	58097	2.686	13.880

Table 14. Sums of absolute differences for all four photographs for each recode tested for Study Site #3.

Category	Recode	388_45	388_47	388_88	388_90	TOTALS
Cover	ISO2	246550	268068	168920	127168	810706
Bare Ground	ISO2	246306	267693	169166	127168	810333
Cover	1_25	209003	241420	146619	94535	691577
Bare Ground	1_25	212144	245018	148918	95991	702071
Cover	12_35	259318	273912	195069	126412	854711
Bare Ground	12_35	260613	276189	196749	127148	860699
Cover	13_45	211676	242798	163202	102826	720502
Bare Ground	13_45	210519	242833	162842	102599	718793
Cover	14_5	110184	168701	90035	59396	428316
Bare Ground	14_5	107777	165536	88538	58097	419948
TOTALS		2074090	2392168	1530058	1021340	7017656

Spatial Extrapolation

In addition to photo-by-photo demixing analysis, a demixing model was also developed by sampling three of the four photographs for each site, as described in the methodology. The three photographs for each site were randomly selected. The demixing model was then tested by attempting to demix a subset of the TM image that matched the footprint of the fourth photograph. Demixing results from this subset were then compared with reference groundcover estimates for the fourth photograph in the same manner as individual photographs were evaluated. Based on evaluations of demixing performance for individual photographs, only the two best performing recodes for each site were tested for extrapolating results from three photographs to a fourth location.

For Study Site #1, photos 380_18, 381_144, and 381_146 were sampled to develop a single demixing model. A subset of a TM image matching the footprint of a fourth photograph, 381_158, was then demixed using this model to estimate abundance of vegetative cover and bare ground in the area of photo 381_158. Recode 12_35 and a two-class unsupervised classification (ISO2), which were identified as the top performing recodes for Study Site #1 based on analysis of individual photographs, were evaluated. Results for these two recodes are summarized in Table 15. Both recodes were comparable in performance, and tended to overestimate cover by approximately 5 to 7 percent and underestimate bare ground by approximately 6 to 8 percent. ISO2 resulted in a slightly lower sum of absolute differences than recode 12_35. This may be due in part to the fact that ISO2 was the top performer for photo 381_158 when analyzed as an individual photograph. The null hypothesis was rejected for both land-cover categories for both recodes.

Table 15. Descriptive and inferential statistics of difference image (estimated [extrapolated demixing] minus reference) for two land-cover categories for photo 381_158 for Study Site #1 using recode 12_35 and ISO2.

Site 1	Recode	t-value	P	CI	abs. diff.	Mean	SD
Cover	12_35	50.83	0.0000	6.951, 7.509	136271	7.230	14.609
Bare Ground	12_35	54.28	0.0000	-8.441, -7.853	140436	-8.147	15.415
Cover	ISO2	39.78	0.0000	5.251, 5.796	128530	5.524	14.260
Bare Ground	ISO2	-46.07	0.0000	-6.684, -6.138	131882	-6.411	14.289

Figures 12 and 13 contrast images of the reference abundance, the estimated abundance derived directly from samples of photo 381_158 only, and the extrapolated estimates of abundance for the same area derived from sampling the other three photographs in Study Site #1. Using recode 12_35, extrapolated estimates of demixing actually appear more similar to reference images than demixing estimates derived directly from photo 381_158. Single-photo estimates appeared to overestimate cover and bare ground in the lower left quadrant of the image, while the extrapolated estimates appeared similar to the reference images for this same area. Using ISO2, the opposite appeared to be true. Extrapolated estimates appeared to overestimate abundance of cover and bare ground, while single-photo estimates appeared similar to reference images.

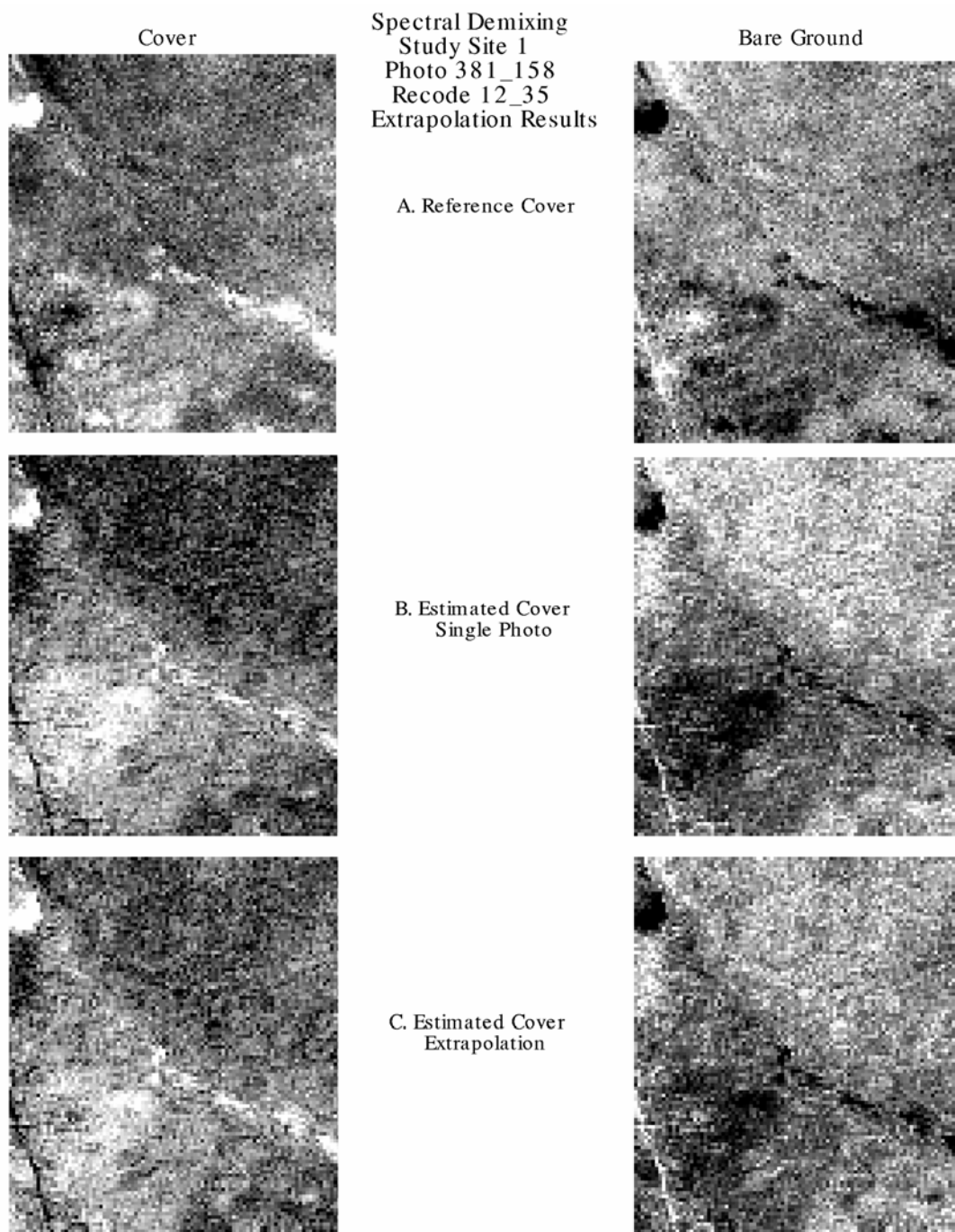


Figure 12. Demixing results for two land-cover categories for photo 381-158 using recode 12_35.

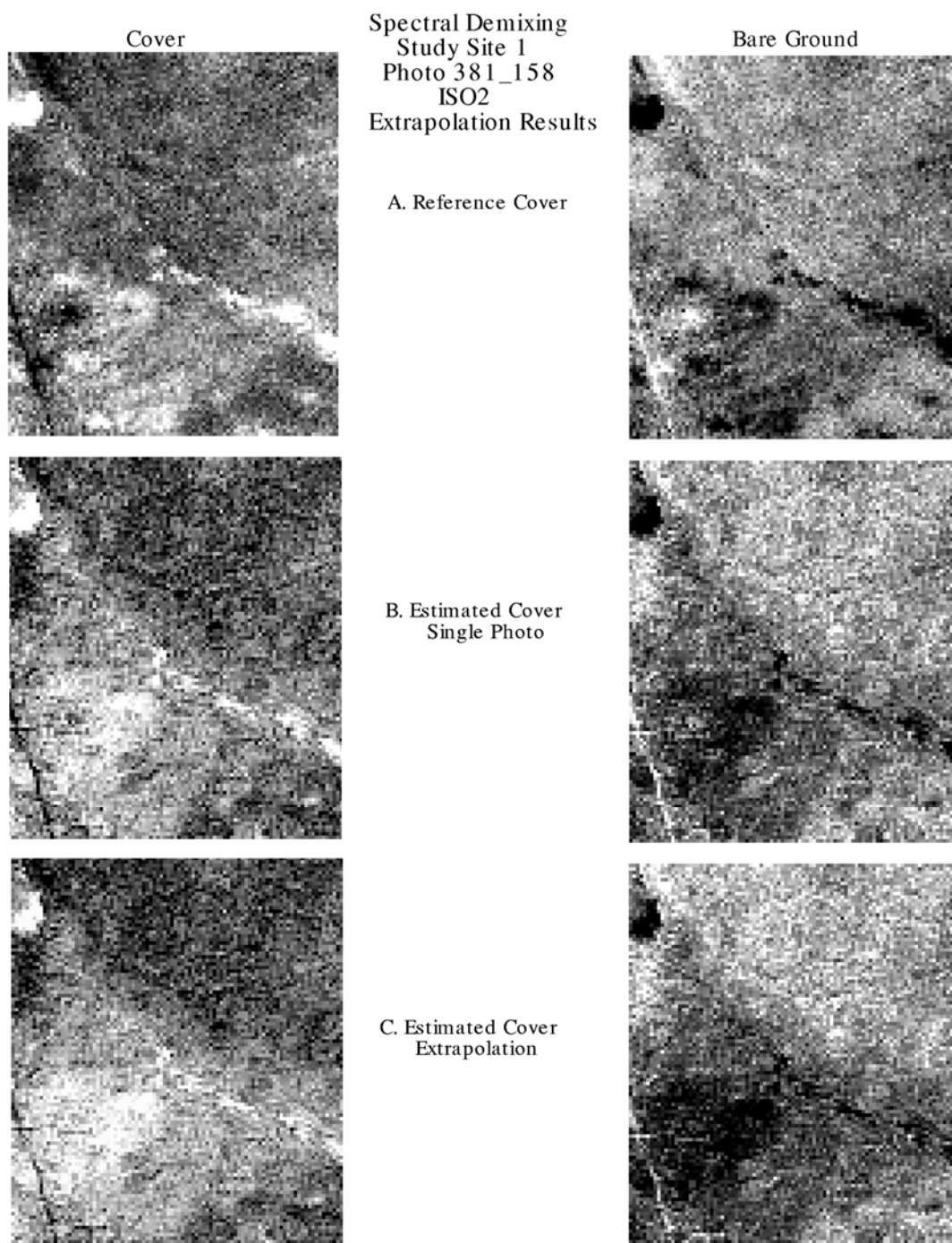


Figure 13. Demixing results for two land-cover categories for photo 381-158 using ISO2.

For Study Site #2, photos 386_122, 386_16, and 386_18 were extrapolated to photo 386_124. Recodes 14_5 and 1_25, identified as the best performers for Study Site #2, were evaluated. Results for these two recodes are summarized in Table 16. Recode 14_5 appeared to perform better than recode 1_25 based on a much lower sum of absolute differences for both land-cover classes, even though recode 1_25 was identified as the top performer when all four individual photographs were evaluated. Recode 14_5 was the second best performing recode for individual photo analysis, and actually was the top performing recode for photo 386_124, which may explain why the sum of absolute differences was considerably lower for recode 14_5 when the demixing model was extrapolated to this photo location. Recode 14_5 underestimated cover and overestimated bare ground by approximately 9 percent, while recode 1_25 overestimated cover and underestimated bare ground by approximately 8 percent. The null hypothesis was rejected for both land-cover categories for both recodes. The variance in mean difference was considerably higher for Study Site #2 than Study Site #1.

Images of reference abundance, estimated abundance derived directly from samples of photo 386_124 only, and extrapolated estimates of abundance for the same area derived from sampling the other three photographs in Study Site #2 are contrasted in Figures 14 and 15. Visual inspection of results from both recodes indicated that recode 14_5 appeared to perform better, both in terms of single-photo and extrapolated estimates matching reference images more closely and single-photo and extrapolated estimates matching each other. The sum of absolute differences also confirmed that recode 14_5 performed best for Study Site #2.

Table 16. Descriptive and inferential statistics of difference image (estimated [extrapolated demixing] minus reference) for two land-cover categories for photo 386_124 for Study Site #2 using recode 14_5 and 1_25.

Site 2	Recode	t-value	P	CI	abs. diff.	Mean	SD
Cover	14_5	-31.69	0.0000	-10.010, -8.843	116691	-9.427	25.825
Bare Ground	14_5	29.74	0.0000	8.438, 9.629	115037	9.034	26.370
Cover	1_25	21.23	0.0000	7.555, 9.092	196351	8.324	34.037
Bare Ground	1_25	-22.36	0.0000	-9.755, -8.182	199598	-8.969	34.816

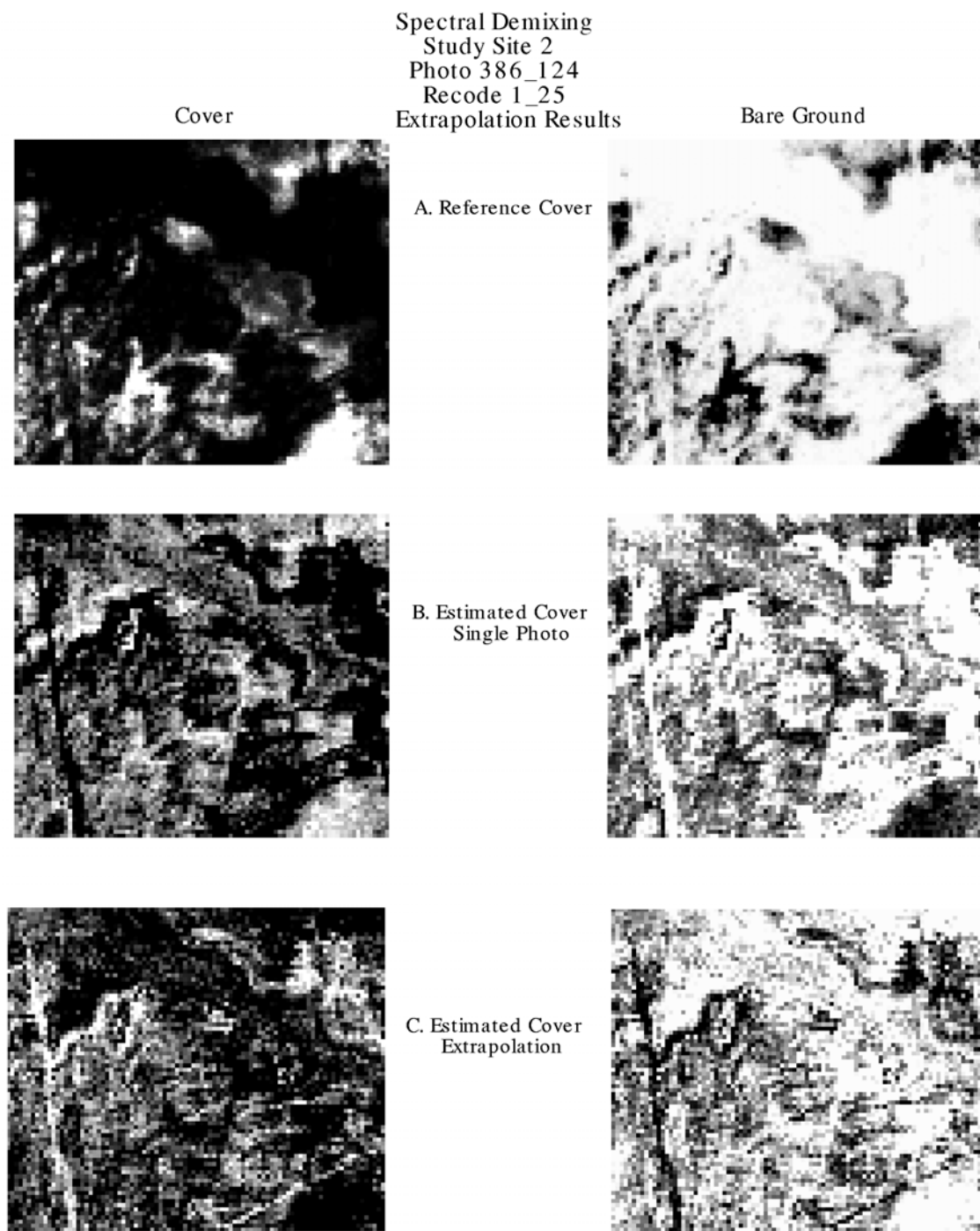


Figure 14. Demixing results for two land-cover categories for photo 386-124 using recode 1_25.

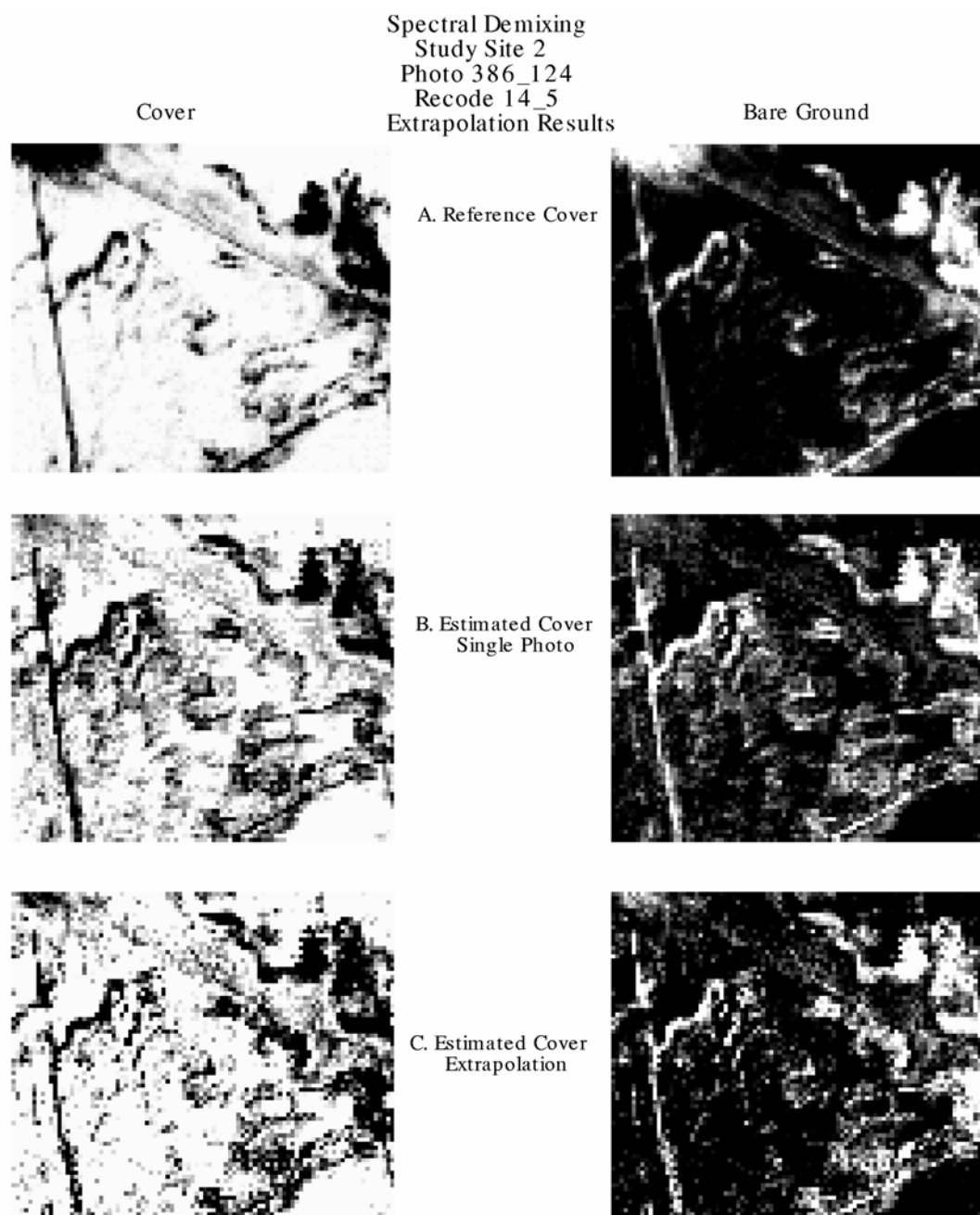


Figure 15. Demixing results for two land-cover categories for photo 386-124 using recode 14_5.

For Study Site #3, photos 388_45, 388_47, and 388_88 were used to extrapolate estimates to 388_90. Recodes 14_5 and 1_25, identified as the best performers for Study Site #3, were evaluated. These results are summarized in Table 17. Recode 14_5 appeared to perform better than recode 1_25, based on a considerably lower sum of absolute differences and mean difference. Although the null hypothesis was rejected for both land-cover classes for both recodes, recode 14_5 overestimated cover and underestimated bare ground by only 3 percent on

average. This mean difference was considerably lower than all other mean differences resulting from spatial extrapolation at the other study sites.

Table 17. Descriptive and inferential statistics of difference image (estimated [extrapolated demixing] minus reference) for two land-cover categories for photo 388_90 for Study Site #3 using recodes 14_5 and 1_25.

Site 3	Recode	t-value	P	CI	abs. diff.	Mean	SD
Cover	14_5	17.61	0.0000	2.773, 3.468	57533	3.136	13.585
Bare Ground	14_5	-18.31	0.0000	-3.978, -3.208	57613	-3.594	13.445
Cover	1_25	49.79	0.0000	16.696, 18.065	149085	17.407	26.820
Bare Ground	1_25	-50.02	0.0000	-18.856, -17.433	152026	-18.153	26.994

Images of reference abundance, estimated abundance derived directly from samples of photo 388_90 only, and extrapolated estimates of abundance for the same area derived from sampling the other three photographs in Study Site #3 are contrasted in Figures 16 and 17. Similar to Study Site #2, visual inspection of results for the two recodes tested indicated that recode 14_5 appeared to perform best. There was more similarity in patterns for single-photo and extrapolated results for recode 14_5. The sum of absolute differences also indicated that recode 14_5 was clearly the top performer.

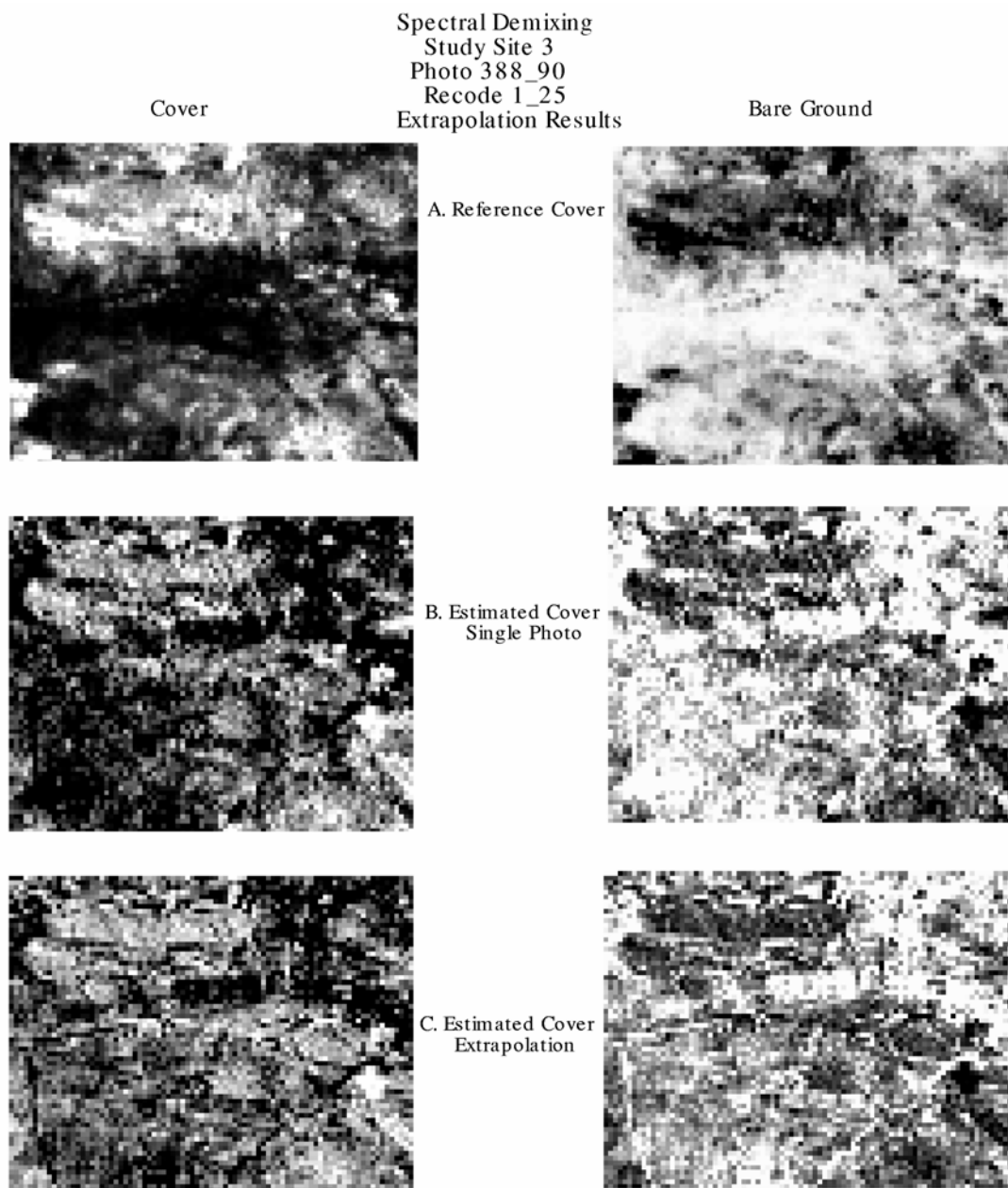


Figure 16. Demixing results for two land-cover categories for photo 388-90 using recode 1_25.

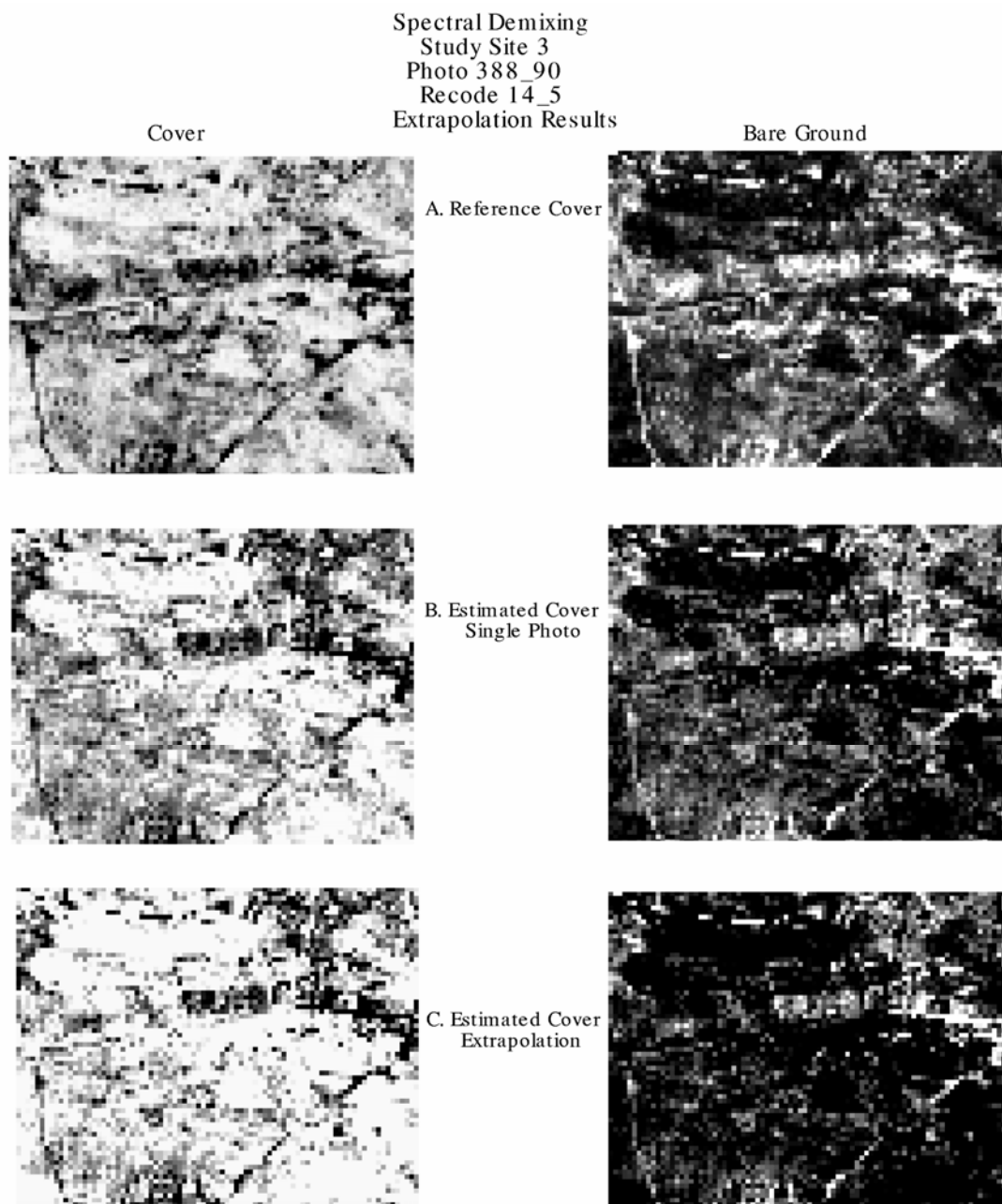


Figure 17. Demixing results for two land-cover categories for photo 388-90 using recode 14_5.

Spectral Index Correlation Analysis

Correlations between nine spectral brightness and greenness indices, as well as six individual TM bands, were evaluated using exploratory regression analysis. The indices and individual TM bands were evaluated as independent variables and correlated with reference measurements of vegetation cover or abundance. The linear relationship between each independent variable and each reference

abundance amount were evaluated based on R^2 values, or Coefficients of Determination. All possible correlations between indices/TM spectral bands and fractional land-cover percent cover values were evaluated for each photograph for all three study sites. Appendix B contains a summary of the adjusted R^2 for all correlations.

Greenness or Vegetation Indices exhibited very low correlations with reference vegetation cover amounts in all photographs, as expected based on previous literature and the unique limitations of the application of vegetation indices in arid environments. In some isolated photographs, individual TM bands, particularly Bands 2 (green) and 3 (red), exhibited some correlation with vegetative abundance. However, only the two spectral brightness indices, Albedo and Tasseled Cap or Kauth-Thomas Brightness (KTB) consistently exhibited strong correlations with reference cover amounts for most photographs in all three study sites.

Therefore, only these two brightness indices were evaluated for their utility for estimating vegetative cover. The regression formula describing the relationship between each of the brightness indices and reference vegetation cover amounts was then applied to each pixel in the spectral brightness indices to derive a fractional percent cover estimate for each land-cover component within that pixel. These estimates of cover were then compared with reference fractional land-cover values in the same manner as spectral demixing.

Five-class Results

Using photo 381_158 from Study Site #1 as an example, Figure 18 shows estimates of abundance derived from correlation analysis using albedo and corresponding reference images of abundance for five land-cover classes. Similar to example output from demixing analysis, brighter pixels represent higher percent cover or abundance for that respective land-cover type. Figure 19 shows similar estimates derived from Kauth-Thomas or Tasseled Cap Brightness.

Relative to visual examination of demixing estimates of abundance, spatial patterns of estimated abundance derived from correlation analysis using both Albedo and KTB appeared to correspond well with reference images. Both indices clearly delineated a road or trail running across the lower left or southwest corner of the image. Two areas of relatively high cover were evident in the reference image. The first was a circular area in the upper left or northwest corner of the image and the second was a somewhat linear feature originating in approximately the center of the image and extending to the southeast on the right half of the photograph. According to the reference image, the circular area in the upper left corner of the image had a large amount of land-cover Category

#1 (Mesquite) and Category #2 (Mesquite/Dune Edge/Shadow/Litter), with slightly smaller amount of Category #3 (Interdunal) and almost no presence of land-cover Categories #4 (Interdunal) and #5 (Bare Ground). Estimates of cover derived from both Albedo and KTB correlations for this same area indicate higher amounts of cover in land-cover Categories #1 through 3, but also show a higher amount of cover for land-cover Category #4. The linear feature of high cover appeared to be predominantly land-cover Category #1 (Mesquite) in the reference images, yet this same feature appears to have relatively high abundance of land-cover Categories #1 through 4 in the estimated cover images. The estimated cover images also did not clearly depict the relatively high abundance of land-cover Categories #2 and #3, which was evident in the reference images in the southwest or lower left quadrant of the image.

Images of estimated abundance derived from Albedo and KTB correlations appeared quite similar to each other for each of the land-cover categories. Images also appeared similar for land-cover Categories #1 through 4 for each individual index. However, examination of abundance values for individual pixels in each of these four land-cover categories revealed that estimates were similar but different. Visual examination of gray-scale images can sometimes be misleading because the histogram from which gray-scale color values are assigned to pixels is based solely on the histogram for that respective land-cover category. For example, the pixel with the highest cover amount for any single land-cover category will be assigned the brightest pixel value for that respective land-cover category. That same pixel may also have the highest cover amount for a different land-cover category, and therefore would be assigned the brightest pixel value for that land-cover category as well, yet the actual abundance amount for that particular land-cover category may be quite different than the actual abundance amount in the first land-cover category.

The same metrics used to evaluate demixing analysis, including results from statistical analysis, were also used to evaluate spectral index correlation analysis. The mean and standard deviation of the reference abundance images were compared to the mean and standard deviation of estimated abundance derived from Albedo and KTB correlations. Table 18 contains these results for photo 381_158.

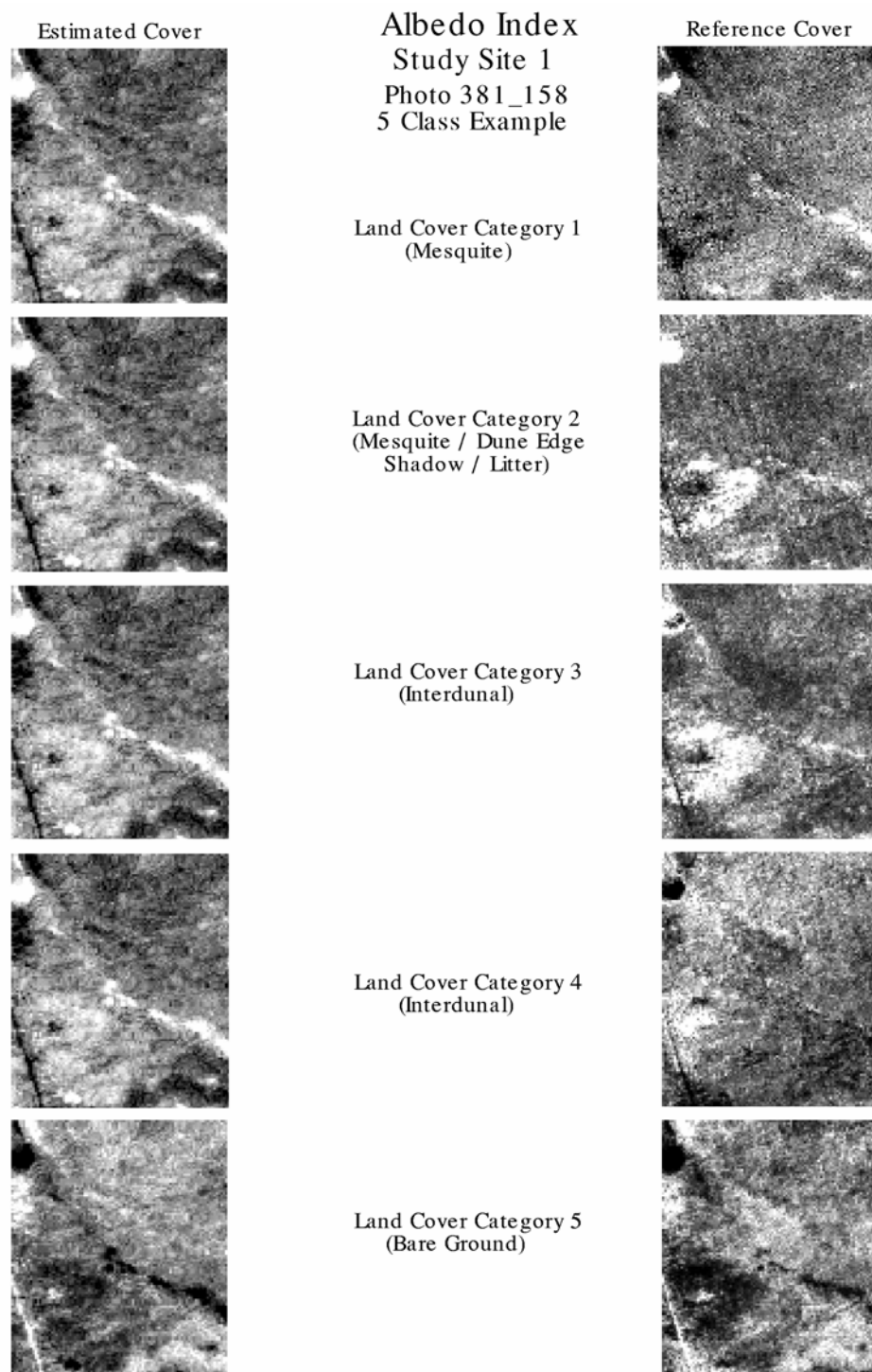


Figure 18. Albedo correlation results for five land-cover categories for photo 381_158 (left column is the albedo-derived estimate of abundance for each category, right column is the reference abundance for each category).

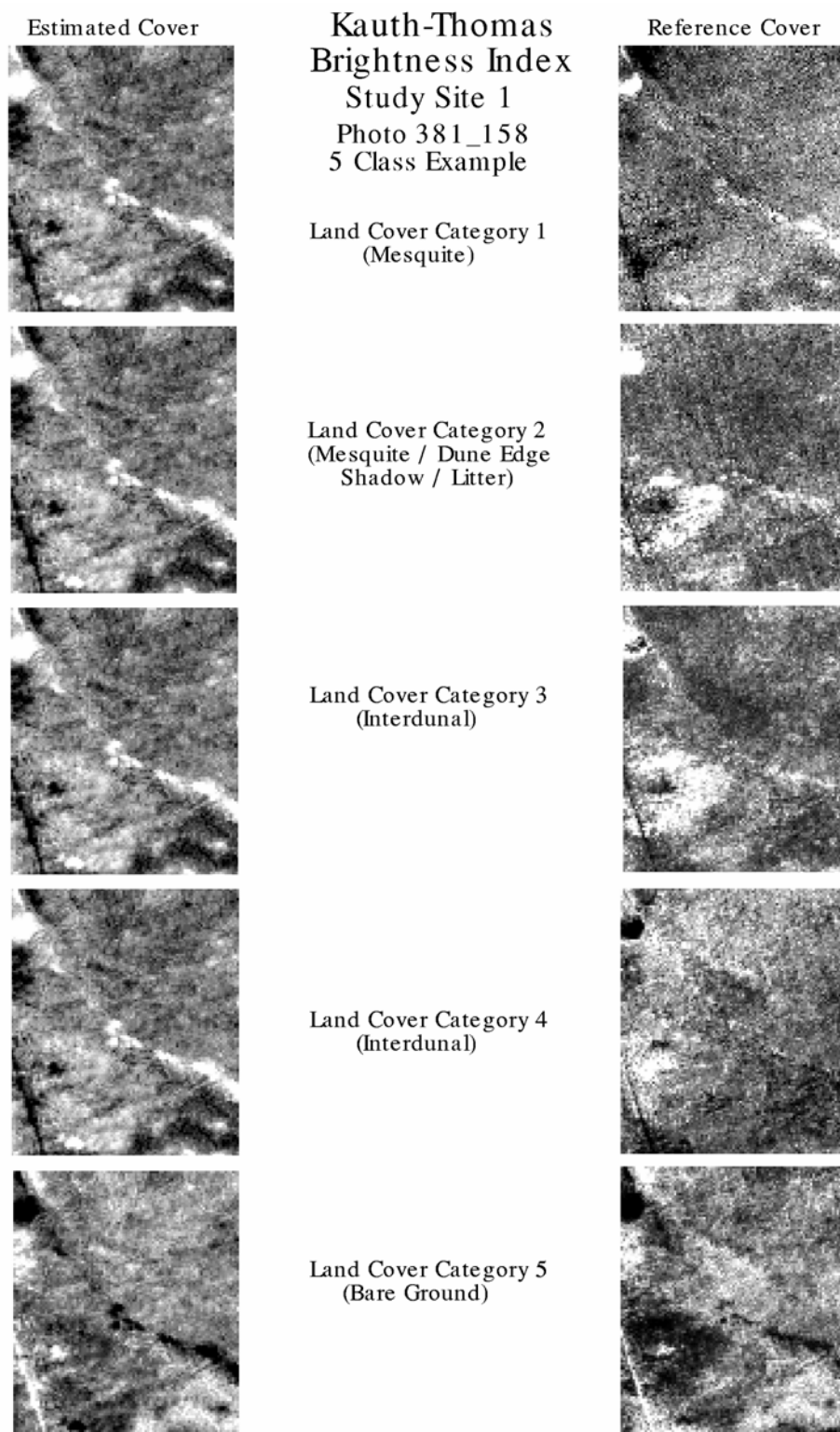


Figure 19. KTB correlation results for five land-cover categories for photo 381_158 (left column is the KTB-derived estimate of abundance for each category, right column is the reference abundance for each category).

Table 18. Mean and standard deviation of abundance for five land-cover categories for photo 381_158, Study Site #1; estimated (spectral index correlations) versus reference.

KTB	ESTIMATED		REFERENCE	
	Mean	SD	Mean	SD
Category				
mesquite (1)	24.171	4.064	24.307	7.530
mesquite/ dune edge/ shadow/ litter (2)	11.340	2.117	11.482	4.192
interdunal (3)	13.262	2.651	13.393	5.488
interdunal (4)	24.704	0.192	24.403	8.255
bare ground (5)	26.658	8.964	26.412	12.927
Totals	100.135		99.997	

ALBEDO	ESTIMATED		REFERENCE	
	Mean	SD	Mean	SD
Category				
mesquite (1)	24.156	3.712	24.307	7.530
mesquite/ dune edge/ shadow/ litter (2)	11.302	2.241	11.482	4.192
interdunal (3)	13.279	2.977	13.393	5.488
interdunal (4)	24.669	0.006	24.403	8.255
bare ground (5)	26.245	8.881	26.412	12.927
Totals	99.651		99.997	

Unlike demixing, where estimates of abundance were constrained to be less than or equal to 100 percent, estimates derived from correlation analysis were not subjected to the same constraints. Therefore, the sum of the estimated abundance of cover for all bands did not always equal 100 percent. However, in all cases, even without constraints, the sum of the estimated abundance for all land-cover types did equal approximately 100 percent. Using a five-class breakout, estimates derived from Albedo and KTB correlations were very similar to reference cover amounts. Standard deviations of the mean estimates of abundance were also lower than standard deviations of abundance in reference images, and were also considerably lower than standard deviations resulting from demixing estimates of cover.

The same statistics that were used to compare demixing estimates of abundance with reference abundance amounts were also used to compare estimates derived from Albedo and KTB correlations with reference abundance amounts. This included a paired Students T-test statistic (t-value), probability value (P), and a 95% confidence interval for mean difference. These statistics were used to evaluate the null hypothesis that the mean difference between the estimated percent cover derived from Albedo and KTB correlations and the reference percent cover values derived from air photo classifications were equal to zero at $\alpha = .05$ or 95% confidence. These statistics, along with the mean difference and the sum of absolute differences for all pixels, are summarized in Table 19 for photo 381_158 for five land-cover classes.

Table 19. Descriptive and inferential statistics of difference image (estimated [spectral index correlations] minus reference) for five land-cover categories for photo 381_158, Study Site #1.

KTB	t-value	P	CI	abs. diff.	Mean	SD
mesquite (1)	-2.77	0.0058	-1.363, -0.232	50487	-0.798	6.366
mesquite/ dune edge/ shadow/ litter (2)	-1.01	0.32	-0.533, 0.172	27260	-0.180	3.969
interdunal (3)	0.55	0.59	-0.332, 0.587	37638	0.128	5.173
interdunal (4)	3.03	0.0026	0.401, 1.883	69396	1.142	8.336
bare ground (5)	-0.29	0.77	-1.009, 0.748	80807	-0.131	9.885

Albedo	t-value	P	CI	abs. diff.	Mean	SD
mesquite (1)	-2.84	0.0047	-1.461, -0.266	52080	-0.863	6.726
mesquite/ dune edge/ shadow/ litter (2)	-1.14	0.26	-0.537, 0.143	26558	-0.197	3.825
interdunal (3)	0.89	0.38	-0.241, 0.637	36131	0.198	4.939
interdunal (4)	2.88	0.0041	0.343, 1.815	69333	1.079	8.282
bare ground (5)	-1.28	0.20	-1.369, 0.287	80221	-0.541	9.316

The null hypothesis was accepted for land-cover Category #2 (Mesquite/Dune Edge/Shadow/Litter), Category #3 (Interdunal), and Category #5 (Bare Ground) for estimates derived from both Albedo and KTB correlations. Mean differences ranged from -0.798 to 1.142 for KTB-derived estimates to -0.863 to 1.079 for Albedo-derived estimates. KTB estimates performed best for land-cover Categories #2 and #3, based on the lowest sum of absolute differences, which were 27260 and 37638, respectively. Albedo estimates also performed best for these two land-cover categories based on the lowest sum of absolute differences.

Albedo estimates for land-cover Category #2 were the best overall, with an absolute difference of 26558. However, neither KTB nor Albedo correlations accurately estimated abundance of land-cover Categories #5, as evident by the relatively higher sum of absolute differences and the mean difference for this category.

Three-class Results

Although estimates of abundance for five land-cover classes derived from Albedo and KTB correlations were much better than estimates derived from demixing for five land-cover classes, there were still some problem areas evident in the visual examination of the five-class results. Therefore, the same 3-class breakout used to evaluate demixing was also used to evaluate spectral index correlations. Figures 20 and 21 contrast the results of Albedo and KTB estimates of abundance with reference images of abundance for three land-cover categories: Honey Mesquite (Category #1), Interdunal Cover (Category #2), and Bare Ground (Category #3).

Spatial patterns of estimated abundance of land-cover Categories #1 (Honey Mesquite) and #3 (Bare Ground) were quite similar to patterns in the corresponding reference images for estimates derived from both Albedo and KTB indices. Both indices correctly estimated a high abundance of honey mesquite in the upper left corner of the image and along a linear pattern in the center of the image. Both indices also clearly delineated a road in the lower left corner of the image for land-cover Category #3. However, both indices failed to identify a pattern of higher amounts of Interdunal Cover (Category #2) in the lower left quadrant of the image. This pattern is clearly identifiable in land-cover Categories #2 and #3 in the reference images, but is not evident in the corresponding estimated cover images, with the exception of a small isolated area of bare ground.

Table 20 lists the mean and standard deviation of abundance for both the reference images and estimates derived from both Albedo and KTB correlations. Both indices resulted in estimates of 30 percent cover of honey mesquite, which agreed with reference amounts. Both indices resulted in estimates of interdunal cover at 26 percent, which again agreed with reference amounts. Estimates of bare ground were only 1 percent higher than reference amounts, at approximately 43 percent. Similar to the five land-cover class breakout, standard deviations resulting from brightness index correlations were much lower than demixing estimates.

Table 21 summarizes the statistical results for the three-class breakout. The null hypothesis was accepted for land-cover Category #1 (Honey Mesquite) and land-cover Category #2 (Interdunal Cover) for Albedo-derived estimates, but rejected for all other land-cover categories using both Albedo- and KTB-derived estimates. In general, estimates derived from both indices slightly underestimated honey mesquite and interdunal cover and slightly overestimated bare ground. The smallest sum of absolute difference and mean difference occurred for honey mesquite, while the largest sum of absolute difference and mean difference occurred for bare ground.

The same five-class and three-class breakouts were evaluated for all photographs at each of the three study sites. Although correlation analysis results were more promising than demixing, five-class and three-class recodes were eliminated from further analysis and correlation analysis was limited to estimating cover versus bare ground by analyzing only those classifications and recodes containing two land-cover categories (Cover and Bare Ground). A three-class breakout was not investigated further because of the problems associated with identifying three unique land-cover classes in the reference aerial photograph.

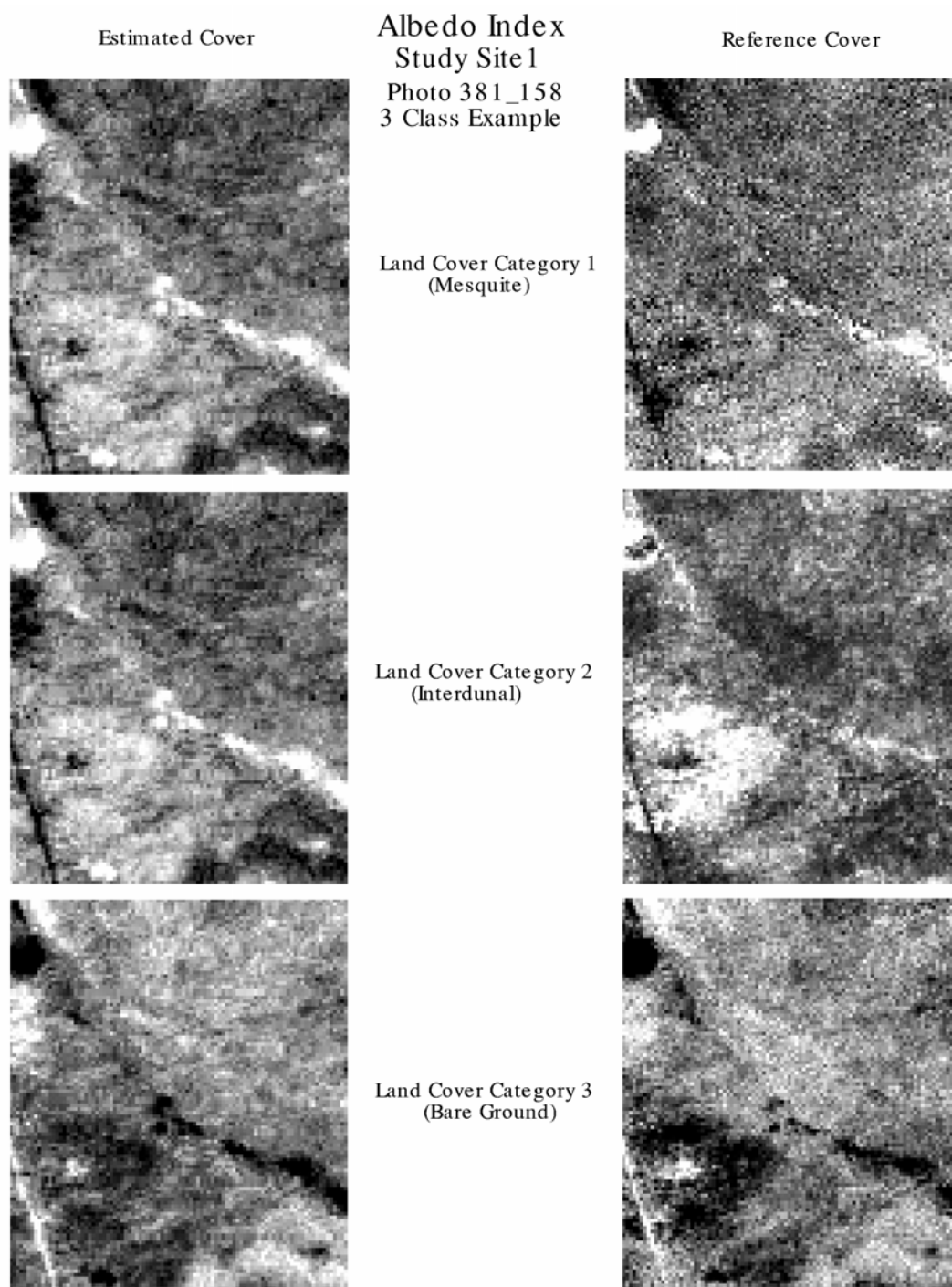


Figure 20. Albedo correlation results for three land cover categories for photo 381_158 (left column is the albedo-derived estimate of abundance for each category, right column is the reference abundance for each category).

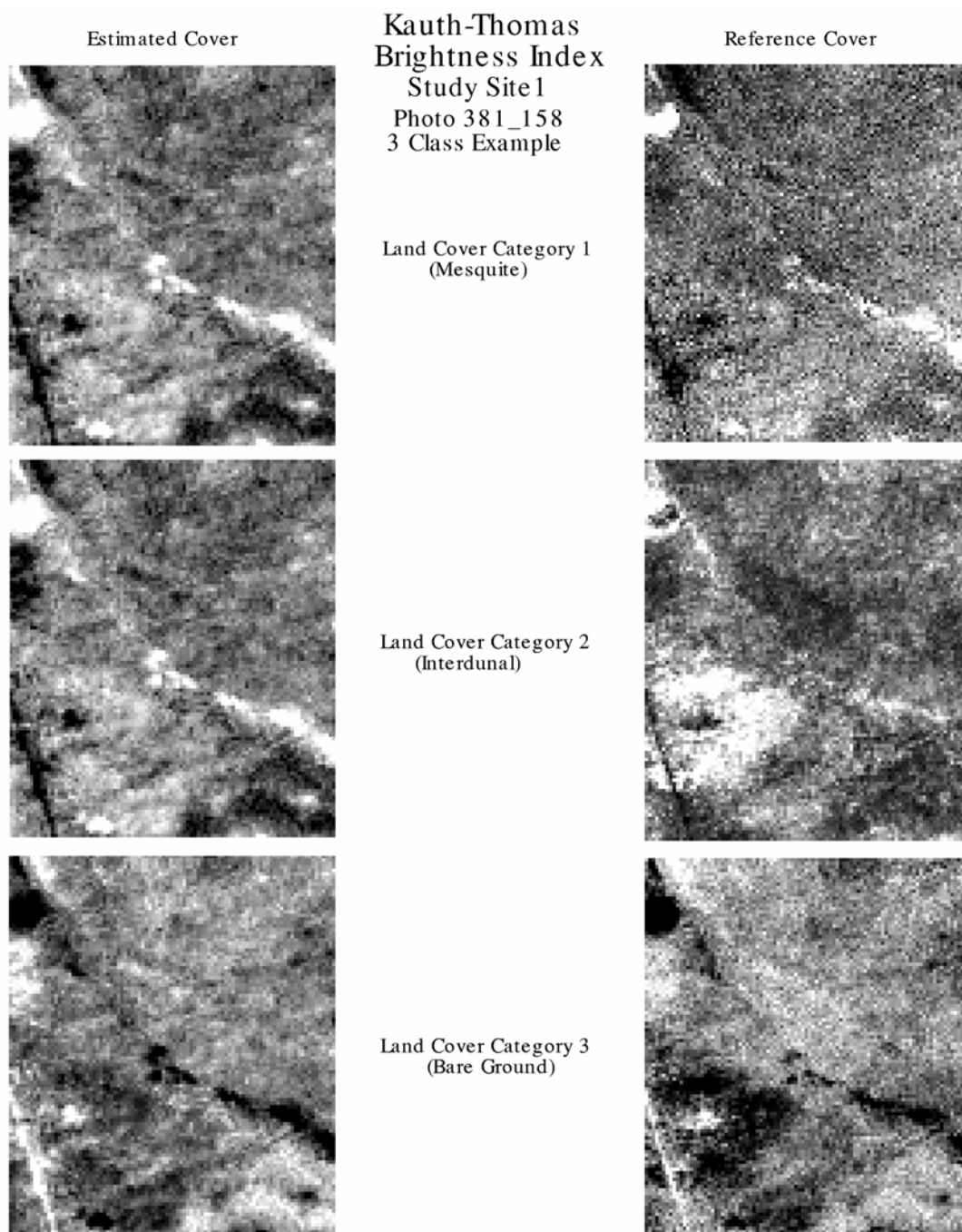


Figure 21. KTB correlation results for three land cover categories for photo 381_158 (left column is the KTB-derived estimate of abundance for each category, right column is the reference abundance for each category).

Table 20. Mean and standard deviation of abundance for three land-cover categories for photo 381_158, Study Site #1; estimated (spectral index correlations) versus reference.

KTB	ESTIMATED		REFERENCE	
	Mean	SD	Mean	SD
mesquite (1)	30.354	4.966	30.590	8.162
interdunal (2)	26.098	4.576	26.594	9.653
bare ground (3)	43.304	9.569	42.818	12.879
Totals	99.756		100.002	

ALBEDO	ESTIMATED		REFERENCE	
	Mean	SD	Mean	SD
mesquite (1)	30.531	4.60	30.590	8.162
interdunal (2)	26.473	5.127	26.594	9.653
bare ground (3)	44.160	9.783	42.818	12.879
Totals	101.164		100.002	

Table 21. Descriptive and inferential statistics of difference image (estimated [spectral index correlations] minus reference) for three land-cover categories for photo 381_158, Study Site #1.

KTB	t-value	P	CI	abs. diff.	Mean	SD
mesquite (1)	-3.94	0.0001	-0.3525, -0.1182	51209	-0.2353	6.1372
interdunal (2)	-5.85	0.0000	-0.6620, -0.3295	67410	-0.4958	8.7082
bare ground (3)	5.81	0.0000	0.3225, 0.6507	70342	0.4866	8.5945

Albedo	t-value	P	CI	abs. diff.	Mean	SD
mesquite (1)	-0.94	0.35	-0.1808, 0.0640	52636	-0.0584	6.4127
interdunal (2)	-1.50	0.13	-0.2793, 0.0371	65302	-0.1211	8.2851
bare ground (3)	17.08	0.0000	1.1883, 1.4965	67655	1.3424	8.0706

Two-class Results

Study Site #1 - Coppice Dunes Maneuver Areas

The same five recodes of land-cover categories into cover and bare ground categories that were used to evaluate demixing results were also used to evaluate results of correlation analysis. Table 22 presents the mean percentage or abundance of cover resulting from each of the different recodes and the two-class unsupervised classification using both Albedo- and KTB-derived indices for photo

381_158. The mean percentage or abundance of bare ground is not included in the table, but is equal to 100 percent minus the cover percent. Similar to the demixing results, the estimates of cover are very similar to the reference amounts. In addition, estimates derived from Albedo correlations and those derived from KTB correlations are also very similar. However, unlike demixing estimates, where the variance in cover estimates was significantly higher than the variance found in the reference images, variance in estimates derived from spectral index correlation was actually lower than the variance found in the reference images.

Table 22. Mean and standard deviation of cover abundance for photo 381_158, Study Site #1 using ISO2 and four recodes: estimated (spectral index correlations) versus reference.

KTB	ESTIMATED		REFERENCE	
	Mean	SD	Mean	SD
ISO2	37.358	6.819	38.480	9.751
1_25	24.171	4.064	24.307	7.530
12_35	35.004	6.214	35.776	9.158
13_45	48.881	8.799	49.178	11.874
14_5	73.342	8.964	73.588	12.927

ALBEDO	ESTIMATED		REFERENCE	
	Mean	SD	Mean	SD
ISO2	38.171	6.668	38.480	9.751
1_25	24.156	3.712	24.307	7.530
12_35	35.867	5.967	35.776	9.158
13_45	48.30	8.950	49.178	11.874
14_5	73.755	8.881	73.588	12.927

Table 23 summarizes the descriptive and inferential statistics that compare results for these five breakouts for photo 381_158. The null hypothesis was rejected for all possible recode combinations using KTB-derived estimates of cover, with the exception of bare ground using recode 1_25. However, recodes 1_25, 12_35, and ISO2 all appeared to estimate abundance of cover and bare ground with some degree of accuracy, as indicated by the relatively low mean differences and absolute differences. Recode 1_25 appeared to be the best performer, with absolute differences of 50487 (Cover) and 50457 (Bare Ground), although absolute differences for recode 12_35 and ISO2 were comparable.

The same three recodes, 1_25, 12_35, and ISO2, were also the best performers for Albedo-derived estimates. Using Albedo, the null hypothesis was accepted for cover using recode 12_35, for both cover and bare ground using recode 14_5,

and for bare ground using recode 1_25. Again, recode 1_25 appeared to be the best performer, with absolute differences of 52080 (Cover) and 52055 (Bare Ground), yet results from recodes 12_35 and ISO2 were comparable. Estimates of abundance derived from each of these brightness indices for these three recodes resulted in mean differences and confidence intervals that were close to zero or straddled zero. This would indicate that any recode that grouped land-cover Category #1 (Honey Mesquite) alone or in combination with land-cover Category #2 (Mesquite/Dune Edge/Shadow/Litter) to a single cover class, and grouped the remaining land-cover categories to bare ground should provide reasonable estimates of abundance of both cover and bare ground using either brightness index for photo 381_158.

The same recodes were evaluated for three additional photographs for Study Site #1 (Coppice Dunes Maneuver Areas) and are summarized in Table 24. Using KTB, results for photo 381_146 were similar, with recode 1_25 performing the best, as indicated by absolute differences of 30388 for both cover and bare ground. The null hypothesis was accepted for recode 1_25 for both Cover and Bare Ground also. Again, recode 12_35 and ISO2 also performed well, based on their relatively low sum of absolute differences.

Table 23. Descriptive and inferential statistics of difference image (estimated [spectral index correlations] minus reference) for two land-cover categories for photo 381_158, Study Site #1 using ISO2 and four recodes.

KTB	Recode	t-value	P	CI	abs. diff.	Mean	SD
Cover	ISO2	-17.54	0.0000	-1.2503, -0.9989	56175	-1.1246	6.5839
Bare Ground	ISO2	17.54	0.0000	0.9989, 1.2503	56175	1.1246	6.5839
Cover	1_25	-2.31	0.021	-0.2531, -0.0209	50487	-0.1370	6.0792
Bare Ground	1_25	0.62	0.53	-0.0791, 0.1531	50457	0.0370	6.0792
Cover	12_35	-12.47	0.0000	-0.8963, -0.6528	53886	-0.7746	6.3761
Bare Ground	12_35	12.47	0.0000	0.6528, 0.8963	53886	0.7746	6.3761
Cover	13_45	-3.99	0.0001	-0.4469, -0.1524	63653	-0.2996	7.7110
Bare Ground	13_45	3.99	0.0001	0.1524, 0.4469	63653	0.2996	7.7110
Cover	14_5	-2.64	0.0083	-0.4312, -0.0635	80807	-0.2474	9.6285
Bare Ground	14_5	2.64	0.0083	0.0635, 0.4312	80807	0.2474	9.6285

Albedo	Recode	t-value	P	CI	abs. diff.	Mean	SD
Cover	ISO2	-4.81	0.0000	-0.4380, -0.1842	55031	-0.3111	6.6481
Bare Ground	ISO2	4.81	0.0000	0.1842, 0.4380	55031	0.3111	6.6481
Cover	1_25	-2.47	0.013	-0.2735, -0.0316	52080	-0.1526	6.3335
Bare Ground	1_25	1.18	0.24	-0.0484, 0.1935	52055	0.0726	6.3335
Cover	12_35	1.40	0.16	-0.0358, 0.2140	53849	0.0891	6.5415
Bare Ground	12_35	3.31	0.0009	0.0860, 0.3358	53925	0.2109	6.5415
Cover	13_45	-12.27	0.0000	-1.0207, -0.7394	61395	-0.8800	7.3670
Bare Ground	13_45	12.27	0.0000	0.7394, 1.0207	61395	0.8800	7.3670
Cover	14_5	1.82	0.068	-0.0124, 0.3465	80221	0.1670	9.3992
Bare Ground	14_5	-1.82	0.068	-0.3465, 0.0124	80221	-0.1670	9.3992

Table 24. Descriptive and inferential statistics of difference image (estimated [spectral index correlations] minus reference) for two land-cover categories for photos 380_18, 381_144, and 381_146, Study Site #1 using ISO2 and four recodes.

KTB 380_18	Recode	t-value	P	CI	abs. diff.	Mean	SD
Cover	ISO2	-51.12	0.0000	-3.872, -3.586	84354	-3.728	8.132
Bare Ground	ISO2	51.12	0.0000	3.586, 3.872	84354	3.728	8.132
Cover	1_25	-59.47	0.0000	-4.486, -4.200	87627	-4.343	8.141
Bare Ground	1_25	64.95	0.0000	4.5995, 4.8858	90038	4.743	8.141
Cover	12_35	-46.38	0.0001	-3.508, -3.223	82301	-3.366	8.088
Bare Ground	12_35	46.38	0.0000	3.223, 3.508	82301	3.366	8.088
Cover	13_45	-24.32	0.092	-2.207, -1.878	88002	-2.042	9.363
Bare Ground	13_45	24.32	0.0000	1.878, 2.207	88002	2.042	9.363
Cover	14_5	27.05	0.0000	3.015, 3.486	131512	3.251	13.398
Bare Ground	14_5	-27.05	0.0000	-3.486, -3.015	131512	-3.251	13.398

Albedo 380_18	Recode	t-value	P	CI	abs. diff.	Mean	SD
Cover	ISO2	-41.65	0.000	-3.398, -3.092	85824	-3.245	8.686
Bare Ground	ISO2	40.36	0.0002	2.992, 3.297	85447	3.145	8.686
Cover	1_25	-70.54	0.0000	-5.679, -5.371	98268	-5.525	8.732
Bare Ground	1_25	71.82	0.0000	5.471, 5.779	98912	5.625	8.732
Cover	12_35	-53.38	0.0000	-4.303, -3.999	89665	-4.1510	8.668
Bare Ground	12_35	52.09,	0.0000	3.899, 4.203	89190	4.0510	8.667
Cover	13_45	-32.69	0.01	-2.973, -2.637	90366	-2.805	9.566
Bare Ground	13_45	32.69	0.011	2.637, 2.973	90366	2.805	9.566
Cover	14_5	31.88	0.0001	3.479, 3.935	126964	3.707	12.964
Bare Ground	14_5	-31.88	0.0002	-3.935, -3.479	126964	-3.707	12.964

KTB 381_144	Recode	t-value	P	CI	abs. diff.	Mean	SD
Cover	ISO2	-34.81	0.000	-4.449, -3.975	77499	-4.212	11.069
Bare Ground	ISO2	34.81	0.000	3.975, 4.449	77499	4.212	11.069
Cover	1_25	-34.44	0.000	-4.339, -3.872	82958	-4.106	10.905
Bare Ground	1_25	36.12	0.000	4.072, 4.539	83406	4.306	10.905
Cover	12_35	-33.55	0.000	-3.970, -3.532	71385	-3.751	10.227
Bare Ground	12_35	33.55	0.000	3.532, 3.970	71385	3.751	10.227
Cover	13_45	-23.26	0.000	-4.061, -3.429	101743	-3.745	14.731
Bare Ground	13_45	23.26	0.000	3.429, 4.061	101743	3.745	14.731
Cover	14_5	-17.68	0.000	-4.355, -3.486	147726	-3.921	20.289
Bare Ground	14_5	17.68	0.000	3.486, 4.355	147726	3.921	20.289

Albedo 381_144	Recode	t-value	P	CI	abs. diff.	Mean	SD
Cover	ISO2	-24.23	0.000	-3.136, -2.666	73058	-2.901	10.951
Bare Ground	ISO2	24.23	0.000	2.666, 3.136	73058	2.901	10.951
Cover	1_25	-34.74	0.000	-4.355, -3.889	81663	-4.122	10.855
Bare Ground	1_25	35.58	0.000	3.989, 4.455	81886	4.222	10.855
Cover	12_35	-38.92	0.000	-4.549, -4.112	70813	-4.331	10.178
Bare Ground	12_35	38.92	0.000	4.112, 4.549	70813	4.331	10.178
Cover	13_45	-24.25	0.000	-4.157, -3.535	98466	-3.846	14.510
Bare Ground	13_45	24.25	0.000	3.535, 4.157	98466	3.846	14.510
Cover	14_5	-16.89	0.000	-4.098, -3.245	143054	-3.672	19.882
Bare Ground	14_5	16.89	0.000	3.245, 4.098	143054	3.672	19.882

KTB 381_146	Recode	t-value	P	CI	abs. diff.	Mean	SD
Cover	ISO2	4.52	0.000	0.202, 0.510	33884	0.355	6.404
Bare Ground	ISO2	-3.25	0.001	-0.410, -0.102	33858	-0.255	6.404
Cover	1_25	-0.90	0.37	-0.202, 0.075	30388	-0.064	5.746
Bare Ground	1_25	0.90	0.37	-0.075, 0.202	30388	0.064	5.746
Cover	12_35	8.30	0.000	0.485, 0.786	33084	0.635	6.242
Bare Ground	12_35	-3.07	0.0021	-0.386, -0.085	32915	-0.235	6.242
Cover	13_45	22.15	0.000	1.897, 2.266	42213	2.081	7.659
Bare Ground	13_45	-22.15	0.000	-2.266, -1.897	42212	-2.081	7.659
Cover	14_5	55.18	0.000	6.879, 7.386	68732	7.133	10.532
Bare Ground	14_5	-55.18	0.000	-7.386, -6.879	68732	-7.133	10.532

Albedo 381_146	Recode	t-value	P	CI	abs. diff.	Mean	SD
Cover	ISO2	4.52	0.000	0.202, 0.510	33801	0.558	6.387
Bare Ground	ISO2	-3.25	0.0012	-0.410, -0.102	33757	-0.458	6.387
Cover	1_25	-4.64	0.000	-0.4614, - 0.1872	30126	-0.324	5.70
Bare Ground	1_25	-0.80	0.43	-0.1928, 0.0814	30138	-0.056	5.70
Cover	12_35	3.21	0.0013	0.095, 0.395	32719	0.245	6.223
Bare Ground	12_35	-4.52	0.000	-0.495, -0.195	32751	-0.345	6.223
Cover	13_45	29.72	0.000	2.574, 2.937	42826	2.754	7.557
Bare Ground	13_45	-29.72	0.000	-2.937, -2.574	42826	-2.754	7.557
Cover	14_5	66.65	0.000	8.023, 8.509	70519	8.266	10.106
Bare Ground	14_5	-66.65	0.000	-8.509, -8.023	70519	-8.266	10.106

However, recode 12_35 appeared to be the top performer for the two remaining photographs for Study Site #1, as indicated by the lowest sum of absolute differences. In photo 380_18, recodes 13_45, 1_25, and ISO2 had only slightly higher absolute differences, and the null hypothesis was accepted for the Cover category using recode 13_45. In photo 381_144, recode 12_5 and ISO2 performed relatively well compared to recode 12_35, but recode 13_45 had a considerably higher sum of absolute difference. The null hypothesis was rejected for all recode/category combinations in this photograph.

Results for albedo for the remaining three photographs for Study Site #1 were similar. Recode 1_25 was the top performer for photo 381_146 and the null hypothesis was accepted for this recode for Bare Ground. Recode 1_25 was the top performer for photo 381_144, with ISO2 and recode 1_25 also performing well. For photo 380_18, ISO2 was the top performer. The null hypothesis was rejected for all recode/category combinations for photos 381_144 and 380_18.

Table 25 shows the total sum of absolute differences for all four photographs for each recode tested for Study Site #1, using both Albedo- and KTB-derived estimates. Although recode 12_35 was not the top performer for each photograph and each index, it did perform relatively well for each photograph. Recode 12_35 also had the lowest sum of absolute differences for all photographs using KTB correlations for Cover (240656) and Bare Ground (240487). Therefore, it was

concluded that recode 12_35 was the best overall performer for both KTB and Albedo correlations for Study Site #1. Again, both recode 1_25 and ISO2 also performed relatively well.

Table 25. Total sum of absolute differences for all four photographs for each recode tested for Study Site #1.

Recode_Index Category	380_18	381_144	381_146	381_158	Totals
ISO2_KTB Cover	84354.00	77499.00	33884.00	56175.00	251912
ISO2_KTB Bare Ground	84354.00	77499.00	33858.00	56175.00	251886
ISO2_ALB Cover	85824.00	73058.00	33801.00	55031.00	247714
ISO2_ALB Bare Ground	85447.00	73058.00	33757.00	55031.00	247293
1_25_KTB Cover	87627.00	82958.00	30388.00	50487.00	251460
1_25_KTB Bare Ground	90038.00	83406.00	30388.00	50457.00	254289
1_25_ALB Cover	98268.00	81663.00	30126.00	52080.00	262137
1_25_ALB Bare Ground	98912.00	81886.00	30138.00	52055.00	262991
12_35_KTB Bare Ground	82301.00	71385.00	32915.00	53886.00	240487
12_35_ALB Cover	89665.00	70813.00	32719.00	53849.00	247046
12_35_ALB Bare Ground	89190.00	70813.00	32751.00	53925.00	246679
13_45_KTB Cover	88002.00	101743.00	42213.00	63653.00	295611
13_45_KTB Bare Ground	88002.00	101743.00	42212.00	63653.00	295610
13_45_ALB Cover	90366.00	98466.00	42826.00	61395.00	293053
13_45_ALB Bare Ground	90366.00	98466.00	42826.00	61395.00	293053
14_5_KTB Cover	131512.00	147726.00	68732.00	80807.00	428777
14_5_KTB Bare Ground	131512.00	147726.00	68732.00	80807.00	428777
14_5_ALB Cover	126964.00	143054.00	70519.00	80221.00	420758
14_5_ALB Bare Ground	126964.00	143054.00	70519.00	80221.00	420758
Totals	1849668	1826016	803304	1161303	5640291

Study Site #2 - Otero Mesa Grasslands

The same four recodes of a five-class unsupervised classification, as well as a two-class unsupervised classification were evaluated using KTB and Albedo correlations for Study Site #2. Table 26 presents results for these four photographs. Using KTB correlations, recode 14_5 was clearly the best performer for photos 386_122, 386_16, and 386_18, and was the second best performer for photo 386_124, where recode 1_25 performed the best. The null hypothesis was accepted for both Cover and Bare Ground using recode 12_35 and 1_25 in photo 386_122 and for Cover and Bare Ground using ISO2 in photo 386_124. In photo 386_16, the null hypothesis was accepted for all recode/category combinations, with the exception of recode 13_45, where P was only slightly below .05 (.048). In photo 386_18, the null hypothesis was also accepted for ISO2 and recode 12_35 for both Cover and Bare Ground, as well as for Bare Ground using recode 14_5. Recode 14_5 slightly overestimated Cover in all four photographs for Study Site #2.

Table 26. Descriptive and inferential statistics of difference image (estimated [spectral index correlations] minus reference) for two land-cover categories for photos 386_122, 386_124, 386_16, and 386_18, Study Site #2 using ISO2 and four recodes.

KTB							
386_122	Recode	t-value	P	CI	abs. diff.	Mean	SD
Cover	ISO2	17.22	0.000	3.874, 4.869	144139	4.371	22.187
Bare Ground	ISO2	-17.22	0.000	-4.869, -3.874	144139	-4.371	22.187
Cover	1_25	-0.93	0.35	-0.476, 0.169	81959	-0.153	14.365
Bare Ground	1_25	-0.89	0.37	-0.469, 0.176	82231	-0.147	14.365
Cover	12_35	0.25	0.80	-0.414, 0.536	135376	0.061	21.176
Bare Ground	12_35	-0.25	0.8	-0.536, 0.414	135376	-0.061	21.176
Cover	13_45	27.74	0.000	6.738, 7.763	138471	7.251	22.851
Bare Ground	13_45	-27.74	0.000	-7.763, -6.738	138471	-7.251	22.851
Cover	14_5	23.56	0.000	2.639, 3.118	32136	2.878	10.681
Bare Ground	14_5	-19.46	0.000	-2.618, -2.139	32976	-2.378	10.681

Albedo 386_122	Recode	t-value	P	CI	abs. diff.	Mean	SD
Cover	ISO2	32.50	0.000	7.516, 8.481	142054	7.998	21.515
Bare Ground	ISO2	-32.50	0.000	-8.481, -7.516	142054	-7.998	21.515
Cover	1_25	-3.96	0.0001	-0.956, -0.232	81264	-0.640	14.116
Bare Ground	1_25	3.96	0.0001	0.323, 0.956	81264	0.640	14.116
Cover	12_35	13.64	0.000	2.742, 3.663	133835	3.303	20.529
Bare Ground	12_35	-13.64	0.000	-3.663, -2.742	133835	-3.203	20.529
Cover	13_45	38.58	0.000	9.280, 10.274	137020	9.777	22.155
Bare Ground	13_45	-38.58	0.000	-10.274, -9.280	137020	-9.777	22.155
Cover	14_5	25.92	0.000	2.884, 3.356	33526	3.120	10.524
Bare Ground	14_5	-23.42	0.000	-3.056, -2.584	33138	-2.820	10.524

KTB 386_124	Recode	t-value	P	CI	abs. diff.	Mean	SD
Cover	ISO2	0.01	1.00	-0.408, 0.412	108226	0.002	18.144
Bare Ground	ISO2	-0.01	1.00	-0.412, 0.408	108226	-0.02	18.144
Cover	1_25	-5.70	0.000	-1.351, -0.660	83818	-1.005	15.296
Bare Ground	1_25	3.43	0.0006	0.260, 0.951	84188	0.605	15.296
Cover	12_35	-4.54	0.000	-1.473, -0.585	121917	-1.029	19.649
Bare Ground	12_35	4.54	0.000	0.585, 1.473	121917	1.029	19.649
Cover	13_45	39.21	0.000	6.757, 7.469	99704	7.113	15.746
Bare Ground	13_45	-39.21	0.000	-7.469, -6.757	99704	-7.113	15.746
Cover	14_5	2.21	0.027	0.045, 0.769	96600	0.068	8.705
Bare Ground	14_5	-2.21	0.027	-0.769, -0.045	96600	0.032	8.705

Albedo 386_124	Recode	t-value	P	CI	abs. diff.	Mean	SD
Cover	ISO2	-3.78	0.0002	-1.179, -0.373	104479	-0.776	17.840
Bare Ground	ISO2	3.78	0.0002	0.373, 1.179	108333	0.776	17.840
Cover	1_25	-1.63	0.10	-0.627, 0.058	83681	-0.284	15.141
Bare Ground	1_25	3.35	0.0008	0.242, 0.927	83257	0.584	15.141
Cover	12_35	-3.20	0.0014	-1.154, -0.277	118844	-0.715	19.418
Bare Ground	12_35	3.20	0.0014	0.277, 1.154	118844	0.715	19.418
Cover	13_45	8.27	0.000	1.106, 1.794	87426	1.450	15.216
Bare Ground	13_45	-8.27	0.000	-1.794, -1.106	87426	-1.450	15.216
Cover	14_5	-15.48	0.000	-2.987, -2.315	90528	-0.152	8.713
Bare Ground	14_5	15.48	0.000	2.315, 2.987	90528	0.052	8.713

KTB							
386_16	Recode	t-value	P	CI	abs. diff.	Mean	SD
Cover	ISO2	0.83	0.41	-0.348, 0.856	66997	0.254	20.096
Bare Ground	ISO2	-0.83	0.41	-0.856, 0.348	66997	-0.254	20.096
Cover	1_25	-0.56	0.58	-0.450, 0.251	30844	-0.099	11.703
Bare Ground	1_25	0.56	0.58	-0.251, 0.450	30844	0.099	11.703
Cover	12_35	-1.10	0.27	-0.843, 0.238	57477	-0.303	18.034
Bare Ground	12_35	1.10	0.27	-0.238, 0.843	57477	0.303	18.034
Cover	13_45	1.97	0.048	0.004, 1.245	71560	0.625	20.711
Bare Ground	13_45	-1.97	0.048	-1.245, -0.004	71560	-0.625	20.711
Cover	14_5	0.52	0.61	-0.192, 0.329	26814	0.068	8.705
Bare Ground	14_5	0.24	0.81	-0.229, 0.292	26919	0.032	8.705

Albedo							
386_16	Recode	t-value	P	CI	abs. diff.	Mean	SD
Cover	ISO2	0.20	0.84	-0.544, 0.668	66669	0.062	20.214
Bare Ground	ISO2	-0.20	0.84	-0.668, 0.544	66669	-0.062	20.214
Cover	1_25	0.72	0.47	-0.221, 0.479	31393	0.129	11.675
Bare Ground	1_25	-0.72	0.47	-0.479, 0.221	31393	-0.129	11.675
Cover	12_35	-3.00	0.0027	-1.381, -0.290	57414	-0.836	18.205
Bare Ground	12_35	3.00	0.0027	0.290, 1.381	57414	0.836	18.205
Cover	13_45	3.97	0.0001	0.636, 1.877	71217	1.257	20.708
Bare Ground	13_45	-3.97	0.0001	-1.877, -0.636	71217	-1.257	20.708
Cover	14_5	-1.14	0.25	-0.413, 0.109	27142	-0.152	8.713
Bare Ground	14_5	0.39	0.70	-0.209, 0.313	27033	0.052	8.713

KTB							
386_18	Recode	t-value	P	CI	abs. diff.	Mean	SD
Cover	ISO2	0.04	0.97	-0.683, 0.712	106594	0.014	25.223
Bare Ground	ISO2	-0.04	0.97	-0.712, 0.683	106594	-0.014	25.223
Cover	1_25	-2.14	0.032	-0.673, -0.029	36958	-0.351	11.634
Bare Ground	1_25	2.14	0.032	0.029, 0.673	36958	0.351	11.634
Cover	12_35	-1.73	0.083	-1.250, 0.077	97823	-0.587	23.997
Bare Ground	12_35	1.73	0.083	-0.077, 1.250	97823	0.587	23.997
Cover	13_45	-2.43	0.015	-1.432, -0.154	97285	-0.793	23.10
Bare Ground	13_45	2.43	0.015	0.154, 1.432	97285	0.793	23.10
Cover	14_5	4.88	0.000	0.305, 0.714	24244	0.510	7.398
Bare Ground	14_5	-1.05	0.29	-0.314, 0.095	24775	-0.110	7.398

Albedo 386_18	Recode	t-value	P	CI	abs. diff.	Mean	SD
Cover	ISO2	0.87	0.38	-0.385, 1.00	105982	0.307	25.029
Bare Ground	ISO2	-0.97	0.38	-1.00, 0.385	105982	-0.307	25.029
Cover	1_25	-2.95	0.0032	-0.798, -0.160	36829	-0.479	11.523
Bare Ground	1_25	2.95	0.0032	0.160, 0.798	36829	0.479	11.523
Cover	12_35	-0.56	0.58	-0.845, 0.470	97570	-0.188	23.770
Bare Ground	12_35	1.75	0.080	-0.070, 1.245	97237	0.588	23.770
Cover	13_45	0.32	0.75	-0.531, 0.739	96462	0.104	22.963
Bare Ground	13_45	-0.32	0.75	-0.739, 0.531	96462	-0.104	22.963
Cover	14_5	0.68	0.50	-0.133, 0.275	24657	0.071	7.369
Bare Ground	14_5	-0.68	0.50	-0.275	24657	-0.071	7.369

Results for Albedo-derived estimates were the same as KTB-derived estimates in terms of the top performing recode for each photograph. The null hypothesis was rejected for all recode/category combinations for photo 386_122 and was only accepted for Cover using recode 1_25 in photo 386_124. However, the null hypothesis was accepted for several recodes in both photos 386_16 and 386_18.

Table 27 summarizes the total sum of absolute differences for all four photographs for both KTB- and Albedo-derived estimates for each recode tested for Study Site #2. Recode 14_5 was identified as the best performer for Study Site #2 using KTB correlations, based on the lowest sum of absolute differences for all photographs. The same recode was also identified as the best performer using Albedo.

Table 27. Total sum of absolute differences for all four photographs for each recode tested for Study Site #2.

Recode_Index Category	386_122	386_124	386_16	386_18	Totals
ISO2_KTB Cover	144139.00	108226.00	66997.00	106594.00	425956
ISO2_KTB Bare Ground	144139.00	108226.00	66997.00	106594.00	425956
ISO2_ALB Cover	142054.00	104479.00	66669.00	105982.00	419184
ISO2_ALB Bare Ground	142054.00	108333.00	66669.00	105982.00	423038
1_25_KTB Cover	81959.00	83818.00	30844.00	36958.00	233579
1_25_KTB Bare Ground	82231.00	84188.00	30844.00	36958.00	234221
1_25_ALB Cover	81264.00	83681.00	31393.00	36829.00	233167
1_25_ALB Bare Ground	81264.00	83257.00	31393.00	36829.00	232743
12_35_KTB Cover	135376.00	121917.00	57477.00	97823.00	412593
12_35_KTB Bare Ground	135376.00	121917.00	57477.00	97823.00	412593
12_35_ALB Cover	133835.00	118844.00	57414.00	97570.00	407663
12_35_ALB Bare Ground	133835.00	118844.00	57414.00	97237.00	407330
13_45_KTB Cover	138471.00	99704.00	71560.00	97285.00	407020
13_45_KTB Bare Ground	138471.00	99704.00	71560.00	97285.00	407020
13_45_ALB Cover	137020.00	87426.00	71217.00	96462.00	392125
13_45_ALB Bare Ground	137020.00	87426.00	71217.00	96462.00	392125
14_5_KTB Cover	32136.00	96600.00	26814.00	24244.00	179794
14_5_KTB Bare Ground	32976.00	96600.00	26919.00	24775.00	181270
14_5_ALB Cover	33526.00	90528.00	27142.00	24657.00	175853
14_5_ALB Bare Ground	33138.00	90528.00	27033.00	24657.00	175356
Totals	2120284	1994246	1015050	1449006	6578586

Study Site #3 - Controlled Burn Area/Otero Mesa Foothills

The same two- class breakouts (Cover vs. Bare Ground) were evaluated for all four photographs for Study Site #3 and are summarized in Table 28. Unlike Study Sites #1 and #2, where different recodes performed best for different photographs, recode 14_5 was clearly the best performer in all four photographs for both KTB and Albedo correlations. Using KTB-derived estimates, the null hypothesis was accepted for Cover and Bare Ground using recode 12_35 in photo 388_45 and using ISO2 in photo 388_90. The null hypothesis was accepted for several recode/category combinations in both photos 388_47 and 388_88. Similarly, using Albedo-derived estimates, the null hypothesis was rejected for all recode/category combinations in photo 388_45 and 388_88. However, the null hypothesis was accepted for several recode/category combinations in photos 388_47 and 388_90. Table 29 lists the total sum of absolute differences for both KTB and Albedo correlations for all four photographs for Study Site #3. Again, recode 14_5 was clearly identified as the top performer for Study Site #3 based on the lowest sum of absolute differences for Cover (293890) and Bare Ground (293475) using Albedo-derived estimates of abundance.

Table 28. Descriptive and inferential statistics of difference image (estimated [spectral index correlations] minus reference) for two land-cover categories for photos 388_45, 388_47, 388_88, and 388_90, Study Site #3 using ISO2 and four recodes.

KTB 388_45	Recode	t-value	P	CI	abs. diff.	Mean	SD
Cover	ISO2	2.02	0.044	0.008, 0.575	139115	0.291	15.433
Bare Ground	ISO2	-2.02	0.044	-0.575, -0.008	139115	-0.291	15.433
Cover	1_25	-4.22	0.000	-0.819, -0.299	130347	-0.559	14.140
Bare Ground	1_25	3.46	0.0005	0.199, 0.719	130389	0.459	14.140
Cover	12_35	-0.48	0.63	-0.377, 0.229	152435	-0.074	16.516
Bare Ground	12_35	0.48	0.63	-0.229, 0.377	152435	0.074	16.516
Cover	13_45	-9.89	0.000	-1.545, -1.034	125907	-1.289	13.918
Bare Ground	13_45	9.89	0.000	1.034, 1.545	125907	1.289	13.918
Cover	14_5	-6.90	0.000	-0.7718, -0.4301	78954	-0.601	9.306
Bare Ground	14_5	6.90	0.000	0.4301, 0.7718	78954	0.601	9.306

Albedo 388_45	Recode	t-value	P	CI	abs. diff.	Mean	SD
Cover	ISO2	5.09	0.000	0.435, 0.99	132712	0.707	14.845
Bare Ground	ISO2	-5.09	0.000	-0.980, -0.435	132712	-0.707	14.845
Cover	1_25	-7.30	0.000	-1.187, -0.684	125525	-0.935	13.676
Bare Ground	1_25	3.40	0.0007	0.184, 0.687	125675	0.435	13.676
Cover	12_35	1.91	0.0056	-0.007, 0.575	145154	0.284	15.861
Bare Ground	12_35	-2.58	0.0098	-0.675, -0.093	145123	-0.384	15.861
Cover	13_45	-6.93	0.000	-1.120, -0.626	119872	-0.873	13.448
Bare Ground	13_45	6.93	0.000	0.626, 1.120	119872	0.873	13.448
Cover	14_5	-2.17	0.030	-0.3590, -0.0180	77954	-0.1885	9.285
Bare Ground	14_5	4.47	0.000	0.2180, 0.5590	78163	0.3885	9.285

KTB 388_47	Recode	t-value	P	CI	abs. diff.	Mean	SD
Cover	ISO2	0.65	0.51	-0.162, 0.323	142690	0.081	14.011
Bare Ground	ISO2	-0.65	0.51	-0.323, 0.162	142690	-0.081	14.011
Cover	1_25	-1.25	0.21	-0.374, 0.083	138124	-0.146	13.219
Bare Ground	1_25	1.25	0.21	-0.083, 0.374	138124	0.146	13.219
Cover	12_35	-1.71	0.088	-0.481, 0.033	154796	-0.224	14.843
Bare Ground	12_35	0.26	0.80	-0.223, 0.291	154821	0.034	14.843
Cover	13_45	1.23	0.22	-0.091, 0.400	142103	0.154	14.174
Bare Ground	13_45	-2.03	0.042	-0.500, -0.009	142077	-0.254	14.174
Cover	14_5	-2.94	0.0033	-0.520, -0.104	113875	-0.312	12.007
Bare Ground	14_5	1.06	0.29	-0.096, 0.320	113543	0.112	12.007

Albedo 388_47	Recode	t-value	P	CI	abs. diff.	Mean	SD
Cover	ISO2	-1.72	0.086	-0.448, 0.030	139445	-0.209	13.800
Bare Ground	ISO2	0.07	0.94	-0.230, 0.248	139455	0.009	13.800
Cover	1_25	2.78	0.0055	0.095, 0.550	136218	0.322	13.144
Bare Ground	1_25	-7.09	0.000	-1.050, -0.595	136975	-0.822	13.144
Cover	12_35	2.13	0.033	0.022, 0.520	148764	0.271	14.377
Bare Ground	12_35	1.02	0.31	-0.120, 0.378	148605	0.129	14.377
Cover	13_45	-1.12	0.26	-0.376, 0.103	138437	-0.137	13.843
Bare Ground	13_45	0.30	0.76	-0.203, 0.276	138415	0.037	13.843
Cover	14_5	-6.26	0.000	-0.858, -0.449	113283	-0.653	11.829
Bare Ground	14_5	2.42	0.015	0.049, 0.458	112661	0.253	11.829

KTB 388_47	Recode	t-value	P	CI	abs. diff.	Mean	SD
Cover	ISO2	0.65	0.51	-0.162, 0.323	142690	0.081	14.011
Bare Ground	ISO2	-0.65	0.51	-0.323, 0.162	142690	-0.081	14.011
Cover	1_25	-1.25	0.21	-0.374, 0.083	138124	-0.146	13.219
Bare Ground	1_25	1.25	0.21	-0.083, 0.374	138124	0.146	13.219
Cover	12_35	-1.71	0.088	-0.481, 0.033	154796	-0.224	14.843
Bare Ground	12_35	0.26	0.80	-0.223, 0.291	154821	0.034	14.843
Cover	13_45	1.23	0.22	-0.091, 0.400	142103	0.154	14.174
Bare Ground	13_45	-2.03	0.042	-0.500, -0.009	142077	-0.254	14.174
Cover	14_5	-2.94	0.0033	-0.520, -0.104	113875	-0.312	12.007
Bare Ground	14_5	1.06	0.29	-0.096, 0.320	113543	0.112	12.007

Albedo 388_47	Recode	t-value	P	CI	abs. diff.	Mean	SD
Cover	ISO2	-1.72	0.086	-0.448, 0.030	139445	-0.209	13.800
Bare Ground	ISO2	0.07	0.94	-0.230, 0.248	139455	0.009	13.800
Cover	1_25	2.78	0.0055	0.095, 0.550	136218	0.322	13.144
Bare Ground	1_25	-7.09	0.000	-1.050, -0.595	136975	-0.822	13.144
Cover	12_35	2.13	0.033	0.022, 0.520	148764	0.271	14.377
Bare Ground	12_35	1.02	0.31	-0.120, 0.378	148605	0.129	14.377
Cover	13_45	-1.12	0.26	-0.376, 0.103	138437	-0.137	13.843
Bare Ground	13_45	0.30	0.76	-0.203, 0.276	138415	0.037	13.843
Cover	14_5	-6.26	0.000	-0.858, -0.449	113283	-0.653	11.829
Bare Ground	14_5	2.42	0.015	0.049, 0.458	112661	0.253	11.829

KTB 388_88	Recode	t-value	P	CI	abs. diff.	Mean	SD
Cover	ISO2	-2.47	0.014	-0.551, -0.063	71757	-0.307	11.294
Bare Ground	ISO2	-1.55	0.12	-0.437, 0.051	71541	-0.193	11.294
Cover	1_25	-0.40	0.69	-0.302, 0.199	74455	-0.051	11.579
Bare Ground	1_25	0.40	0.69	-0.199, 0.302	74455	0.051	11.579
Cover	12_35	-1.52	0.13	-0.451, 0.058	75624	-0.197	11.780
Bare Ground	12_35	-0.02	0.98	-0.258, 0.251	75631	-0.003	11.780
Cover	13_45	4.14	0.000	0.267, 0.748	70485	0.508	11.129
Bare Ground	13_45	-1.69	0.091	-0.448, 0.033	70571	-0.208	11.129
Cover	14_5	8.10	0.000	0.748, 1.226	66069	0.987	11.056
Bare Ground	14_5	-4.00	0.0001	-0.726, -0.248	66494	-0.487	11.056

Albedo 388_88	Recode	t-value	P	CI	abs. diff.	Mean	SD
Cover	ISO2	-2.89	0.0038	-0.607, -0.116	71647	-0.362	11.356
Bare Ground	ISO2	2.89	0.0038	0.116, 0.607	71647	0.362	11.356
Cover	1_25	3.62	0.0003	0.212, 0.710	74345	0.461	11.547
Bare Ground	1_25	-2.05	0.040	-0.510, -0.012	74115	-0.261	11.547
Cover	12_35	3.97	0.0001	0.261, 0.770	75706	0.515	11.792
Bare Ground	12_35	-3.97	0.0001	-0.770, -0.261	75706	-0.515	11.792
Cover	13_45	-2.95	0.0032	-0.606, -0.122	70487	-0.364	11.216
Bare Ground	13_45	2.95	0.0032	0.122, 0.606	70487	0.364	11.216
Cover1	14_5	6.19	0.000	0.513, 0.990	64795	0.752	11.025
Bare Ground	14_5	-6.19	0.000	-0.990, -0.513	64795	-0.752	11.025

KTB 388_90	Recode	t-value	P	CI	abs. diff.	Mean	SD
Cover	ISO2	-1.37	0.17	-0.477, 0.084	50946	-0.196	11.004
Bare Ground	ISO2	1.37	0.17	-0.084, 0.477	50946	0.196	11.004
Cover	1_25	3.36	0.0008	0.191, 0.726	48459	0.459	10.487
Bare Ground	1_25	-3.36	0.0008	-0.726, -0.191	48459	-0.459	10.487
Cover	12_35	2.02	0.043	0.010, 0.620	55448	0.315	11.976
Bare Ground	12_35	-2.02	0.043	-0.620, -0.010	55448	-0.315	11.976
Cover	13_45	-5.31	0.000	-0.994, -0.458	48922	-0.726	10.524
Bare Ground	13_45	4.23	0.000	0.379, 1.032	48922	0.726	10.524
Cover	14_5	-2.59	0.0095	-0.510, -0.071	39274	-0.291	8.613
Bare Ground	14_5	2.59	0.0095	0.071, 0.510	39274	0.291	8.613

Albedo 388_90	Recode	t-value	P	CI	abs. diff.	Mean	SD
Cover	ISO2	3.10	0.0020	0.171, 0.759	53254	0.465	11.535
Bare Ground	ISO2	-3.10	0.0020	-0.759, -0.171	53254	-0.465	11.535
Cover	1_25	0.26	0.79	-0.243, 0.318	50978	0.037	11.001
Bare Ground	1_25	0.44	0.66	-0.218, 0.343	50935	0.061	11.001
Cover	12_35	-4.23	0.000	-1.032, -0.379	60033	-0.706	12.819
Bare Ground	12_35	4.23	0.000	0.379, 1.032	60033	0.706	12.819
Cover	13_45	2.17	0.030	0.029, 0.573	49040	0.301	10.668
Bare Ground	13_45	-2.17	0.030	-0.573, -0.029	49040	-0.301	10.668
Cover	14_5	-1.36	0.18	-0.358, 0.065	37857	-0.146	8.298
Bare Ground	14_5	1.36	0.18	-0.065, 0.358	37857	0.146	8.298

Table 29. Total sum of absolute differences for all four photographs for each recode tested for Study Site #3.

Recode_Index Category	388_45	388_47	388_88	388_90	Totals
ISO2_KTB Cover	139115.00	142689.00	71757.00	50946.00	404507
ISO2_KTB Bare Ground	139115.00	142689.00	71541.00	50946.00	404291
ISO2_ALB Cover	132711.00	139445.00	71647.00	53254.00	397057
ISO2_ALB Bare Ground	132711.00	139455.00	71647.00	53254.00	397067
1_25_KTB Cover	130347.00	138124.00	74455.00	48459.00	391385
1_25_KTB Bare Ground	130389.00	138124.00	74455.00	48459.00	391427
1_25_ALB Cover	125524.00	136218.00	74345.00	50978.00	387065
1_25_ALB Bare Ground	125674.00	136975.00	74115.00	50935.00	387699
12_35_KTB Cover	152435.00	154795.00	75624.00	55448.00	438302
12_35_KTB Bare Ground	152435.00	154821.00	75631.00	55448.00	438335
12_35_ALB Cover	145154.00	148764.00	75706.00	60033.00	429657
12_35_ALB Bare Ground	145123.00	148605.00	75706.00	60033.00	429467
13_45_KTB Cover	125907.00	142103.00	70485.00	48922.00	387417
13_45_KTB Bare Ground	125907.00	142077.00	70571.00	48922.00	387477
13_45_ALB Cover	119872.00	138436.00	70487.00	49040.00	377835
13_45_ALB Bare Ground	119872.00	138415.00	70487.00	49040.00	377814
14_5_KTB Cover	78954.00	113874.00	66069.00	39274.00	298171
14_5_KTB Bare Ground	78954.00	113542.00	66494.00	39274.00	298264
14_5_ALB Cover	77954.00	113284.00	64795.00	37857.00	293890
14_5_ALB Bare Ground	78163.00	112660.00	64795.00	37857.00	293475
Totals	2456316	2735095	1430812	988379	7610602

Spatial Extrapolation

Similar to spectral demixing extrapolation analysis, a correlation between two spectral brightness indices (KTB and Albedo) and percent cover/bare ground was developed by sampling three of the four photographs for each site, as described in the methodology. The regression equation explaining the relationship between the spectral brightness index (independent variable) and percent cover/bare ground (dependent variable) based on a sample of three photographs was then used to estimate abundance of vegetative cover for an area matching the footprint of the fourth photograph. To accomplish this, both Albedo and KTB values were calculated for every pixel of a TM subset matching the footprint of the fourth photograph. Based on evaluations of correlation analysis for individual photographs, only the two best performing recodes for each site were tested for extrapolating results from three photographs to the fourth. The same three sample photographs and remaining test photograph that were used to evaluate demixing extrapolation were also used to evaluate correlation extrapolation for each site.

Table 30 presents inferential and descriptive statistics for Study Site #1. Recode 12_35 and the two-class unsupervised classification were tested and extrapolated using Albedo and KTB. Both recodes performed relatively well, with mean differences between the estimated and the reference abundance ranging from -1.7 percent (KTB/12_35/Cover) to 0.44 percent (KTB/ISO2/Bare Ground). Recode 12_35 performed the best for both Albedo and KTB, as indicated by the lowest sum of absolute differences. Mean differences were between 0 and 1 percent for Albedo and 1 and 2 percent for KTB. The null hypothesis was rejected for all recode/land-cover category combinations. The top performing recode/index combination was Albedo/12_35, based on the lowest sum of absolute differences, although all recode/index combinations were comparable in performance.

Figures 22 through 25 contain images of reference abundance, estimated abundance derived directly from samples of photo 381_158 only, and extrapolated estimates of abundance for the same area derived from sampling the other three photographs in Study Site #1. Relative to visual inspection of demixing estimates, patterns for single-photo and extrapolated estimates were much more similar to reference images and to each other for both Albedo- and KTB-derived estimates. Visual inspection seemed to indicate that both recodes performed well for both single-photo and extrapolated estimates. Statistics confirmed that all recodes were similar in performance.

Table 30. Descriptive and inferential statistics of difference image (estimated [extrapolated spectral index correlations] minus reference abundance) for two land-cover categories for photo 381_158 for Study Site #1 using recode 12_35 and ISO2.

KTB	Recode	t-value	P	CI	abs. diff.	Mean	SD
Cover	12_35	-28.99	0.0000	-1.9208, -1.6774	55727	-1.799	6.373
Bare Ground	12_35	28.99	0.0000	1.6774, 1.9208	55727	1.7990	6.3736
Cover	ISO2	-22.22	0.0000	-1.5672, -1.3131	56944	-1.4401	6.6546
Bare Ground	ISO2	6.79	0.0000	0.3131, 0.5672	55727	0.4401	6.6546

Albedo	Recode	t-value	P	CI	abs. diff.	Mean	SD
Cover	12_35	5.09	0.0000	0.1989, 0.4481	53946	0.3235	6.5278
Bare Ground	12_35	1.20	0.0023	-0.0481, 0.2011	53985	0.0765	6.5278
Cover	ISO2	-5.14	0.0000	-0.4606, -0.2061	55017	-0.3333	6.6657
Bare Ground	ISO2	-7.22	0.0000	-0.5964, -0.3417	55012	-0.4690	6.6708

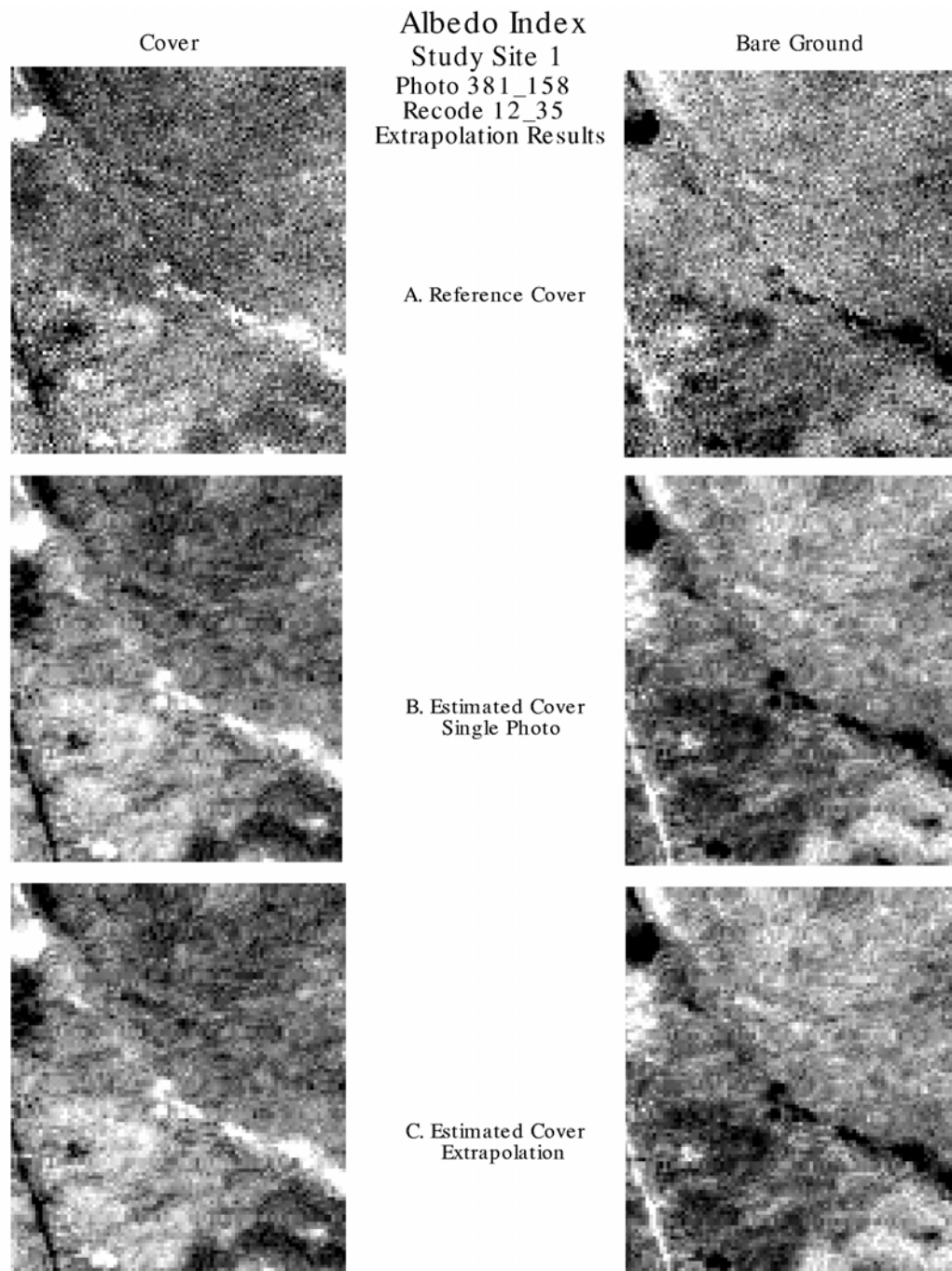


Figure 22. Albedo correlation results for two land cover categories for photo 381_158 using recode 12_35.

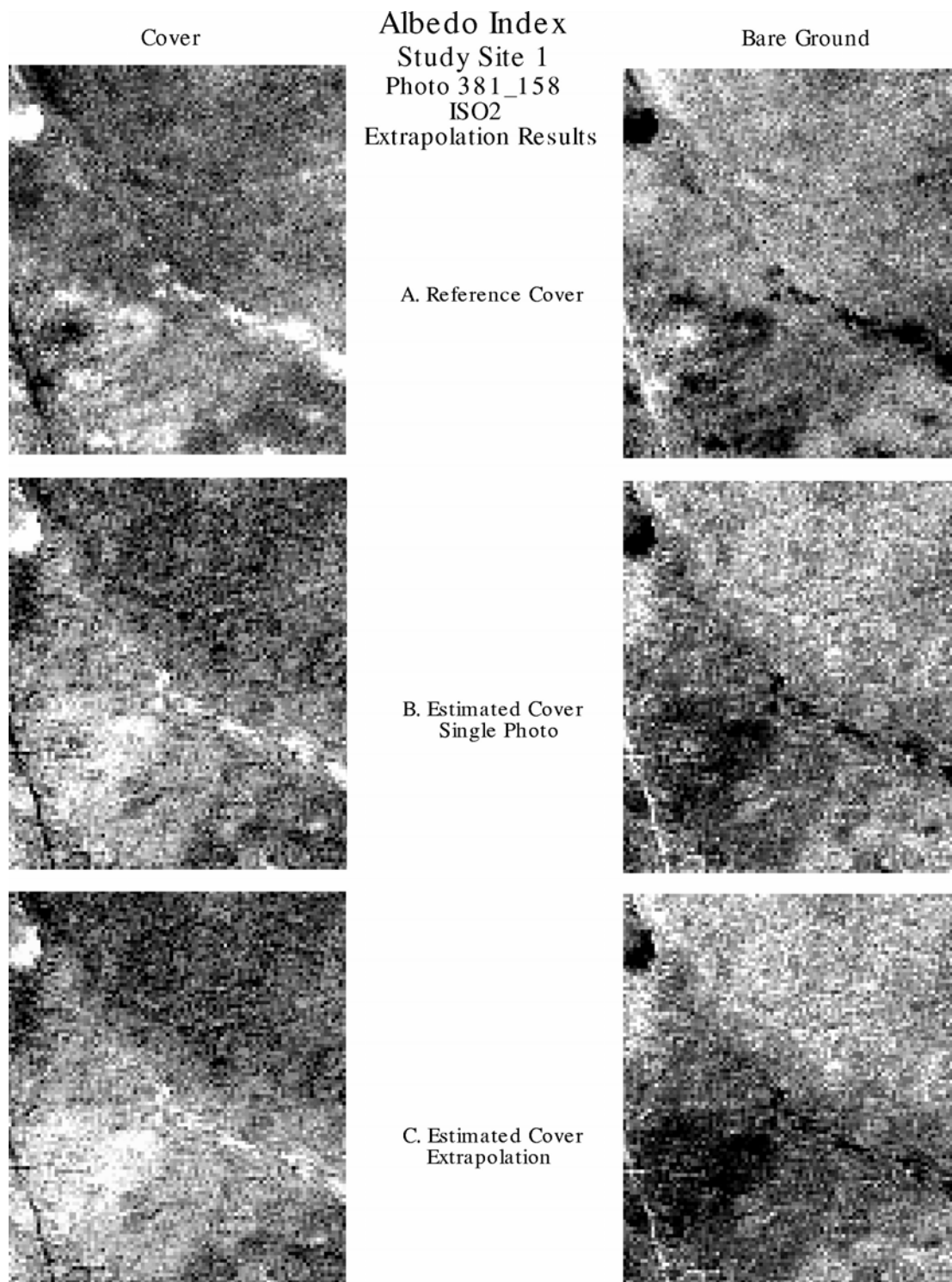


Figure 23. Albedo correlation results for two land cover categories for photo 381_158 using recode 12_35.

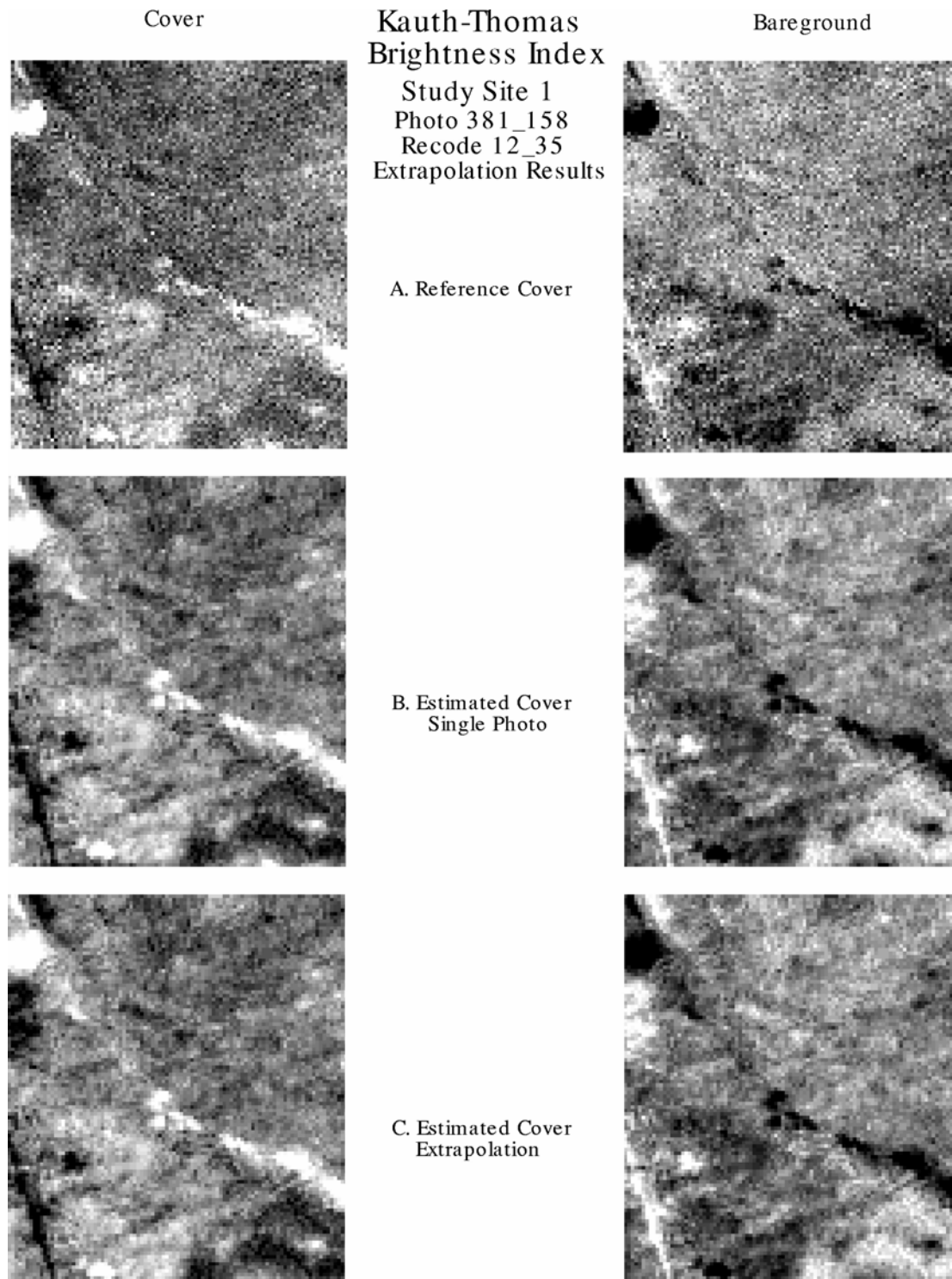


Figure 24. KTB correlation results for two land cover categories for photo 381_158 using recode 12_35.

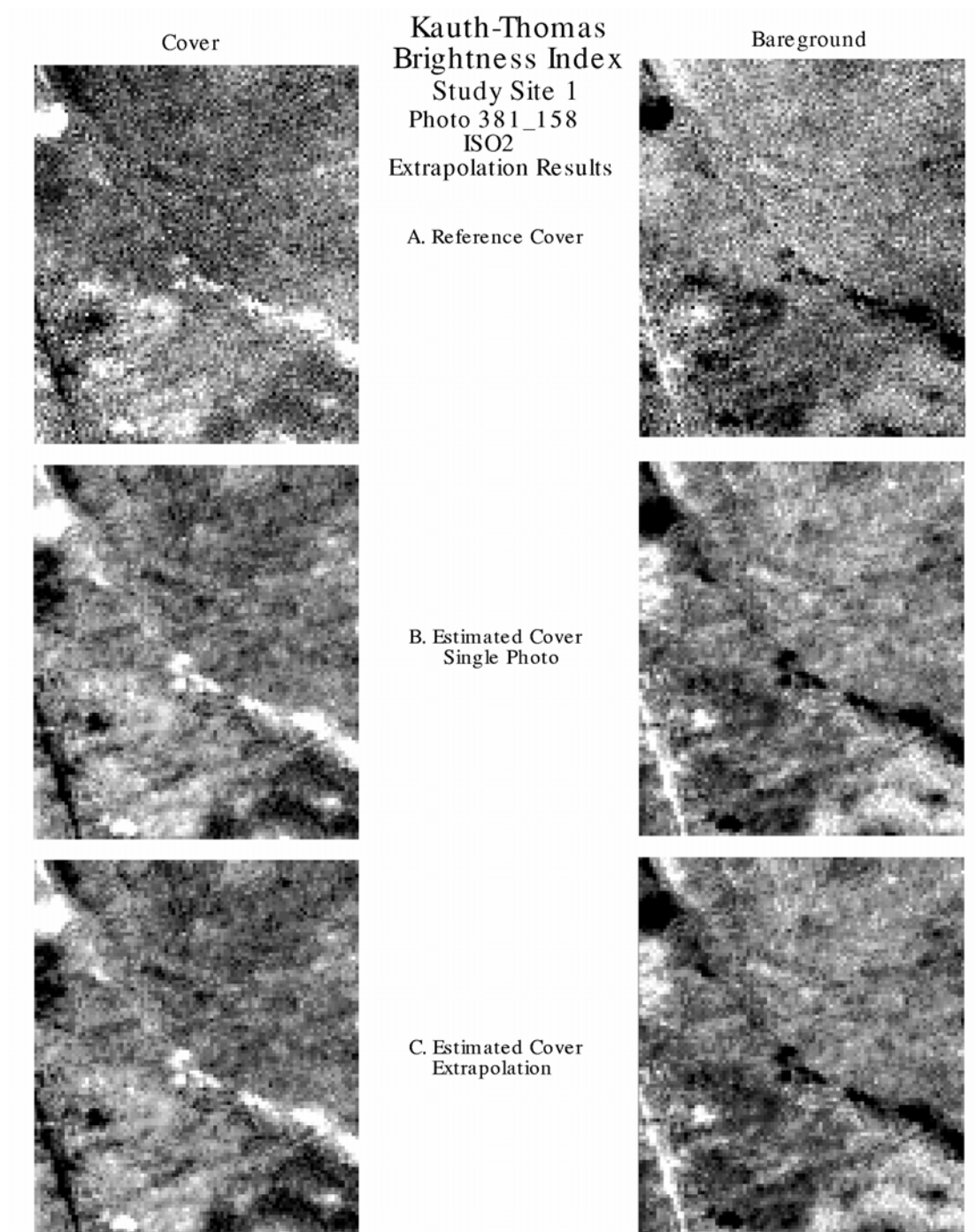


Figure 25. KTB correlation results for two land cover categories for photo 381_158 using ISO2.

Table 31 summarizes the inferential and descriptive statistics for Study Site #2. Recodes 14_5 and 1_25 were used to evaluate extrapolated estimates of cover and bare ground using KTB and Albedo. Mean differences ranged from -7.9 percent (KTB/14_5/Bare Ground) to 7.7 percent (KTB/14_5/Cover). Recode 1_25 performed the best for both Albedo and KTB, as indicated by the lowest sum of absolute differences. Mean differences were between -7.75 and 7.55 percent for Albedo and -7.91 and 7.79 percent for KTB. Similar to Study Site #1, the null hypothesis was rejected for all recode/land-cover category combinations, but variance of the mean difference was considerably higher than Study Site #1. The top performing recode/index combination was Albedo/1_25.

Table 31. Descriptive and inferential statistics of difference image (estimated [extrapolated spectral index correlations] abundance minus reference abundance) for two land-cover categories for photo 386_124 for Study Site #2 using recode 14_5 and 1_25.

KTB	Recode	t-value	P	CI	abs. diff.	Mean	SD
Cover	14_5	33.32	0.0000	7.334, 8.252	81084	7.793	20.304
Bare Ground	14_5	-33.92	0.0000	-8.369, -7.454	80790	-7.911	20.245
Cover	1_25	-20.30	0.0000	-4.078, -3.360	75804	-3.719	15.904
Bare Ground	1_25	20.00	0.0000	3.296, 4.013	75853	3.655	15.859

Albedo	Recode	t-value	P	CI	abs. diff.	Mean	SD
Cover	14_5	32.71	0.0000	7.098, 8.003	79879	7.550	20.034
Bare Ground	14_5	-32.28	0.0000	-8.223, -7.281	79532	-7.752	20.844
Cover	1_25	-23.97	0.0000	-4.702, -3.991	74978	-4.346	15.737
Bare Ground	1_25	22.37	0.0000	3.966, 4.727	74978	4.347	16.864

Images of reference abundance, estimated abundance derived directly from samples of photo 386_124 only, and extrapolated estimates of abundance for the same area derived from sampling the other three photographs in Study Site #2 are contrasted in Figures 26 through 29. Visual examination indicated that the results appeared similar between Albedo- and KTB-derived estimates for the same recode tested. However, there were significant differences between the two recodes. Single-photo and extrapolated results for recode 14_5 appeared more similar to reference images than estimates derived from recode 1_25. In general, extrapolated results were similar to single-photo results for both indices and both recodes.

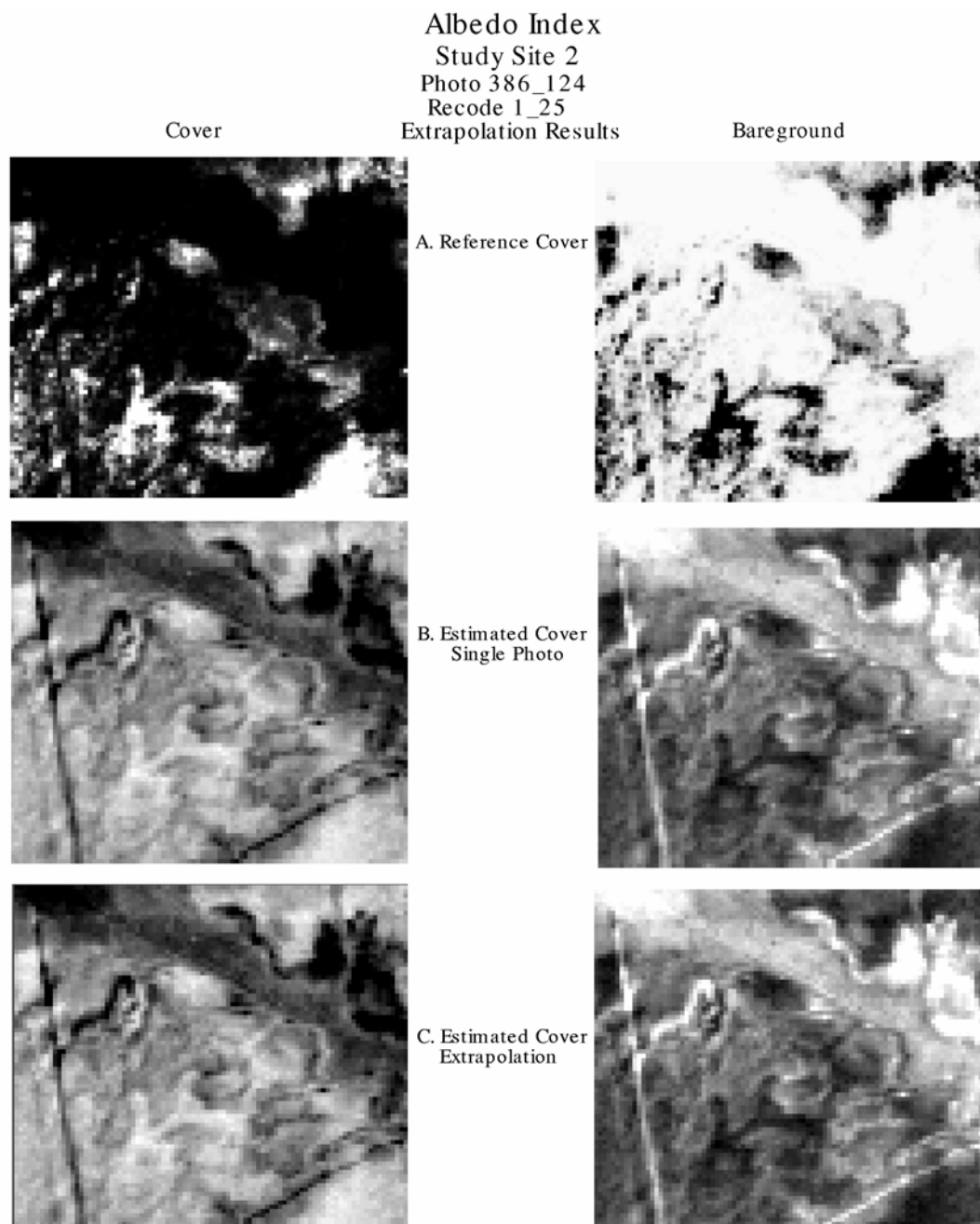


Figure 26. Albedo correlation results for two land cover categories for photo 386_124 using recode 1_25.

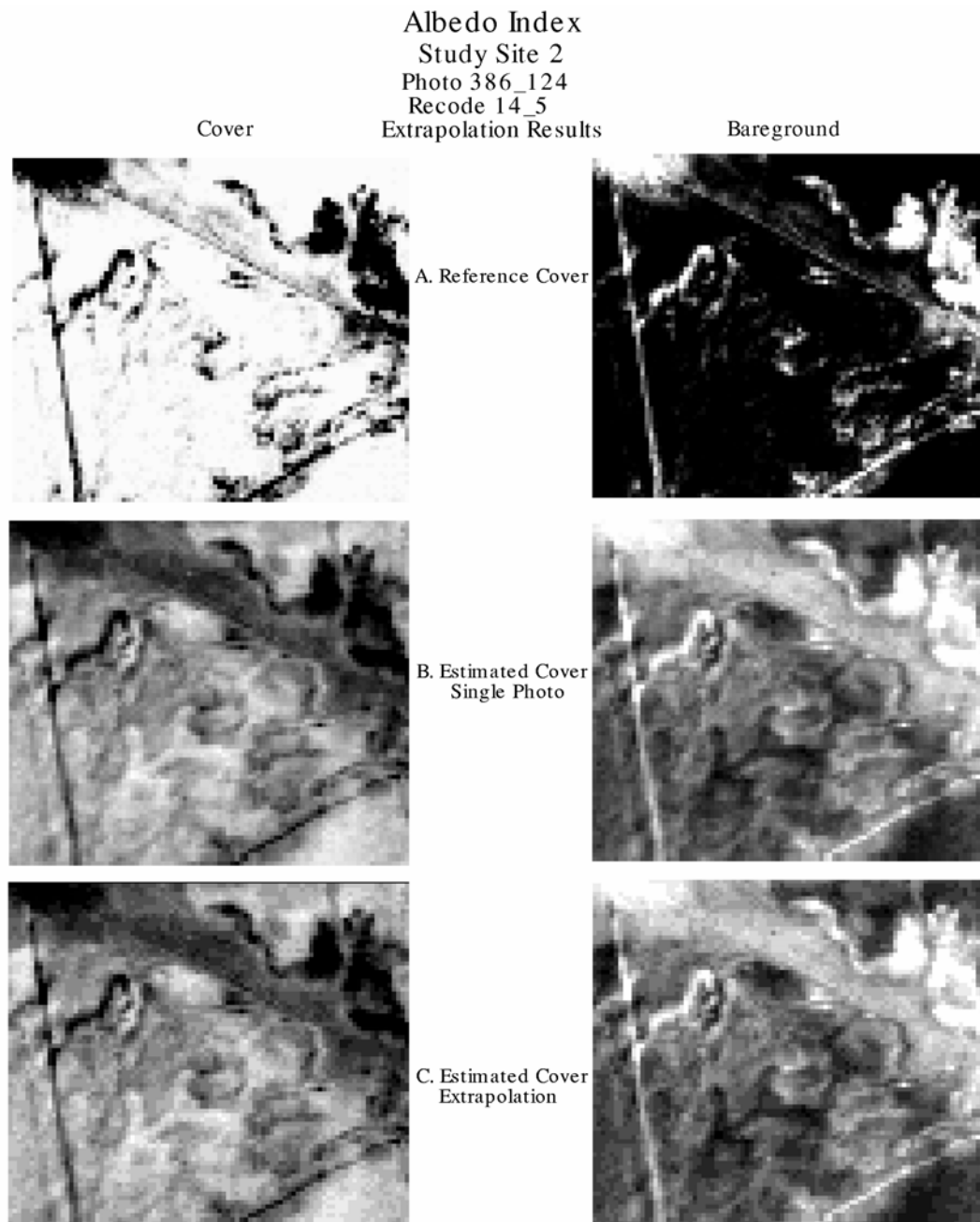


Figure 27. Albedo correlation results for two land cover categories for photo 386_124 using recode 14_5.

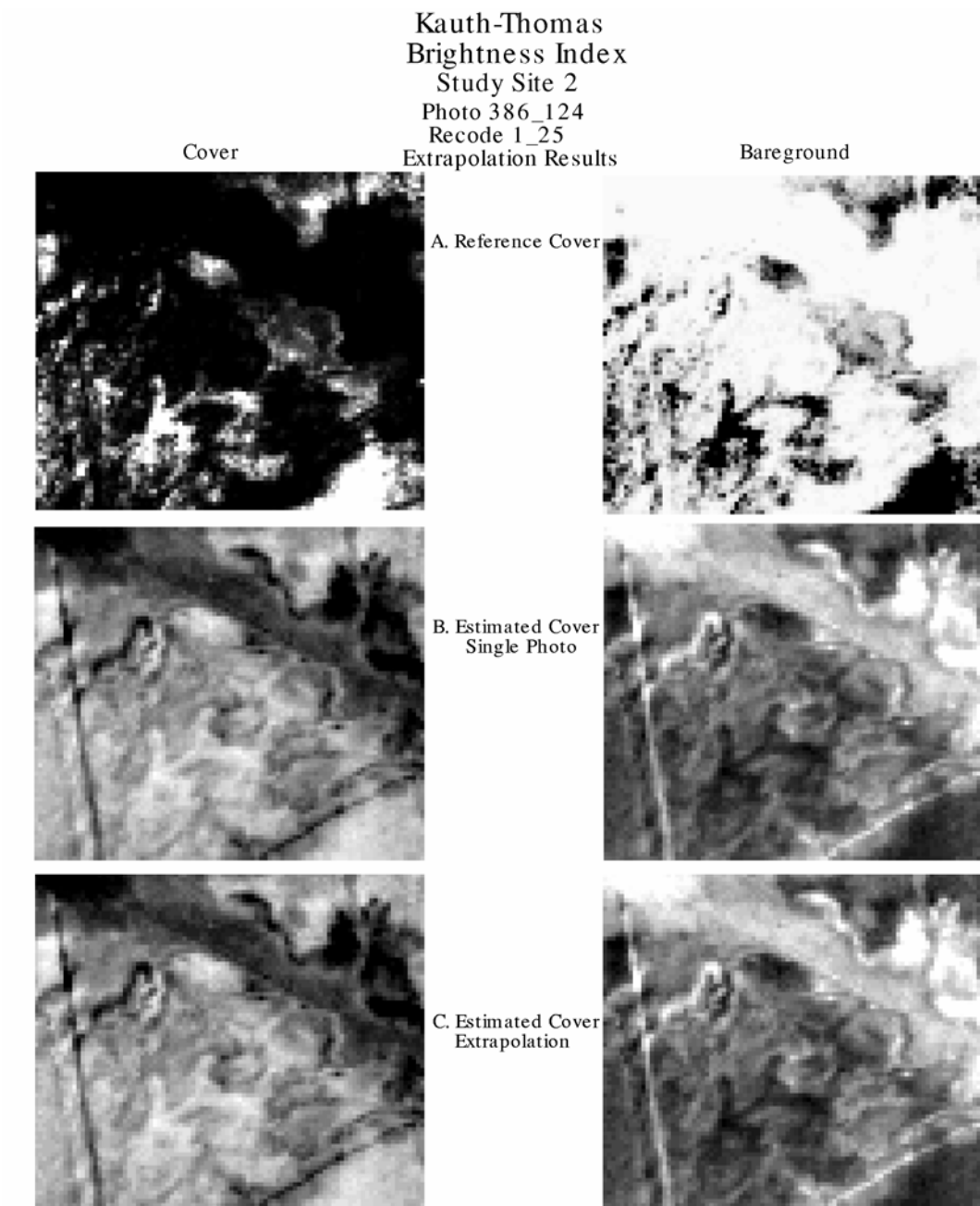


Figure 28. KTB correlation results for two land cover categories for photo 386_124 using recode 1_25.

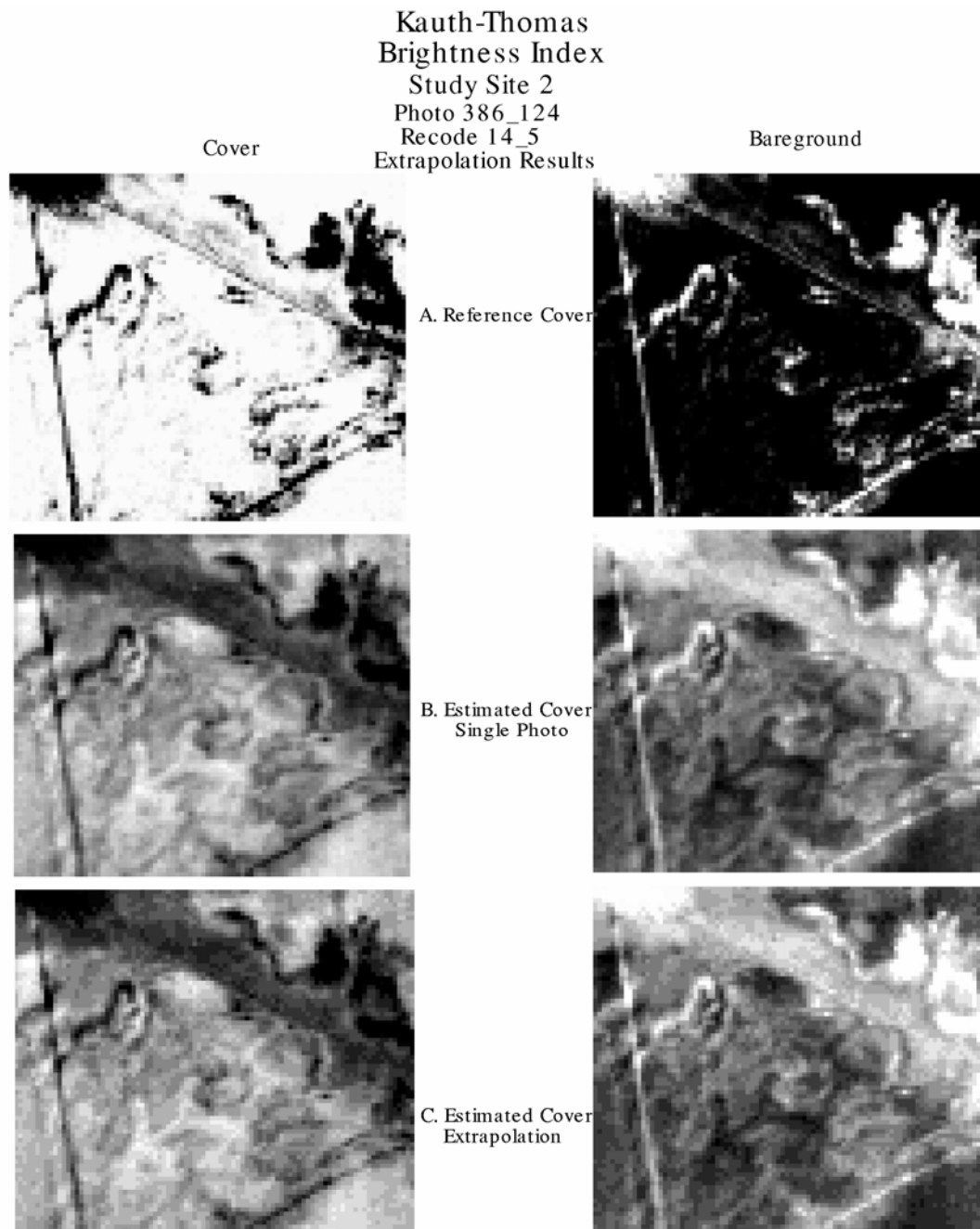


Figure 29. KTB correlation results for two land cover categories for photo 386_124 using recode 14_5.

Table 32 contains the inferential and descriptive statistics for Study Site #3. Recodes 14_5 and 1_25 were also used to evaluate extrapolation results, since these were identified as the top performing recodes in the analysis of individual photographs. Mean differences ranged from -6.6 percent (Albedo/1_25/Bare Ground) to 7.1 percent (Albedo/1_25/Cover). Recode 14_5 performed the best for both Albedo and KTB, as indicated by the lowest sum of absolute differences. Mean differences ranged from -6.60 to 7.10 percent for Albedo and -3.85 to 3.45 percent for KTB. Similar to Study Sites #1 and #2, the null hypothesis was rejected for all recode/land-cover category combinations, but variance of the mean difference was lower than Study Site #2 and only slightly higher than Study Site #1. Although mean differences were lower for KTB-derived estimates, the top performing recode/index combination was Albedo/14_5.

Images of reference abundance, estimated abundance derived directly from samples of photo 388_90 only, and extrapolated estimates of abundance for the same area derived from sampling the other three photographs in Study Site #3 are contrasted in Figures 30 through 33. Similar to results for Study Site #2, recode 14_5 appeared to perform better than recode 1_25, based on the similarity between both single-photo and extrapolated estimates, and reference images. Again results for both indices appeared similar, but there were significant differences between the two recodes tested. Extrapolation appeared to work well for both indices and recodes.

Table 32. Descriptive and inferential statistics of difference image (estimated [extrapolated spectral index correlations] abundance minus reference abundance) for two land-cover categories for photo 388_90 for Study Site #3 using recodes 14_5 and 1_25.

KTB	Recode	t-value	P	CI	abs. diff.	Mean	SD
Cover	14_5	-29.65	0.0000	-4.106, -3.597	52681	-3.852	9.994
Bare Ground	14_5	26.72	0.0000	3.198, 3.704	51613	3.451	9.934
Cover	1_25	-10.95	0.0000	-2.418, -1.684	67826	-2.051	14.409
Bare Ground	1_25	10.89	0.0000	1.666, 2.399	67826	2.032	14.364

Albedo	Recode	t-value	P	CI	abs. diff.	Mean	SD
Cover	14_5	37.85	0.0000	3.929, 4.359	40272	4.144	8.423
Bare Ground	14_5	-31.73	0.0000	-4.714, -4.166	40958	-4.440	10.765
Cover	1_25	45.99	0.0000	6.799, 7.405	69274	7.102	11.882
Bare Ground	1_25	-36.84	0.0000	-6.953, -6.250	67735	-6.601	13.786

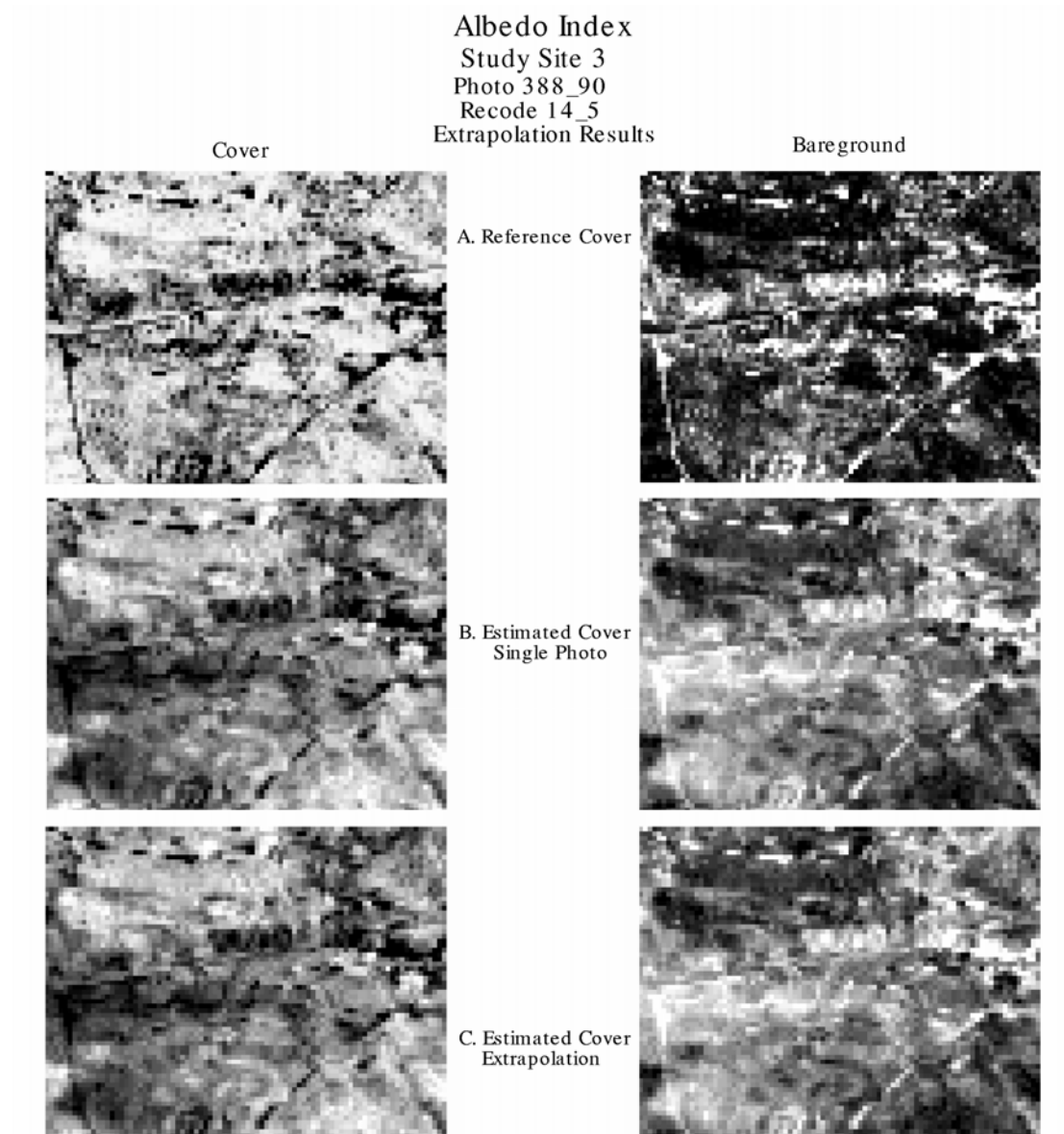


Figure 30. Albedo correlation results for two land cover categories for photo 388_90 using recode 14_5.

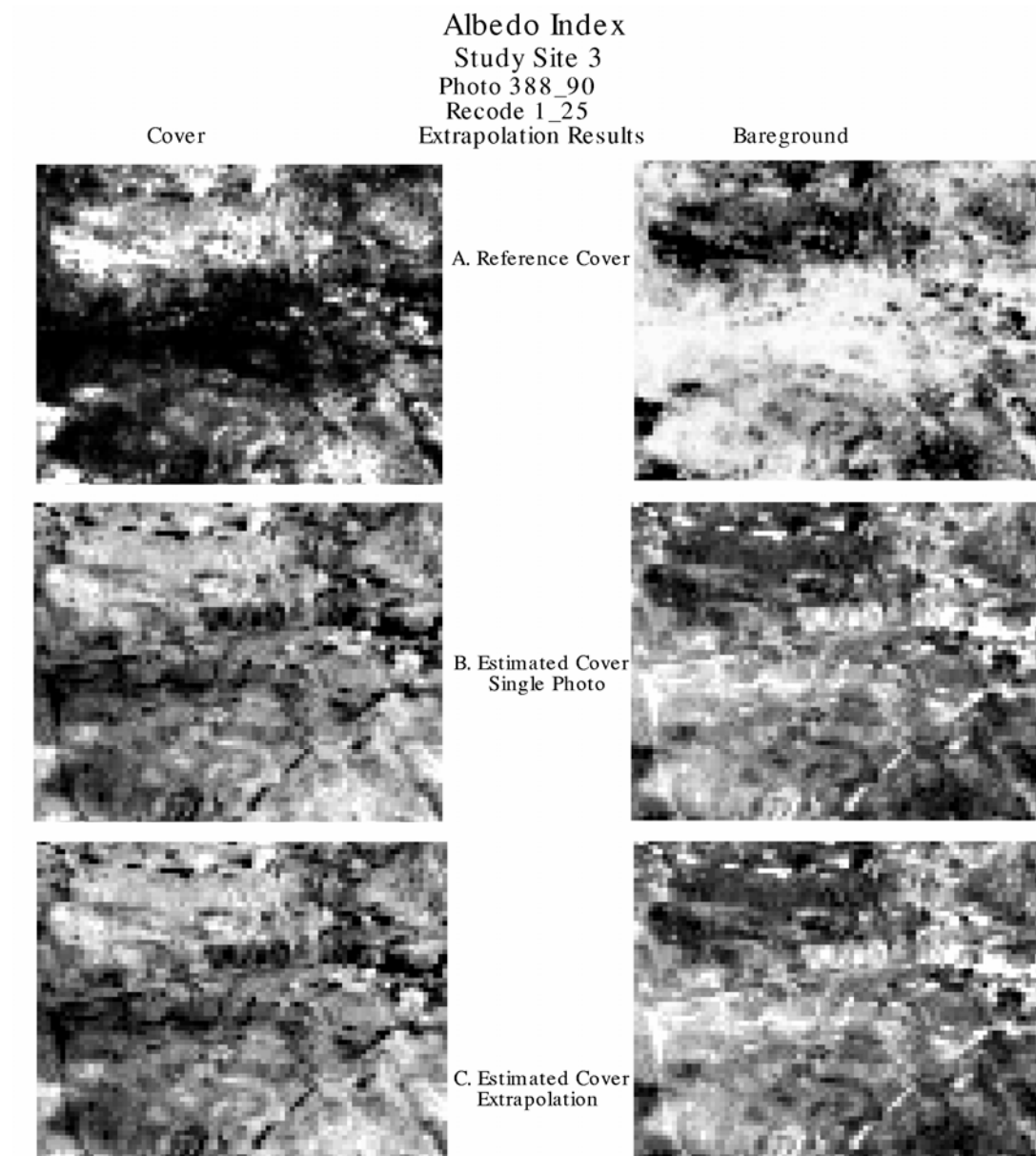


Figure 31. Albedo correlation results for two land cover categories for photo 388_90 using recode 1_25.

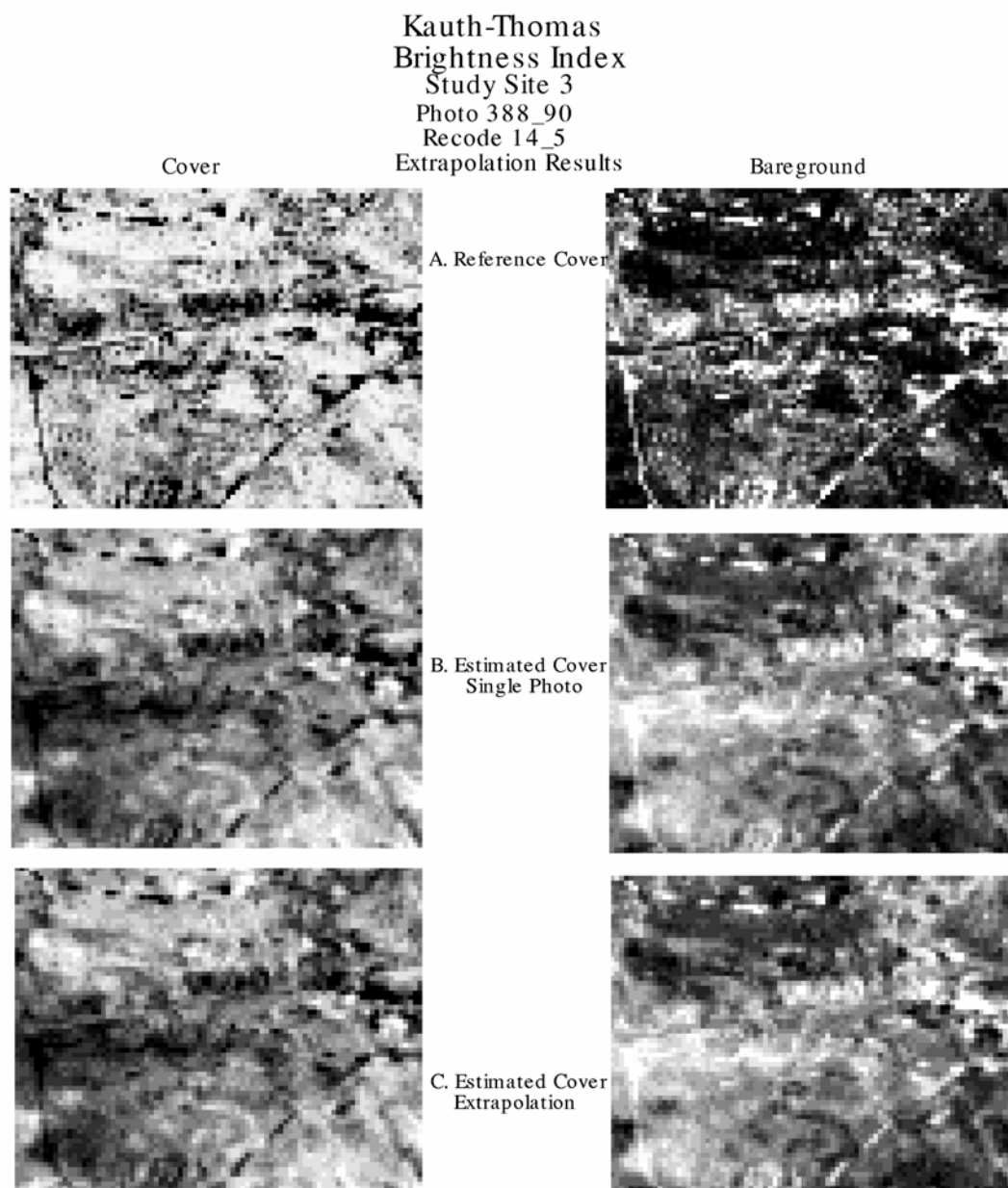


Figure 32. KTB correlation results for two land cover categories for photo 388_90 using recode 14_5.

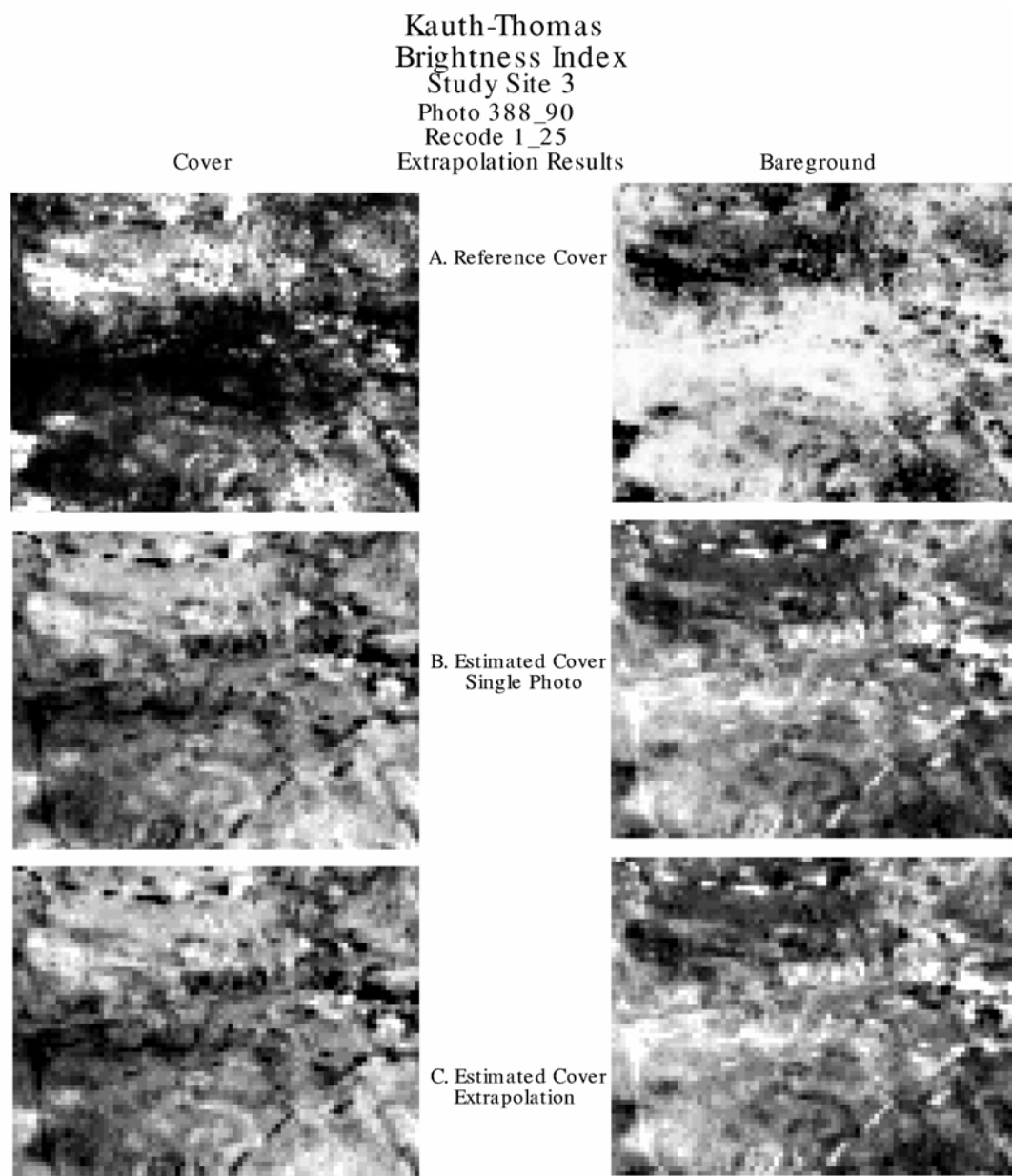


Figure 33. KTB correlation results for two land cover categories for photo 388_90 using recode 1_25.

Summary of Results

In all CIR photograph samples, bare ground was clearly delineated using an unsupervised, five-category classification. Dense shrub or grass cover was also clearly identified as a separate spectral class. However, the remaining spectral categories appeared to delineate a gradient of foliar cover and canopy closure

rather than a distinction between different plant species. Attempts were made to estimate abundance of five land-cover categories using demixing and spectral index correlations, but results indicated this would not be possible. Therefore, all five land-cover categories were reclassified as either Cover or Bare Ground. However, some land-cover categories were difficult to classify as Cover or Bare Ground. Therefore, a number of different reclassifications were tested, each with a slightly different grouping of the original five land-cover categories. Categories were assigned so that higher category numbers represented lower abundance of cover (Category 1= Highest Cover, Category 5 = Bare Ground). The top performing recodes for Study Sites #2 and #3 were recode 1_25, where land-cover Category #1 was reclassified as Cover and all remaining land-cover categories were reclassified as Bare Ground; or recode 14_5, where land-cover Categories 1 through 4 were reclassified as Cover and Land-cover Category #5 was reclassified as Bare Ground. One exception to this was Study Site #1 (Coppice Dunes Maneuver Areas), where a reclassification of land-cover Categories #1 and #2 to Cover and land-cover Categories 3 through 5 as Bare Ground performed slightly better than other reclassifications. Although photographs selected were within relatively close proximity to each other within each individual study site, there was still considerable heterogeneity in abundance of vegetative cover between individual photographs for any given study site. This would explain why different reclassification or recodes, and in some cases, different demixing or spectral index correlation models performed best for each photograph. However, the top performing models and respective recodes for each study site were selected based on examination of descriptive statistics for all photographs for each site.

Study Site #1 - Coppice Dunes Maneuver Areas

Correlations between the KTB index and reference abundance values based on a reclassification of Categories 1 and 2 into vegetated Cover and Categories 3 through 5 into Bare Ground (recode 12_35) provided the best estimates of vegetated cover. Correlations between Albedo and reference abundance values for the same recode resulted in comparable performance. Recode 1_25, as well as a two-class unsupervised classification also performed relatively well using both KTB and Albedo correlation models. The top performing demixing model was derived using the 12_35 recode as well. However, the best performing spectral index correlation (KTB/12_35) clearly outperformed the best demixing model, as evident by the considerably lower sum of absolute difference between estimated and reference vegetative cover/bare ground abundance for KTB (481503) and demixing (1012788). In summary, the KTB correlation provides the best model for estimating and extrapolating vegetative cover estimates across Study Area #1, although Albedo correlation models produced comparable results. Recode 12_35 performed only slightly better than recode 1_25, again suggesting that ei-

ther recode produced comparable results. Determination of the appropriate recode or reclassification (Cover or Bare Ground) of Category #2 in unsupervised classifications of photographs for this study site was difficult, even after field reconnaissance. Land-cover Category #2 generally appeared to correspond to the edges of mesquite-covered dunes and was generally one to three pixels wide (1 to 3 m). This was originally thought to be due to an edge effect around the coppice dunes that could be a combination of shadows, litter, and solar geometry due to sloping effect of the dunes. However, this spectral category did not occur at any particular spatial orientation to the dune, and in some isolated cases, occurred in interdunal areas not associated with any dune formation. Therefore, it was concluded to be a combination of litter; decreased mesquite foliar, stem, and branch densities; and some shadowing. Additional field validation would be required to determine which recode is appropriate for estimating cover. However, either recode should provide comparable estimates, and errors associated with the misclassification of Category #2 should be minimal. Neither spectral index correlations nor demixing were able to estimate interdunal vegetation cover with any consistency.

Study Site #2 - Otero Mesa Grasslands

Correlations between Albedo and reference abundance values based on a reclassification of Categories 1 through 4 as Cover and Category 5 as Bare Ground (recode 14_5) provided the best estimates of cover. Correlations between KTB and reference abundance values for the same recode resulted in comparable performance. Recode 1_25 also performed relatively well using both KTB and Albedo correlation models. The top performing demixing model was derived using the 1_25 recode, although recode 14_5 also performed relatively well. However, the best performing spectral index correlation (Albedo/14_5) clearly outperformed the best demixing model, as evident by the considerably lower sum of absolute difference between the estimated and reference vegetative Cover/Bare Ground abundance for Albedo (351209) and demixing (677145). In summary, the Albedo correlation provided the best model for estimating and extrapolating vegetative cover estimates across Study Area #2, although KTB correlation models produced comparable results. Recode 1_25 also performed relatively well for both spectral index correlations, but recode 14_5 was clearly the top performer. The opposite was true for demixing, where recode 14_5 performed relatively well, but recode 1_25 was clearly the top performer. Both spectral index correlations and demixing were able to estimate percent cover and bare ground, but were unable to provide reasonable estimates of different vegetative cover types.

Study Site #3 - Controlled Burn Area/Otero Mesa Foothills

Correlations between Albedo and reference abundance values based on a reclassification of Categories 1 through 4 into Cover and Category 5 into Bare Ground (recode 14_5) provided the best estimates of cover. Correlations between KTB and reference abundance values for the same recode resulted in comparable performance. The top performing demixing model was derived using the same recode. However, the best performing spectral index correlation (Albedo/14_5) clearly outperformed the best demixing model, as evident by the considerably lower sum of absolute difference between estimated and reference cover/bare ground abundance for Albedo (587365) and demixing (848264). In summary, the Albedo correlation provided the best model for estimating and extrapolating vegetative cover estimates across Study Area #3, although KTB correlation models produced comparable results. Recode 14_5 was clearly the top performing recode for both spectral index correlation models and demixing. Both the spectral index correlations and demixing were able to estimate percent cover and bare ground, but were unable to provide reasonable estimates of different vegetative cover types.

Using spectral index correlation models KTB/12_35 for Site#1, Albedo/14_5 for Site #2, and Albedo/14_5 for Site #3, a two-band image (Band 1 = Cover; Band 2 = Bare Ground) was created for each study site, with each pixel value representing estimated percent cover or bare ground for that location. A generalized map depicting the approximate boundaries of the three study sites was created and then used to determine which model should be applied to different areas of the installation. Images for each of the study sites were then mosaiced together to create a single image of estimated cover for the entire installation.

6 Conclusions and Recommendations

Conclusions

The objective of this research was to investigate alternative methods for characterizing and monitoring vegetative cover at Fort Bliss, Texas, that would be cost effective, yet provide quantitative estimates of both total cover, and cover by species type, across the entire installation. The alternative methods that were investigated were designed to overcome deficiencies in currently available ground monitoring efforts by using and integrating remote sensing technologies into a characterization and monitoring protocol. Secondly, methods were evaluated that potentially could provide a means to quantify and monitor vegetative cover information from coarse resolution satellite imagery. Historically, coarse resolution satellite imagery has only been used for characterization of relative rather than quantifiable changes in total vegetative cover. The primary focus of this research was to evaluate spectral demixing and correlations between spectral indices and vegetation abundance as potential methods for estimating total percent cover, and preferably, percent cover for distinct land-cover types or plant species, within a single coarse resolution satellite image pixel. These same techniques were also evaluated for their utility in extrapolating fractional cover estimates of distinct land-cover types across various regions of the installation from a limited number of reference samples. Both methods used high-resolution color infrared photography as a sampling technique for collecting reference or “ground truth” measurements of percent total vegetative cover and bare ground. Therefore, the results of this research provided not only an evaluation of demixing and correlation analysis for estimating and extrapolating vegetative cover estimates using coarse resolution satellite imagery, but also an evaluation of a sampling and validation methodology that uses high-resolution photography rather than ground surveys.

Vegetative Cover Estimation

Field sampling will always be a necessity for natural resources characterization and monitoring efforts, but exclusive reliance on field sampling will always remain cost prohibitive, especially for such large land areas as Fort Bliss. Therefore, to adequately sample a large area, Fort Bliss DOE land managers can benefit from alternative sampling techniques such as high-resolution photography or

digital imagery to augment existing field sampling efforts. In many cases, observations from high-resolution imagery are unacceptable as surrogate measurements of ecological data measured on the ground for survey and monitoring purposes. However, for the purpose of measuring *total* aerial vegetative cover and bare ground for specific sites, high-resolution aerial photography was adequate as a sampling technique for the Fort Bliss semiarid environment.

Cover Estimation for Unique Land-cover/Vegetation Types

Results from this study indicated that estimates of percent cover by specific land-cover type or vegetative species could not be derived consistently from classifications of high-resolution aerial photography. Attempts to estimate total cover for both five and three unique land-cover classes resulted in an unacceptable level of error. This was concluded through both visual inspection and field reconnaissance. In all CIR photograph samples, bare ground was clearly delineated using an unsupervised, five-category classification. Dense shrub or grass cover was also clearly identified as a separate spectral class. However, the remaining spectral categories appeared to delineate a gradient of foliar cover and canopy closure rather than a distinction between different plant species.

Specifically, for the Coppice Dunes Study Site (Study Site #1), one of the goals was to develop a cost-effective method to quantify and monitor interdunal vegetation cover. The site was representative of a large percentage of the total area that is used for tracked and wheeled training maneuvers at Fort Bliss. Within these coppice dune areas, impacts from the training mission are concentrated in the interdunal areas, typically resulting in a loss of total interdunal vegetative cover. Therefore, a goal was to develop a cost-effective method to characterize and monitor this specific cover type. Unfortunately, results from this study indicated that it was not possible to clearly distinguish interdunal vegetation from other land-cover types, including bare ground.

Spectral Demixing for Estimating Total Vegetation Cover

Spectral demixing was evaluated as a potential methodology for extracting percent vegetative cover estimates from coarse resolution (> 25 m) satellite imagery. In this study, estimates of percent cover derived from spectral demixing were evaluated against reference or “ground truth” percent cover derived from high-resolution aerial photography. Attempts to estimate total cover for five and three land-cover classes using spectral demixing resulted in an unacceptable level of error. Attempts to estimate total vegetative cover, independent of vegetation type, and bare ground produced mixed results. In most test photographs for Study Site #1, the mean difference between demixing estimates of cover and

“ground truth” percent cover values was less than 2 percent, but was significantly higher for Study Sites #2 and #3. The variance of the estimated total cover from demixing was much higher than the variance of the reference values, even for Study Site #1. A null hypothesis that there was no significant difference between estimates of total cover derived from demixing and reference cover amounts was rejected for more than half of the sample photographs. Visual inspection of demixing results also confirmed that for a select few sample sites, demixing provided accurate estimates of cover, but for the majority of the sites, there was a significant amount of error. Therefore, it was concluded that spectral demixing was unable to consistently estimate percent cover within an acceptable level of error.

Spectral Index Correlations for Estimating Total Vegetative Cover

Similar to spectral demixing, the correlation between spectral index values derived from coarse resolution imagery and reference or “ground truth” percent cover values derived from high-resolution aerial photography was evaluated as a potential methodology for estimating and extrapolating total vegetative cover estimates. Attempts to estimate total cover for five and three land-cover classes using spectral index correlations resulted in estimates that were consistently better than estimates derived from spectral demixing. A null hypothesis that there was no significant difference between estimates of total cover derived from spectral index correlations and reference cover amounts was accepted for three of five land-cover categories in Study Site #1, with the largest mean difference between estimated total cover and reference cover being approximately 1 percent. When total cover for only three distinct land-cover classes was estimated for Study Site #1, the null hypothesis was accepted for two of the three categories and mean differences were again approximately 1 percent. The two land-cover classes where the null hypothesis was accepted were honey mesquite and interdunal vegetation. Although these results were promising, as described above, the original land-cover categories derived from the reference aerial photography delineated a gradient of foliar cover and canopy closure rather than a distinction between different plant species. As a result, all land-cover types that were clearly identified as mesquite or bare ground were lumped into Categories 1 and 3, respectively, and all remaining pixels were lumped into the interdunal category. Therefore, it was concluded that spectral index correlations show promise for estimating total percent cover of different categories of foliar cover and canopy closure. If a method could be developed to more accurately identify an “interdunal” vegetation category from high-resolution aerial photography, it is expected that spectral index correlations would provide an accurate and cost-effective characterization and monitoring tool for coppice dune environments similar to Study Site #1. However, because there was uncertainty as to whether

the interdunal category in the reference photographs was an accurate representation of total interdunal cover, it was determined that spectral index correlations would have more utility for estimating two categories of land-cover: vegetation and bare ground.

A number of different combinations of five land-cover classes were grouped into either a “vegetated” or “bare ground” category for each of the study sites. Different combinations performed better than others and varied between photographs in individual sites and also between sites. In addition, both spectral indexes (Albedo and KTB) produced similar results. The null hypothesis that there was no significant difference between estimates of total cover derived from spectral index correlations and reference cover amounts was accepted for at least one index and recode combination in 11 of the 12 photographs evaluated, with photo 381_144 (Study Site #1) being the only photograph where the null hypothesis was rejected for all index and recode combinations. Therefore, based on inferential and descriptive statistics, it was concluded that spectral index correlations did provide an accurate estimate of total cover at each of the study sites.

Spatial Extrapolation of Total Vegetative Cover Estimates

Based on the results and conclusions described above, it was concluded that a methodology that uses spectral index correlations rather than spectral demixing would provide the best utility for estimating and extrapolating total vegetative cover estimates across the entire installation. The three study sites in this research were selected to characterize three very general landform/vegetation zones at Fort Bliss (Study Site #1 – Coppice Dunes, Study Site #2 – Otero Mesa Grasslands, Study Site #3 – Controlled Burn Area/Otero Mesa Foothills). Ideally, the best performing combination of spectral index and recode could be clearly identified for each study site and then applied uniformly across all other areas of the installation that are similar to that respective study site. In this study, it was difficult to identify a specific index and recode combination that was a best performer for a specific study site, because results varied between photographs within a single site. Therefore, it was concluded that the index and recode combination that resulted in the lowest absolute difference between estimated total cover and reference total cover would be used to identify the best performing index and recode combination. In turn, these best performing combinations would be used to extrapolate total cover estimates across each study site.

Using spectral index correlation models KTB/12_35 for Site#1, Albedo/14_5 for Site #2, and Albedo/14_5 for Site #3, a two-band image (Band 1 = Cover; Band 2 = Bare Ground) was created for each study site, with each pixel value represent-

ing the estimated percent cover or bare ground for that location. A generalized map depicting the approximate boundaries of the three study sites was created and then used to determine which model should be applied to different areas of the installation. Images for each of the study sites were then mosaiced together to create a single image of estimated cover for the entire installation.

Visual inspection of the estimated cover map for the entire installation resulted in the following conclusions. Spectral index correlations were demonstrated to be effective in estimating total vegetative cover for specific areas. Attempts to extrapolate cover estimates across the entire installation, however, will require a significant refinement of the stratification of the installation into unique landform/vegetation zones. It was recognized that these three study sites do not adequately represent all landform/vegetation types at Fort Bliss. In addition, there was no clear determination of boundaries between these very generalized landform/vegetation types. The issue of stratification is discussed in more detail in the Recommendations section below. However, the use of correlations between spectral indexes derived from coarse resolution imagery and reference cover amounts derived from high-resolution aerial photography does provide an accurate and cost-effective method for quantifying total vegetative cover, and with refinements, shows promise for extrapolating these estimates over much larger geographic regions.

Recommendations

There are always challenges, as there were in this investigation, in interpreting photographic or spectral images and translating that information to quantitative ecological data. Any type of sampling that uses remote observations should always be validated with in-situ measurements. In this research, *historical* photography and satellite imagery were used to evaluate spectral demixing and correlation analysis. Therefore, ground observations of vegetative cover at the time the imagery and photography were collected were not available. If ground observations had been available, problems associated with the uncertainty in assigning spectral classes derived from photography into Cover versus Bare Ground information classes would have been minimized, thus improving the reference cover estimates derived from aerial photography classifications. Minimizing these types of errors would have improved the reference cover values used to develop demixing and correlation models, thus improving the accuracy of abundance estimates derived from these models. Therefore, the recommendation is to coordinate any future collection of aerial photography and satellite imagery with coincident field surveys of the area.

In addition to the lack of field validation data, there were other aspects of the techniques evaluated that could potentially be improved. Specifically, further research is required to determine the number and location of samples necessary to adequately sample and characterize the diversity of land-cover types and land uses at Fort Bliss. Results from this research attempted to characterize three general regions of Fort Bliss: the Coppice Dunes Maneuver Areas, the Otero Mesa Grasslands, and the transition zone between Tularosa Valley and Otero Mesa, in close proximity to the Controlled Burn Study Site. There was considerable diversity within these large, generalized land areas that was not adequately sampled in this study. There was also considerable diversity in abundance of various land-cover types within the relatively small areas that were sampled with CIR photography for each study site. Therefore, the recommendation is to develop a more detailed stratification process that would identify more unique landform/vegetation types. The goal would be to develop more strata of smaller area, resulting in a higher degree of homogeneity in land cover and plant species within each strata. Once such stratification is developed, a larger sample of photography that is distributed across all strata should increase the accuracy of these estimates.

In addition, both the CIR photography and TM imagery used to evaluate demixing and correlation analysis were collected in late October and early November 1994. This was well beyond the peak precipitation events and corresponding peak greenness and photosynthetically active period of most vegetation at Fort Bliss, which typically occurs in August and September. As a result, because of minimal green biomass and photosynthetic activity at this time, minimal Near Infrared spectral response was observed in the CIR photography and satellite imagery. This may have adversely affected spectral demixing results, where each spectral endmember or land-cover type to be characterized must be spectrally unique from all other endmembers. In addition, spectral indices, and in particular, spectral greenness indices, may have also been adversely affected by the timing of the image collection. Therefore, the recommendation is to collect any future imagery during the peak photosynthetic activity of vegetation. This may improve estimates of abundance derived from demixing and correlation analysis.

Despite these potential areas for improvement, results from this research were promising and the techniques that were demonstrated and evaluated have great potential for future characterization and monitoring of land condition at Fort Bliss. Estimates of vegetative cover derived from these techniques may never be exact for any given pixel location, yet they will provide more information on total vegetative cover than what can be measured from field surveys alone. Estimates are provided for every pixel, across the entire geographic footprint of the coarse

resolution satellite image. In addition, these estimates of total vegetative cover are quantitative rather than relative. Field surveys alone provide quantitative measures of total cover, but only for specific survey locations. Field surveys are also cost-prohibitive, and even a large ground survey only covers a very small percentage of large installations such as Fort Bliss. Estimates can be derived by supplementing existing field surveys with relatively low-cost samples of high-resolution photography or imagery and coarse resolution satellite imagery.

Several options exist for implementation of the techniques evaluated in this investigation to support future resource characterization and monitoring objectives of the Fort Bliss DOE. One alternative would be to sample with a combination of ground surveys and high-resolution photography or imagery on a regular interval, but not necessarily on an annual basis, for example. Using this alternative, either demixing or spectral index correlation models would be developed from the most recent sample and applied to TM imagery for successive years in which field and aerial samples are not collected. During these interim years, the only inventory requirement would be a single coarse resolution satellite image and field validation plots, thereby reducing the total cost of the monitoring program. Once a new sample of high-resolution imagery is collected, the demixing or spectral index correlations could be recalibrated.

A second alternative would be to sample with high-resolution imagery on an annual basis. The accuracy of abundance estimates derived from demixing and spectral index correlation models should increase with the frequency at which sampling occurs, but increased sampling frequency would incur a greater cost. A third option would be to sample sensitive areas or areas of intense use at a higher frequency than those areas of the installation that are used less frequently, thereby reducing the total cost of monitoring while focusing characterization and monitoring efforts on critical areas of the installation. Characterization and monitoring objectives of installation land managers, as well as resources allocated to meeting these monitoring objectives, will ultimately dictate how such a monitoring program might be implemented. Regardless of sampling frequency, if suggested improvements to the techniques evaluated in this investigation are researched, validated, and implemented, spectral index correlations and demixing techniques should improve the capability of Fort Bliss managers to characterize and monitor land condition on the installation.

References

- Adams, J.B., M.O. Smith, and A.R. Gillespie. 1985. "Simple Models for Complex Natural Surfaces: A Strategy for the Hyperspectral Era of Remote Sensing," *NASA Research Report - NASA Grant NAGW-85*, pp 16-21.
- Adams, J.B., D.E. Sabol, V. Kapos, R. Almeida Filho, D.A. Roberts, M. Smith, and A. Gillespie. 1995. "Classification of Multispectral Images Based on Fractions of Endmembers: Application to Land-Cover Change in the Brazilian Amazon," *Remote Sensing of Environment*, vol 52, pp 137-154.
- Anderson, G.L., J.D. Hanson, and R.H. Haas. 1993. "Evaluating Landsat Thematic Mapper Derived Vegetation Indices for Estimating Above Ground Biomass on Semiarid Rangelands," *Remote Sensing of Environment*, Aug, vol 45, no. 2, pp 165-175.
- Asrar, G., R.L. Weiser, D.E. Johnson, E.T. Kanemasu, and J.M. Killeen. 1986. "Distinguishing Among Tallgrass Prairie Cover Types from Measurements of Multispectral Reflectance," *Remote Sensing of Environment*, vol 19, pp 159-169.
- Bateson, A., and B. Curtiss. 1996. "A Method for Manual Endmember Selection and Spectral Unmixing," *Remote Sensing of Environment*, vol 55, pp 229-243.
- Borel, C.C. and S.A.W. Gerstl. 1994. "Nonlinear Spectral Mixing Models for Vegetative and Soil Surfaces," *Remote Sensing of Environment*, vol 47, pp 403-416.
- Boyd, W.E. 1986. "Correlation of Rangelands Brush Canopy Cover with Landsat MSS Data," *Journal of Range Management*, 39(3), pp 268-271.
- Boykin, K.G., P.L. Matusik, D. Houde-Nethers, and B.C. Thompson. 1997. "Biotic and Physical Attributes of Surface and Near-Surface Water Sites on Fort Bliss Military Reservation: Inventory and Comparative Assessment," New Mexico Cooperative Fish and Wildlife Research Unit.
- Budd, L.F., R.B. Arend, J.W. Hurst, and V.H. Anderson. 1979. "Fort Bliss Environmental Analysis and Impact Assessment", Environmental Impact Statement (EIS) No. DARK-07-78-c-0151, Photographic Interpretation, Hanover, NH.
- Crist, E.P., and R.C. Ciccone. 1984. "Application of the Tassled Cap Concept to Simulated Thematic Mapper Data," *Photogrammetric Engineering and Remote Sensing*, vol 50, no. 3, pp 343-352.
- Curran, P.J. 1980. "Multispectral Remote Sensing of Vegetation Amount," *Progress in Physical Geography*, 4:315-341.

- Duncan, J., D. Stow, J. Franklin, and A. Hope. 1993. "Assessing the relationship between spectral vegetation indices and shrub cover in the Jornada Basin, New Mexico," *International Journal of Remote Sensing*, vol 14, no. 18, pp 3395-3416.
- ERDAS Field Guide, Fourth Edition, ERDAS Inc., 1997.
- Farrand, W.H., R.B. Singer and E. Merenyi. 1994. "Retrieval of Apparent Surface Reflectance from AVIRIS Data: A Comparison of Empirical Line, Radiative Transfer, and Spectral Mixture Methods," *Remote Sensing of Environment*, vol 47, pp 311-321.
- Foody, G.M. and D.P. Cox. 1994. "Sub-pixel land cover composition estimation using a linear mixture model and fuzzy membership functions," *International Journal of Remote Sensing*, vol 15, no. 3, pp 619-631.
- Foschi, P.G. 1994. "A Geometric Approach to a Mixed Pixel Problem: Detecting Subpixel Woody Vegetation," *Remote Sensing of Environment* 50:317-327.
- Frank, T.D. 1984. "The Effect of Change in Vegetation Cover and Erosion Patterns on Albedo and Texture of LANDSAT Images in a Semiarid Environment," *Annals of the Association of American Geographers*, 74(3):393-407.
- Frank, T.D. 1985. "Differentiating Semiarid Environments Using LANDSAT Reflectance Indexes," *Professional Geographer*, 37(1):36-46.
- Franklin, J., J. Duncan, and D.L. Turner. 1993. "Reflectance of Vegetation and Soil in Chihuahuan Desert Plan Communities from Ground Radiometry Using SPOT Wavebands," *Remote Sensing of Environment*, vol 46, pp 291-304.
- Graetz, R.D. and M.R. Gentle. 1982. "The Relationship Between Reflectance in the LANDSAT Wavebands and the Composition of an Australian Semi-Arid Shrub Rangeland," *Photogrammetric Engineering and Remote Sensing*, 11:1721-1730.
- Huete, A.R. 1986. "Separation of Soil-Plant Spectral Mixtures by Factor Analysis," *Remote Sensing of Environment*, vol 19, pp 237-251.
- Huete, A. R. 1988. "A Soil-Adjusted Vegetation Index (SAVI)," *Remote Sensing of Environment*, vol 25, pp 295-309.
- Hughes, N.A., and A. Henderson-Sellers. 1982. "System Albedo as Sensed by Satellites, Its Definition and Variability," *International Journal of Remote Sensing*, 5(1), pp 1-11.
- Jensen, J.R. 1986. *Introductory Digital Image Processing*, Prentice Hall, Englewood Cliffs, NJ,
- Kauth, R.J., P.F. Lambeck, W. Richardson, G.S. Thomas, and A.P. Pentland. 1978. "Feature Extraction Applied to Agricultural Crops As Seen by Landsat," *Proceedings of the Technical Sessions Vol II, The LACIE Symposium*, Oct 1978, NASA Johnson Space Center.
- Lillesand, T.M. and R.W. Kiefer. 1987. *Remote Sensing and Image Interpretation*, Second Edition, John Wiley and Sons, New York, New York.

- Markham, B.L., and J. L. Barker. 1986. "LANDSAT MSS and TM Post-Calibration Dynamic Ranges, Exoatmospheric Reflectances and At-Satellite Temperatures," EOSAT Technical Notes, 1:3-8.
- Marsh, S.E., P. Switzer, W.S. Kowalik, R. Lyon. 1980. "Resolving the Percentage of Component Terrains within Single Resolution Elements," *Photogrammetric Engineering and Remote Sensing*, vol 46, no. 8, pp 1070-1086.
- McDaniel, K.C., and R.H. Haas. 1982. "Assessing Mesquite-Grass Vegetation Condition from Landsat," *Photogrammetric Engineering and Remote Sensing*, vol 48, no. 3, pp 441-450.
- Mehlop, P., E. Muldavin, T. Benett, S. Wood, S. Yanoff, N. Douglas, and S. Radjy. 1996. "Vegetation of Fort Bliss Texas and New Mexico: Final Report Volume II Vegetation Map," New Mexico Natural Heritage Program, Biology Dept., U. of New Mexico.
- Musick, H.B. 1984. "Assessment of Landsat Multispectral Scanner Spectral Indexes for Monitoring Arid Rangeland", *IEEE Transactions on Geoscience and Remote Sensing*, vol GE-22, no. 6, pp 512-520.
- Musick, H.B. 1986. "Temporal Change of LANDSAT MSS Albedo Estimates in Arid Rangeland," *Remote Sensing of Environment*, vol 20, pp 107-120.
- Pech, R.P., R.D. Graetz, and A.W. Davis. 1986. "Reflectance Modeling and the Derivation of Vegetation Indices for and Australian Semi-arid Shrubland," *International Journal of Remote Sensing*, vol 7, no. 3, pp 389-403.
- Peters, A.J., M.D. Eve, E.H. Holt, and W. Whitford. 1997. "Analysis of Desert Plant Community Growth Patterns with High Temporal Resolution Satellite Spectra," *Journal of Applied Ecology*, vol 34, pp 418-432.
- Peterson, G.W., K.F. Connors, D.A. Miller, R.L. Day, and T.W. Gardner, 1987. "Aircraft and Satellite Remote Sensing of Desert Soils and Landscapes," *Remote Sensing of Environment*, vol. 23, pp. 253-271.
- Pickup, G., V.H. Chewings, and D.J. Nelson. 1993. "Estimating Changes in Vegetation Cover Over Time in Arid Rangelands Using Landsat MSS Data," *Remote Sensing of Environment*, vol 43, no. 3, pp 243-263.
- Press, William H. Brian P. Flannery, Saul A. Teukolsky, William T. Vetterling. 1992. *Numerical Recipes in FORTRAN*, Cambridge University Press.
- Price, K.P., D. A. Pyke, and L. Mendes. 1992. "Shrub Dieback in a Semiarid Ecosystem; The Integration of Remote Sensing and Geographic Information Systems for Detecting Vegetation Change," *Photogrammetric Engineering and Remote Sensing*, vol 58, no. 4, pp 455-463.
- Price, J. 1987. "Calibration of Satellite Radiometers and the Comparison of Vegetation Indices," *Remote Sensing of Environment*, vol 21:15-27.

- Puyou-Lascassies, P., G. Flouzat, M. Gay, and C. Vignolles. 1994. "Validation of the Use of Multiple Linear Regression as a Tool for Unmixing Coarse Spatial Resolution Images," *Remote Sensing of Environment*, vol 49, pp 155-166.
- Qi, J., A. Chehbouni, A.R. Huete, Y.H. Kerr, and S. Sorooshian. 1994. "A Modified Soil Adjusted Vegetation Index," *Remote Sensing of Environment*, vol 48 pp 119-126.
- Ray, T.W. and B.C. Murray. 1996. "Nonlinear Spectral Mixing in Desert Vegetation," *Remote Sensing of Environment*, vol 55, pp 59-64.
- Richardson, A.J. and C.L. Wiegand. 1977. "Distinguishing Vegetation from Soil Background Information," *Photogrammetric Engineering*, vol 43, no. 12, pp 1541-1552.
- Roberts, D.A., M.O. Smith, J.B. Adams, and A.R. Gillespie. 1991. "Leaf Spectral Types, Residuals, and Canopy Shade in an AVIRIS Image," *Proceedings: 3rd Airborne Visible/Infrared Imaging Spectrometer (AVIRIS) Workshop* (R.O. Green, ed.), pp 43-50.
- Roberts, D.A., M.O. Smith, and J.B. Adams. 1993. "Green Vegetation, Nonphotosynthetic Vegetation, and Soils in AVIRIS Data," *Remote Sensing of Environment*, vol 44, pp 255-269.
- Robinove, C.J. 1982. "Computation with Physical Values from LANDSAT Digital Data," *Photogrammetric Engineering and Remote Sensing*, vol 5, pp 781-784.
- Robinove, C.J., P.S. Chavez, D. Gehring, and R. Holmgren. 1981. "Arid Land Monitoring Using LANDSAT Albedo Difference Images," *Remote Sensing of Environment*, vol 11, pp 133-156.
- Rondeaux, G. M. Steven, and F. Baret. 1996. "Optimization of Soil-Adjusted Vegetation Indices," *Remote Sensing of Environment*, vol 55, pp 95-107.
- Rouse, J.W., R. H. Haas, J.A. Schell, D.W. Deering, and J.C. Harlan. 1974. "Monitoring vegetation systems in the great plains with ERTS," *Third ERTS Symposium*, NASA SP-351 I:309-317.
- Sanden, E.M., C.M. Britton, and J.H. Everitt. 1996. "Total Ground-Cover Estimates from Corrected Scene Brightness Measurements," *Photogrammetric Engineering and Remote Sensing*, vol 62, no. 2, pp 147-150.
- Satterwhite, M.B. 1984. "Discriminating Vegetation and Soils Using Landsat MSS and Thematic Mapper Bands and Band Ratios," Technical Paper, *50th Ann. Meeting American Society of Photogrammetry*, vol 2, pp 479-490, American Society of Photogrammetry, Falls Church, VA.
- Senseman, G.M., C.F. Bagley, and S.A. Tweddale. 1996. "Correlation of Rangeland Cover Measures to Satellite-Imagery-Derived Vegetation Indices," *Geocarto International*, 11(3):29-38.
- Smith, M.O., S.L. Ustin, J.B. Adams, and A.R. Gillespie. 1990. "Vegetation in Deserts: 1. A Regional Measure of Abundance from Multispectral Images," *Remote Sensing of Environment*, vol 31, pp 1-26.

- Smith, M.O., J. Adams, and D. Sabol. 1994. "Spectral Mixture Analysis - New Strategies for the Analysis of Multispectral Data," *Imaging Spectrometry - A Tool for Environmental Observations*, J. Hill and J. Megier (eds.) pp 125-143.
- Smith, M., D. Roberts, J. Hill, W. Mehl, B. Hosgood, J. Verdebout, G. Schmuck, C. Koechler, and J. Adams. 1994. "A New Approach to Quantifying Abundance of Materials in Multispectral Images," *IEEE-IGARSS 1994. International Geoscience and Remote Sensing Symposium*, vol 4, pp 2372-2374.
- Sohn, Y. and R. McCoy. 1997. "Mapping Desert Shrub Rangeland Using Spectral Unmixing and Modelling Spectral Mixtures with TM Data," *Photogrammetric Engineering and Remote Sensing*, vol 63, no. 6, pp 707-716.
- Tazik, D.J, S.D. Warren, V.E. Diersing, R.B. Shaw, R.J. Brozka, C.F. Bagley, and W.R Whitworth. 1992. *U.S. Army Land Condition-Trend Analysis (LCTA) Plot Inventory Field Methods*, Technical Report N-92/03/ADA247931 (U.S. Army Construction Engineering Research Laboratory, February 1992).
- Tucker, C.J. 1979. "Red and Photographic Infrared Linear Combinations for Monitoring Vegetation," *Remote Sensing of Environment*, vol 8, pp 121-150.
- Tueller, P. 1989 "Remote Sensing Technology for Rangeland Management Applications," *Journal of Range Management*, 42(6):442-453.
- Tueller P.T. 1987. "Remote Sensing Science Applications in Arid Environments," *Remote Sensing of Environment*, vol 23, pp 143-154.
- U.S. Army. 1978. "Fort Bliss Texas Terrain Analysis", Terrain Analysis Center, U.S. Army Topographic Laboratories, Fort Belvoir, VA.
- USDA. 1980. "Soil Survey of Dona Ana County, New Mexico", USDA Soil Conservation Service with the U.S. Department of Interior, Bureau of Land Management, and New Mexico Agricultural Experiment Station.
- Ustin, S. L., et al. 1986. "Thematic Mapper Studies of Semiarid Shrub Communities", *BioScience*, vol 36, no. 7, pp 446-452.
- Yool, S.R., M.J. Makaio, and J.M. Watts. 1997. "Techniques for computer-assisted mapping of rangeland change," *Journal of Range Management*, vol 50(3), pp 307-314.

Appendix A: Graphic Depiction of the Linear Spectral Demixing Process Flow

LINEAR SPECTRAL DEMIXING PROCESS FLOW

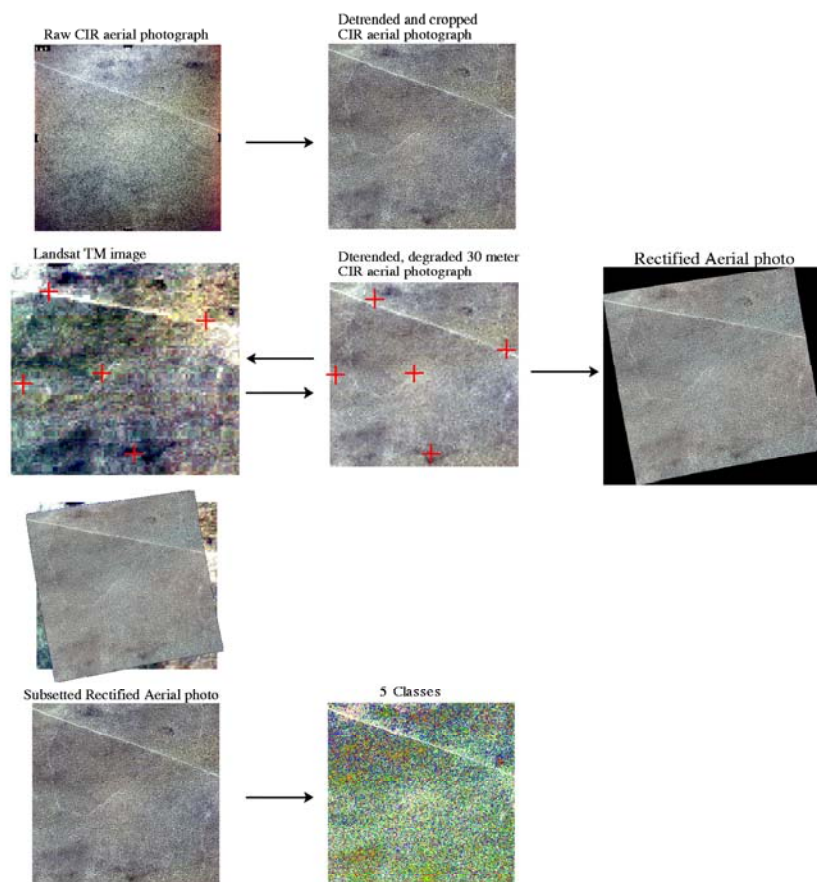
A. CREATE SUBSETS

B. DETREND SUBSETS

C. GEOREFERENCE SUBSETS

D. CHECK GEOREFERENCING

E. CLASSIFY DETRENDED SUBSETS



LINEAR SPECTRAL DEMIXING
PROCESS FLOW

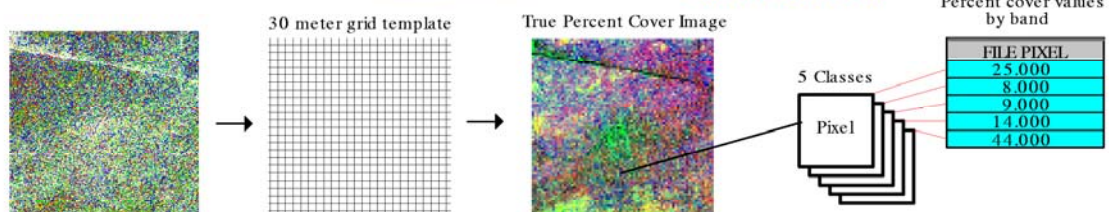
F. RECTIFY THE CLASSIFICATIONS

5 Class

G. SUBSET COMMON AREA

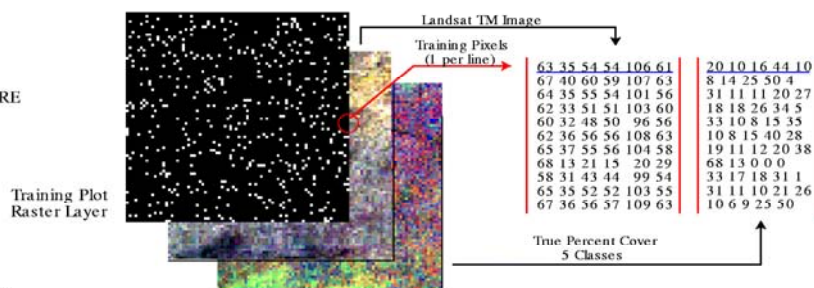
Landsat TM image

H. CALCULATE TRUE PERCENT COVER IMAGES

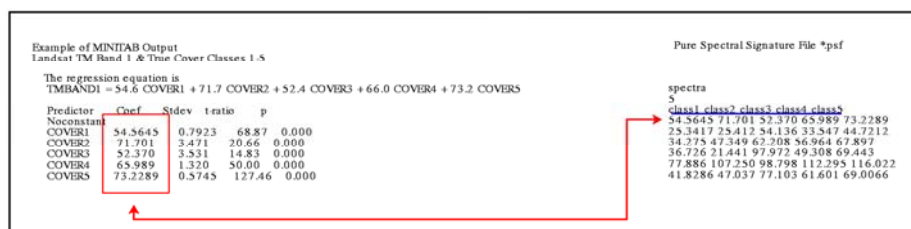


LINEAR SPECTRAL DEMIXING PROCESS FLOW

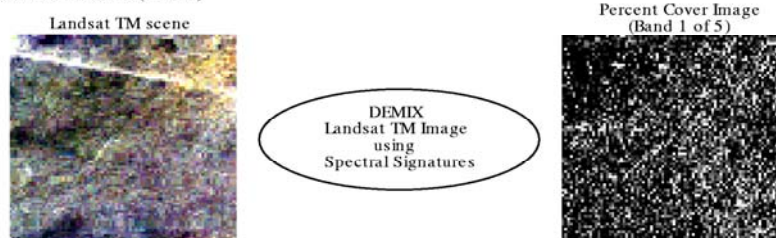
I. CREATE PURE SPECTRAL SIGNATURE TRAINING DATA



J. DERIVE PURE SIGNATURE VALUES



K. CREATE PERCENT COVER IMAGERY (DEMIX)



Appendix B: Summary of the Adjusted R^2 for all Correlations

INDICIES

380_18			380_18			380_18			380_18			380_18		
IND ISO2			IND 12_35			IND 13_45			IND 1_25			IND 14_5		
R-sq	COV1	COV2	R-sq	COV1	COV2	R-sq	COV1	COV2	R-sq	COV1	COV2	R-sq	COV1	COV2
TMBAND1	32.40	32.40	TMBAND1	30.80	30.80	TMBAND1	40.00	40.00	TMBAND1	25.00	25.00	TMBAND1	42.30	42.30
TMBAND2	40.30	40.30	TMBAND2	37.90	37.90	TMBAND2	48.80	48.80	TMBAND2	28.10	28.10	TMBAND2	46.50	46.50
TMBAND3	44.30	44.30	TMBAND3	42.40	42.40	TMBAND3	51.30	51.30	TMBAND3	31.80	31.80	TMBAND3	45.30	45.30
TMBAND4	34.40	34.40	TMBAND4	32.70	32.70	TMBAND4	43.50	43.50	TMBAND4	23.40	23.40	TMBAND4	45.80	45.80
TMBAND5	33.50	33.50	TMBAND5	32.50	32.50	TMBAND5	36.40	36.40	TMBAND5	27.60	27.60	TMBAND5	27.50	27.50
TMBAND7	37.10	37.10	TMBAND7	35.80	35.80	TMBAND7	40.90	40.90	TMBAND7	30.20	30.20	TMBAND7	32.00	32.00
KTBright	47.20	47.20	KTBright	45.20	45.20	KTBright	55.10	55.10	KTBright	35.10	35.10	KTBright	50.00	50.00
KTGreen	26.30	26.30	KTGreen	24.90	24.90	KTGreen	26.70	26.70	KTGreen	21.70	21.70	KTGreen	19.10	19.10
IRR	6.50	6.50	IRR	6.40	6.40	IRR	4.70	4.70	IRR	6.00	6.00	IRR	0.60	0.60
NDVI	6.50	6.50	NDVI	6.40	6.40	NDVI	4.60	4.60	NDVI	6.00	6.00	NDVI	0.60	0.60
SQRT	6.50	6.50	SQRT	6.40	6.40	SQRT	4.60	4.60	SQRT	6.00	6.00	SQRT	0.60	0.60
MSAVI	6.50	6.50	MSAVI	6.40	6.40	MSAVI	4.60	4.60	MSAVI	6.00	6.00	MSAVI	0.60	0.60
TNDVI	6.50	6.50	TNDVI	6.40	6.40	TNDVI	4.60	4.60	TNDVI	6.00	6.00	TNDVI	0.60	0.60
Veg_Index	5.70	5.70	Veg_Index	5.60	5.60	Veg_Index	3.80	3.80	Veg_Index	5.30	5.30	Veg_Index	0.40	0.40
Albedo	45.10	45.10	Albedo	42.90	42.90	Albedo	54.30	54.30	Albedo	32.30	32.30	Albedo	52.30	52.30

381_146			381_146			381_146			381_146			381_146		
IND ISO2			IND 12_35			IND 13_45			IND 1_25			IND 14_5		
R-sq	COV1	COV2	R-sq	COV1	COV2	R-sq	COV1	COV2	R-sq	COV1	COV2	R-sq	COV1	COV2
TMBAND1	28.90	28.90	TMBAND1	27.90	27.90	TMBAND1	40.40	40.40	TMBAND1	34.50	34.50	TMBAND1	54.50	54.50
TMBAND2	40.50	40.50	TMBAND2	39.50	39.50	TMBAND2	53.10	53.10	TMBAND2	42.60	42.60	TMBAND2	63.20	63.20
TMBAND3	44.80	44.80	TMBAND3	43.70	43.70	TMBAND3	55.20	55.20	TMBAND3	40.00	40.00	TMBAND3	58.70	58.70
TMBAND4	41.50	41.50	TMBAND4	40.00	40.00	TMBAND4	53.20	53.20	TMBAND4	33.20	33.20	TMBAND4	55.10	55.10
TMBAND5	38.80	38.80	TMBAND5	37.30	37.30	TMBAND5	43.30	43.30	TMBAND5	31.20	31.20	TMBAND5	40.90	40.90
TMBAND7	35.00	35.00	TMBAND7	33.50	33.50	TMBAND7	37.90	37.90	TMBAND7	28.50	28.50	TMBAND7	34.80	34.80
KTBright	49.20	49.20	KTBright	47.50	47.50	KTBright	60.10	60.10	KTBright	42.80	42.80	KTBright	62.90	62.90
KTGreen	11.70	11.70	KTGreen	11.90	11.90	KTGreen	13.70	13.70	KTGreen	20.40	20.40	KTGreen	20.30	20.30
IRR	3.00	3.00	IRR	3.40	3.40	IRR	2.20	2.20	IRR	6.10	6.10	IRR	2.80	2.80
NDVI	2.90	2.90	NDVI	3.30	3.30	NDVI	2.20	2.20	NDVI	5.90	5.90	NDVI	2.80	2.80
SQRT	3.00	3.00	SQRT	3.30	3.30	SQRT	2.20	2.20	SQRT	6.00	6.00	SQRT	2.80	2.80
MSAVI	2.80	2.80	MSAVI	3.20	3.20	MSAVI	2.10	2.10	MSAVI	5.80	5.80	MSAVI	2.80	2.80
TNDVI	2.90	2.90	TNDVI	3.20	3.20	TNDVI	2.10	2.10	TNDVI	5.90	5.90	TNDVI	2.80	2.80
Veg_Index	1.10	1.10	Veg_Index	1.30	1.30	Veg_Index	0.60	0.60	Veg_Index	3.40	3.40	Veg_Index	1.10	1.10
Albedo	47.90	47.90	Albedo	46.50	46.50	Albedo	61.20	61.20	Albedo	44.60	44.60	Albedo	68.10	68.10

381_144			381_144			381_144			381_144			381_144		
IND ISO2			IND 12_35			IND 13_45			IND 1_25			IND 14_5		
R-sq	COV1	COV2	R-sq	COV1	COV2	R-sq	COV1	COV2	R-sq	COV1	COV2	R-sq	COV1	COV2
TMBAND1	48.20	48.20	TMBAND1	46.70	46.70	TMBAND1	49.00	49.00	TMBAND1	36.00	36.00	TMBAND1	51.40	51.40
TMBAND2	64.70	64.70	TMBAND2	63.00	63.00	TMBAND2	61.80	61.80	TMBAND2	36.60	36.60	TMBAND2	55.00	55.00
TMBAND3	54.90	54.90	TMBAND3	53.50	53.50	TMBAND3	50.00	50.00	TMBAND3	26.50	26.50	TMBAND3	39.30	39.30
TMBAND4	44.70	44.70	TMBAND4	42.50	42.50	TMBAND4	40.80	40.80	TMBAND4	15.60	15.60	TMBAND4	30.80	30.80
TMBAND5	52.30	52.30	TMBAND5	52.40	52.40	TMBAND5	46.10	46.10	TMBAND5	27.00	27.00	TMBAND5	34.70	34.70
TMBAND7	54.70	54.70	TMBAND7	54.90	54.90	TMBAND7	48.20	48.20	TMBAND7	29.50	29.50	TMBAND7	34.30	34.30
KTBright	63.00	63.00	KTBright	61.60	61.60	KTBright	57.90	57.90	KTBright	31.30	31.30	KTBright	46.70	46.70
KTGreen	46.70	46.70	KTGreen	47.20	47.20	KTGreen	45.50	45.50	KTGreen	45.10	45.10	KTGreen	45.50	45.50
IRR	21.20	21.20	IRR	22.50	22.50	IRR	18.70	18.70	IRR	24.70	24.70	IRR	15.80	15.80
NDVI	21.10	21.10	NDVI	22.40	22.40	NDVI	18.70	18.70	NDVI	24.70	24.70	NDVI	16.00	16.00
SQRT	21.20	21.20	SQRT	22.50	22.50	SQRT	18.70	18.70	SQRT	24.70	24.70	SQRT	15.90	15.90
MSAVI	21.00	21.00	MSAVI	22.30	22.30	MSAVI	18.60	18.60	MSAVI	24.70	24.70	MSAVI	16.20	16.20
TNDVI	21.10	21.10	TNDVI	22.40	22.40	TNDVI	18.70	18.70	TNDVI	24.70	24.70	TNDVI	16.10	16.10
Veg_Index	18.80	18.80	Veg_Index	20.10	20.10	Veg_Index	17.00	17.00	Veg_Index	23.40	23.40	Veg_Index	15.60	15.60
Albedo	62.30	62.30	Albedo	60.40	60.40	Albedo	58.50	58.50	Albedo	32.00	32.00	Albedo	49.60	49.60

381_158			381_158			381_158			381_158			381_158		
IND ISO2			IND 12_35			IND 13_45			IND 1_25			IND 14_5		
R-sq	COV1	COV2	R-sq	COV1	COV2	R-sq	COV1	COV2	R-sq	COV1	COV2	R-sq	COV1	COV2
TMBAND1	27.30	27.30	TMBAND1	23.30	23.30	TMBAND1	35.20	35.20	TMBAND1	12.40	12.40	TMBAND1	28.80	28.80
TMBAND2	40.00	40.00	TMBAND2	35.90	35.90	TMBAND2	47.20	47.20	TMBAND2	20.80	20.80	TMBAND2	33.80	33.80
TMBAND3	46.50	46.50	TMBAND3	42.70	42.70	TMBAND3	54.10	54.10	TMBAND3	25.70	25.70	TMBAND3	40.50	40.50
TMBAND4	40.10	40.10	TMBAND4	36.00	36.00	TMBAND4	49.90	49.90	TMBAND4	17.50	17.50	TMBAND4	42.20	42.20
TMBAND5	17.90	17.90	TMBAND5	18.50	18.50	TMBAND5	15.70	15.70	TMBAND5	16.80	16.80	TMBAND5	14.40	14.40
TMBAND7	18.10	18.10	TMBAND7	19.70	19.70	TMBAND7	14.40	14.40	TMBAND7	18.90	18.90	TMBAND7	10.80	10.80
KTBright	48.00	48.00	KTBright	44.80	44.80	KTBright	53.70	53.70	KTBright	28.40	28.40	KTBright	43.60	43.60
KTGreen	17.80	17.80	KTGreen	16.90	16.90	KTGreen	17.50	17.50	KTGreen	15.20	15.20	KTGreen	9.00	9.00
IRR	3.80	3.80	IRR	4.00	4.00	IRR	2.80	2.80	IRR	6.10	6.10	IRR	0.50	0.50
NDVI	3.80	3.80	NDVI	4.00	4.00	NDVI	2.80	2.80	NDVI	6.00	6.00	NDVI	0.50	0.50
SQRT	3.80	3.80	SQRT	3.90	3.90	SQRT	2.80	2.80	SQRT	6.00	6.00	SQRT	0.50	0.50
MSAVI	3.80	3.80	MSAVI	3.90	3.90	MSAVI	2.80	2.80	MSAVI	5.90	5.90	MSAVI	0.60	0.60
TNDVI	3.80	3.80	TNDVI	4.00	4.00	TNDVI	2.80	2.80	TNDVI	6.00	6.00	TNDVI	0.60	0.60
Veg_Index	3.00	3.00	Veg_Index	3.20	3.20	Veg_Index	2.00	2.00	Veg_Index	5.40	5.40	Veg_Index	0.20	0.20
Albedo	48.80	48.80	Albedo	44.00	44.00	Albedo	58.10	58.10	Albedo	25.00	25.00	Albedo	45.40	45.40

INDICIES

386_18			386_18			386_18			386_18			386_18		
IND ISO2			IND 12_35			IND 13_45			IND 1_25			IND 14_5		
R-sq	COV1	COV2	R-sq	COV1	COV2	R-sq	COV1	COV2	R-sq	COV1	COV2	R-sq	COV1	COV2
TMBAND1	10.90	10.90	TMBAND1	5.80	5.80	TMBAND1	13.80	13.80	TMBAND1	2.30	2.30	TMBAND1	6.10	6.10
TMBAND2	23.70	23.70	TMBAND2	15.80	15.80	TMBAND2	26.70	26.70	TMBAND2	10.90	10.90	TMBAND2	7.90	7.90
TMBAND3	32.50	32.50	TMBAND3	22.40	22.40	TMBAND3	35.80	35.80	TMBAND3	15.50	15.50	TMBAND3	10.80	10.80
TMBAND4	31.80	31.80	TMBAND4	22.00	22.00	TMBAND4	35.60	35.60	TMBAND4	15.30	15.30	TMBAND4	11.80	11.80
TMBAND5	17.70	17.70	TMBAND5	11.60	11.60	TMBAND5	22.10	22.10	TMBAND5	4.20	4.20	TMBAND5	6.70	6.70
TMBAND7	19.40	19.40	TMBAND7	10.70	10.70	TMBAND7	24.50	24.50	TMBAND7	4.60	4.60	TMBAND7	8.00	8.00
KTBright	25.40	25.40	KTBright	16.80	16.80	KTBright	29.90	29.90	KTBright	9.20	9.20	KTBright	9.60	9.60
KTGreen	4.90	4.90	KTGreen	1.60	1.60	KTGreen	6.10	6.10	KTGreen	0.60	0.60	KTGreen	1.80	1.80
IRR	0.00	0.00	IRR	0.00	0.00	IRR	0.00	0.00	IRR	0.00	0.00	IRR	0.40	0.40
NDVI	0.00	0.00	NDVI	0.00	0.00	NDVI	0.00	0.00	NDVI	0.00	0.00	NDVI	0.30	0.30
SQRT	0.00	0.00	SQRT	0.00	0.00	SQRT	0.00	0.00	SQRT	0.00	0.00	SQRT	0.30	0.30
MSAVI	0.00	0.00	MSAVI	0.00	0.00	MSAVI	0.00	0.00	MSAVI	0.00	0.00	MSAVI	0.30	0.30
TNDVI	0.00	0.00	TNDVI	0.00	0.00	TNDVI	0.00	0.00	TNDVI	0.00	0.00	TNDVI	0.30	0.30
Veg_Index	0.20	0.20	Veg_Index	0.20	0.20	Veg_Index	0.40	0.40	Veg_Index	0.10	0.10	Veg_Index	0.80	0.80
Albedo	27.00	27.00	Albedo	17.80	17.80	Albedo	30.90	30.90	Albedo	11.30	11.30	Albedo	10.00	10.00

386_16			386_16			386_16			386_16			386_16		
IND ISO2			IND 12_35			IND 13_45			IND 1_25			IND 14_5		
R-sq	COV1	COV2	R-sq	COV1	COV2	R-sq	COV1	COV2	R-sq	COV1	COV2	R-sq	COV1	COV2
TMBAND1	27.20	27.20	TMBAND1	26.10	26.10	TMBAND1	27.30	27.30	TMBAND1	17.80	17.80	TMBAND1	23.60	23.60
TMBAND2	48.00	48.00	TMBAND2	51.60	51.60	TMBAND2	39.20	39.20	TMBAND2	38.50	38.50	TMBAND2	18.40	18.40
TMBAND3	50.50	50.50	TMBAND3	54.00	54.00	TMBAND3	39.10	39.10	TMBAND3	39.40	39.40	TMBAND3	10.60	10.60
TMBAND4	49.90	49.90	TMBAND4	54.50	54.50	TMBAND4	38.40	38.40	TMBAND4	41.70	41.70	TMBAND4	14.10	14.10
TMBAND5	47.80	47.80	TMBAND5	48.30	48.30	TMBAND5	41.70	41.70	TMBAND5	29.70	29.70	TMBAND5	22.70	22.70
TMBAND7	47.50	47.50	TMBAND7	47.80	47.80	TMBAND7	41.00	41.00	TMBAND7	28.10	28.10	TMBAND7	22.20	22.20
KTBright	58.70	58.70	KTBright	61.20	61.20	KTBright	48.50	48.50	KTBright	42.30	42.30	KTBright	21.70	21.70
KTGreen	14.50	14.50	KTGreen	13.30	13.30	KTGreen	14.30	14.30	KTGreen	6.70	6.70	KTGreen	7.00	7.00
IRR	2.80	2.80	IRR	2.70	2.70	IRR	2.20	2.20	IRR	1.30	1.30	IRR	0.00	0.00
NDVI	2.80	2.80	NDVI	2.60	2.60	NDVI	2.20	2.20	NDVI	1.20	1.20	NDVI	0.00	0.00
SQRT	2.80	2.80	SQRT	2.60	2.60	SQRT	2.20	2.20	SQRT	1.30	1.30	SQRT	0.00	0.00
MSAVI	2.70	2.70	MSAVI	2.50	2.50	MSAVI	2.20	2.20	MSAVI	1.10	1.10	MSAVI	0.00	0.00
TNDVI	2.70	2.70	TNDVI	2.50	2.50	TNDVI	2.20	2.20	TNDVI	1.20	1.20	TNDVI	0.00	0.00
Veg_Index	0.80	0.80	Veg_Index	0.60	0.60	Veg_Index	0.70	0.70	Veg_Index	0.10	0.10	Veg_Index	0.30	0.30
Albedo	57.80	57.80	Albedo	61.20	61.20	Albedo	47.20	47.20	Albedo	44.50	44.50	Albedo	20.30	20.30

386_124			386_124			386_124			386_124			386_124		
IND ISO2			IND 12_35			IND 13_45			IND 1_25			IND 14_5		
R-sq	COV1	COV2	R-sq	COV1	COV2	R-sq	COV1	COV2	R-sq	COV1	COV2	R-sq	COV1	COV2
TMBAND1	85.30	85.30	TMBAND1	73.20	73.20	TMBAND1	91.70	91.70	TMBAND1	42.80	42.80	TMBAND1	69.50	69.50
TMBAND2	83.90	83.90	TMBAND2	74.20	74.20	TMBAND2	89.80	89.80	TMBAND2	46.70	46.70	TMBAND2	75.60	75.60
TMBAND3	70.90	70.90	TMBAND3	72.60	72.60	TMBAND3	85.00	85.00	TMBAND3	47.50	47.50	TMBAND3	79.00	79.00
TMBAND4	74.20	74.20	TMBAND4	70.00	70.00	TMBAND4	78.00	78.00	TMBAND4	46.90	46.90	TMBAND4	79.50	79.50
TMBAND5	76.80	76.80	TMBAND5	69.10	69.10	TMBAND5	82.30	82.30	TMBAND5	44.30	44.30	TMBAND5	76.30	76.30
TMBAND7	74.40	74.40	TMBAND7	65.60	65.60	TMBAND7	80.00	80.00	TMBAND7	41.30	41.30	TMBAND7	73.30	73.30
KTBright	81.10	81.10	KTBright	73.20	73.20	KTBright	86.40	86.40	KTBright	46.90	46.90	KTBright	79.20	79.20
KTGreen	69.00	69.00	KTGreen	54.20	54.20	KTGreen	75.90	75.90	KTGreen	29.50	29.50	KTGreen	46.20	46.20
IRR	13.20	13.20	IRR	7.80	7.80	IRR	15.50	15.50	IRR	3.80	3.80	IRR	4.20	4.20
NDVI	13.30	13.30	NDVI	7.80	7.80	NDVI	15.50	15.50	NDVI	3.80	3.80	NDVI	4.10	4.10
SQRT	13.30	13.30	SQRT	7.70	7.70	SQRT	15.50	15.50	SQRT	3.80	3.80	SQRT	4.10	4.10
MSAVI	13.10	13.10	MSAVI	7.80	7.80	MSAVI	15.30	15.30	MSAVI	3.70	3.70	MSAVI	3.90	3.90
TNDVI	13.30	13.30	TNDVI	7.80	7.80	TNDVI	15.50	15.50	TNDVI	3.80	3.80	TNDVI	4.00	4.00
Veg_Index	2.50	2.50	Veg_Index	0.60	0.60	Veg_Index	3.40	3.40	Veg_Index	0.10	0.10	Veg_Index	0.00	0.00
Albedo	83.20	83.20	Albedo	74.80	74.80	Albedo	88.60	88.60	Albedo	47.60	47.60	Albedo	78.90	78.90

386_122			386_122			386_122			386_122			386_122		
IND ISO2			IND 12_35			IND 13_45			IND 1_25			IND 14_5		
R-sq	COV1	COV2	R-sq	COV1	COV2	R-sq	COV1	COV2	R-sq	COV1	COV2	R-sq	COV1	COV2
TMBAND1	34.10	34.10	TMBAND1	37.00	37.00	TMBAND1	27.40	27.40	TMBAND1	29.80	29.80	TMBAND1	8.20	8.20
TMBAND2	43.20	43.20	TMBAND2	47.10	47.10	TMBAND2	33.00	33.00	TMBAND2	38.60	38.60	TMBAND2	4.40	4.40
TMBAND3	43.30	43.30	TMBAND3	47.30	47.30	TMBAND3	32.80	32.80	TMBAND3	38.80	38.80	TMBAND3	3.70	3.70
TMBAND4	43.90	43.90	TMBAND4	48.40	48.40	TMBAND4	31.40	31.40	TMBAND4	43.20	43.20	TMBAND4	1.40	1.40
TMBAND5	33.60	33.60	TMBAND5	39.00	39.00	TMBAND5	21.40	21.40	TMBAND5	29.10	29.10	TMBAND5	0.10	0.10
TMBAND7	27.00	27.00	TMBAND7	33.20	33.20	TMBAND7	14.80	14.80	TMBAND7	22.40	22.40	TMBAND7	0.20	0.20
KTBright	40.80	40.80	KTBright	45.90	45.90	KTBright	28.30	28.30	KTBright	37.90	37.90	KTBright	1.20	1.20
KTGreen	4.70	4.70	KTGreen	5.50	5.50	KTGreen	4.40	4.40	KTGreen	0.10	0.10	KTGreen	7.90	7.90
IRR	1.30	1.30	IRR	1.80	1.80	IRR	0.20	0.20	IRR	7.80	7.80	IRR	4.10	4.10
NDVI	1.30	1.30	NDVI	1.80	1.80	NDVI	0.20	0.20	NDVI	7.80	7.80	NDVI	4.20	4.20
SQRT	1.30	1.30	SQRT	1.80	1.80	SQRT	0.20	0.20	SQRT	7.80	7.80	SQRT	4.20	4.20
MSAVI	1.40	1.40	MSAVI	1.90	1.90	MSAVI	0.20	0.20	MSAVI	7.90	7.90	MSAVI	4.30	4.30
TNDVI	1.30	1.30	TNDVI	1.80	1.80	TNDVI	0.20	0.20	TNDVI	7.80	7.80	TNDVI	4.30	4.30
Veg_Index	7.00	7.00	Veg_Index	8.30	8.30	Veg_Index	3.10	3.10	Veg_Index	15.60	15.60	Veg_Index	3.20	3.20
Albedo	44.40	44.40	Albedo	48.90	48.90	Albedo	32.90	32.90	Albedo	41.10	41.10	Albedo	3.10	3.10

INDICIES

388_45			388_45			388_45			388_45			388_45		
IND ISO2			IND 12_35			IND 13_45			IND 14_5			1_25		
R-sq	COV1	COV2	R-sq	COV1	COV2	R-sq	COV1	COV2	R-sq	COV1	COV2	R-sq	COV1	COV2
TMBAND1	38.10	38.10	TMBAND1	37.80	37.80	TMBAND1	38.60	38.60	TMBAND1	29.10	29.10	TMBAND1	29.80	29.80
TMBAND2	50.30	50.30	TMBAND2	45.30	45.30	TMBAND2	52.30	52.30	TMBAND2	46.50	46.50	TMBAND2	32.80	32.80
TMBAND3	46.90	46.90	TMBAND3	38.20	38.20	TMBAND3	51.30	51.30	TMBAND3	50.30	50.30	TMBAND3	24.70	24.70
TMBAND4	45.80	45.80	TMBAND4	37.10	37.10	TMBAND4	50.40	50.40	TMBAND4	50.40	50.40	TMBAND4	23.30	23.30
TMBAND5	35.60	35.60	TMBAND5	27.70	27.70	TMBAND5	40.60	40.60	TMBAND5	43.10	43.10	TMBAND5	14.40	14.40
TMBAND7	40.60	40.60	TMBAND7	32.90	32.90	TMBAND7	44.90	44.90	TMBAND7	47.30	47.30	TMBAND7	19.20	19.20
KTBright	48.60	48.60	KTBright	39.80	39.80	KTBright	53.40	53.40	KTBright	53.00	53.00	KTBright	24.40	24.40
KTGreen	15.10	15.10	KTGreen	15.90	15.90	KTGreen	14.50	14.50	KTGreen	10.10	10.10	KTGreen	14.40	14.40
IRR	9.00	9.00	IRR	7.80	7.80	IRR	9.10	9.10	IRR	7.10	7.10	IRR	6.30	6.30
NDVI	8.90	8.90	NDVI	7.70	7.70	NDVI	9.00	9.00	NDVI	7.10	7.10	NDVI	6.10	6.10
SQRT	9.00	9.00	SQRT	7.70	7.70	SQRT	9.10	9.10	SQRT	7.10	7.10	SQRT	6.20	6.20
MSAVI	8.90	8.90	MSAVI	7.40	7.40	MSAVI	8.90	8.90	MSAVI	7.10	7.10	MSAVI	5.90	5.90
TNDVI	8.70	8.70	TNDVI	7.60	7.60	TNDVI	9.00	9.00	TNDVI	7.20	7.20	TNDVI	6.00	6.00
Veg_Index	0.80	0.80	Veg_Index	0.70	0.70	Veg_Index	0.70	0.70	Veg_Index	0.40	0.40	Veg_Index	0.80	0.80
Albedo	51.20	51.20	Albedo	43.60	43.60	Albedo	55.10	55.10	Albedo	52.00	52.00	Albedo	29.10	29.10

388_47			388_47			388_47			388_47			388_47		
IND ISO2			IND 12_35			IND 13_45			IND 14_5			1_25		
R-sq	COV1	COV2	R-sq	COV1	COV2	R-sq	COV1	COV2	R-sq	COV1	COV2	R-sq	COV1	COV2
TMBAND1	29.70	29.70	TMBAND1	36.90	36.90	TMBAND1	30.40	30.40	TMBAND1	21.00	21.00	TMBAND1	36.20	36.20
TMBAND2	40.90	40.90	TMBAND2	45.90	45.90	TMBAND2	43.40	43.40	TMBAND2	34.70	34.70	TMBAND2	42.50	42.50
TMBAND3	40.00	40.00	TMBAND3	40.20	40.20	TMBAND3	43.30	43.30	TMBAND3	39.50	39.50	TMBAND3	34.60	34.60
TMBAND4	36.90	36.90	TMBAND4	37.40	37.40	TMBAND4	40.90	40.90	TMBAND4	36.00	36.00	TMBAND4	31.40	31.40
TMBAND5	27.30	27.30	TMBAND5	24.80	24.80	TMBAND5	26.60	26.60	TMBAND5	23.50	23.50	TMBAND5	22.00	22.00
TMBAND7	29.60	29.60	TMBAND7	24.20	24.20	TMBAND7	28.60	28.60	TMBAND7	29.00	29.00	TMBAND7	20.60	20.60
KTBright	39.00	39.00	KTBright	39.00	39.00	KTBright	40.80	40.80	KTBright	35.60	35.60	KTBright	34.20	34.20
KTGreen	23.40	23.40	KTGreen	26.50	26.50	KTGreen	22.10	22.10	KTGreen	18.40	18.40	KTGreen	26.90	26.90
IRR	10.30	10.30	IRR	10.80	10.80	IRR	9.70	9.70	IRR	8.80	8.80	IRR	11.40	11.40
NDVI	10.70	10.70	NDVI	11.00	11.00	NDVI	10.10	10.10	NDVI	9.50	9.50	NDVI	11.20	11.20
SQRT	10.50	10.50	SQRT	10.90	10.90	SQRT	10.00	10.00	SQRT	9.20	9.20	SQRT	11.30	11.30
MSAVI	10.80	10.80	MSAVI	11.00	11.00	MSAVI	10.20	10.20	MSAVI	9.70	9.70	MSAVI	11.00	11.00
TNDVI	10.60	10.60	TNDVI	10.90	10.90	TNDVI	10.00	10.00	TNDVI	9.50	9.50	TNDVI	11.10	11.10
Veg_Index	2.90	2.90	Veg_Index	2.80	2.80	Veg_Index	2.50	2.50	Veg_Index	3.30	3.30	Veg_Index	3.00	3.00
Albedo	41.30	41.30	Albedo	43.90	43.90	Albedo	44.20	44.20	Albedo	37.20	37.20	Albedo	39.10	39.10

388_88			388_88			388_88			388_88			388_88		
IND ISO2			IND 12_35			IND 13_45			IND 14_5			1_25		
R-sq	COV1	COV2	R-sq	COV1	COV2	R-sq	COV1	COV2	R-sq	COV1	COV2	R-sq	COV1	COV2
TMBAND1	63.90	63.90	TMBAND1	64.60	64.60	TMBAND1	61.10	61.10	TMBAND1	45.10	45.10	TMBAND1	58.10	58.10
TMBAND2	72.60	72.60	TMBAND2	70.60	70.60	TMBAND2	71.00	71.00	TMBAND2	57.40	57.40	TMBAND2	60.00	60.00
TMBAND3	72.10	72.10	TMBAND3	67.20	67.20	TMBAND3	72.60	72.60	TMBAND3	64.30	64.30	TMBAND3	54.10	54.10
TMBAND4	69.30	69.30	TMBAND4	66.40	66.40	TMBAND4	69.60	69.60	TMBAND4	53.50	53.50	TMBAND4	52.10	52.10
TMBAND5	62.30	62.30	TMBAND5	60.30	60.30	TMBAND5	61.60	61.60	TMBAND5	44.20	44.20	TMBAND5	49.80	49.80
TMBAND7	56.10	56.10	TMBAND7	51.50	51.50	TMBAND7	60.40	60.40	TMBAND7	51.40	51.40	TMBAND7	40.50	40.50
KTBright	78.10	78.10	KTBright	74.90	74.90	KTBright	77.00	77.00	KTBright	61.10	61.10	KTBright	61.30	61.30
KTGreen	35.50	35.50	KTGreen	33.10	33.10	KTGreen	38.90	38.90	KTGreen	37.10	37.10	KTGreen	30.60	30.60
IRR	13.30	13.30	IRR	11.50	11.50	IRR	17.00	17.00	IRR	17.20	17.20	IRR	11.40	11.40
NDVI	13.90	13.90	NDVI	12.00	12.00	NDVI	17.40	17.40	NDVI	18.40	18.40	NDVI	11.60	11.60
SQRT	13.50	13.50	SQRT	11.70	11.70	SQRT	17.10	17.10	SQRT	17.70	17.70	SQRT	11.40	11.40
MSAVI	13.60	13.60	MSAVI	11.50	11.50	MSAVI	17.30	17.30	MSAVI	18.60	18.60	MSAVI	11.00	11.00
TNDVI	13.50	13.50	TNDVI	11.50	11.50	TNDVI	17.40	17.40	TNDVI	18.20	18.20	TNDVI	11.20	11.20
Veg_Index	3.30	3.30	Veg_Index	2.30	2.30	Veg_Index	5.30	5.30	Veg_Index	8.20	8.20	Veg_Index	2.40	2.40
Albedo	77.60	77.60	Albedo	74.70	74.70	Albedo	76.10	76.10	Albedo	61.80	61.80	Albedo	61.90	61.90

388_90			388_90			388_90			388_90			388_90		
IND ISO2			IND 12_35			IND 13_45			IND 14_5			1_25		
R-sq	COV1	COV2	R-sq	COV1	COV2	R-sq	COV1	COV2	R-sq	COV1	COV2	R-sq	COV1	COV2
TMBAND1	61.20	61.20	TMBAND1	63.40	63.40	TMBAND1	55.80	55.80	TMBAND1	31.80	31.80	TMBAND1	56.70	56.70
TMBAND2	66.20	66.20	TMBAND2	63.60	63.60	TMBAND2	64.70	64.70	TMBAND2	48.00	48.00	TMBAND2	55.40	55.40
TMBAND3	64.50	64.50	TMBAND3	58.30	58.30	TMBAND3	66.30	66.30	TMBAND3	55.20	55.20	TMBAND3	49.30	49.30
TMBAND4	61.00	61.00	TMBAND4	53.30	53.30	TMBAND4	63.80	63.80	TMBAND4	55.70	55.70	TMBAND4	43.30	43.30
TMBAND5	62.10	62.10	TMBAND5	63.40	63.40	TMBAND5	56.60	56.60	TMBAND5	29.90	29.90	TMBAND5	54.90	54.90
TMBAND7	60.00	60.00	TMBAND7	60.80	60.80	TMBAND7	55.10	55.10	TMBAND7	31.00	31.00	TMBAND7	53.20	53.20
KTBright	75.90	75.90	KTBright	72.50	72.50	KTBright	73.90	73.90	KTBright	51.50	51.50	KTBright	61.70	61.70
KTGreen	23.50	23.50	KTGreen	27.60	27.60	KTGreen	19.50	19.50	KTGreen	8.20	8.20	KTGreen	27.40	27.40
IRR	7.90	7.90	IRR	9.10	9.10	IRR	7.00	7.00	IRR	3.60	3.60	IRR	10.20	10.20
NDVI	7.70	7.70	NDVI	8.90	8.90	NDVI	6.80	6.80	NDVI	3.60	3.60	NDVI	9.90	9.90
SQRT	7.80	7.80	SQRT	9.00	9.00	SQRT	6.90	6.90	SQRT	3.60	3.60	SQRT	10.10	10.10
MSAVI	7.30	7.30	MSAVI	8.40	8.40	MSAVI	6.60	6.60	MSAVI	3.60	3.60	MSAVI	9.50	9.50
TNDVI	7.60	7.60	TNDVI	8.70	8.70	TNDVI	6.80	6.80	TNDVI	3.70	3.70	TNDVI	9.80	9.80
Veg_Index	0.80	0.80	Veg_Index	1.30	1.30	Veg_Index	0.50	0.50	Veg_Index	0.10	0.10	Veg_Index	1.90	1.90
Albedo	72.60	72.60	Albedo	68.00	68.00	Albedo	72.20	72.20	Albedo	54.80	54.80	Albedo	57.90	57.90

REPORT DOCUMENTATION PAGE					Form Approved OMB No. 0704-0188	
Public reporting burden for this collection of information is estimated to average 1 hour per response, including the time for reviewing instructions, searching existing data sources, gathering and maintaining the data needed, and completing and reviewing this collection of information. Send comments regarding this burden estimate or any other aspect of this collection of information, including suggestions for reducing this burden to Department of Defense, Washington Headquarters Services, Directorate for Information Operations and Reports (0704-0188), 1215 Jefferson Davis Highway, Suite 1204, Arlington, VA 22202-4302. Respondents should be aware that notwithstanding any other provision of law, no person shall be subject to any penalty for failing to comply with a collection of information if it does not display a currently valid OMB control number. PLEASE DO NOT RETURN YOUR FORM TO THE ABOVE ADDRESS.						
1. REPORT DATE (DD-MM-YYYY) 12-2003		2. REPORT TYPE Final			3. DATES COVERED (From - To)	
4. TITLE AND SUBTITLE Spectral Demixing and Spectral Index Correlations for Subpixel Quantification of Land-cover Components From Coarse Resolution Imagery at Fort Bliss, Texas				5a. CONTRACT NUMBER		
				5b. GRANT NUMBER		
				5c. PROGRAM ELEMENT NUMBER		
6. AUTHOR(S) Scott Tweddale, William Jackson, and Paul Pope				5d. PROJECT NUMBER MIPR		
				5e. TASK NUMBER 95-63		
				5f. WORK UNIT NUMBER		
7. PERFORMING ORGANIZATION NAME(S) AND ADDRESS(ES) U.S. Army Engineer Research and Development Center (ERDC) Construction Engineering Research Laboratory (CERL) PO Box 9005 Champaign, IL 61826-9005				8. PERFORMING ORGANIZATION REPORT NUMBER ERDC/CERL TR-03-26		
9. SPONSORING / MONITORING AGENCY NAME(S) AND ADDRESS(ES) U.S. Army Air Defense Artillery Center U.S. Army Environmental Center Directorate of Environment SFIM-AEC-ECN Fort Bliss, TX 79916-0058 Building E4475 Aberdeen Proving Ground, MD 21010-5401				10. SPONSOR/MONITOR'S ACRONYM(S) ATZC-DOE-C		
				11. SPONSOR/MONITOR'S REPORT NUMBER(S)		
12. DISTRIBUTION / AVAILABILITY STATEMENT Approved for public release; distribution is unlimited.						
13. SUPPLEMENTARY NOTES Copies are available from the National Technical Information Service, 5285 Port Royal Road, Springfield, VA 22161.						
14. ABSTRACT Fort Bliss, Texas, is a Training and Doctrine Command (TRADOC) installation located in the northern Chihuahuan Desert of western Texas and south-central New Mexico. Encompassing approximately 445,170 hectares (1.1 million acres), it is the single largest TRADOC installation. Because Fort Bliss is located within an arid ecosystem characterized by slow vegetative growth, its land is more susceptible to long-term disturbance. Fort Bliss natural resource managers require a timely and cost-effective method for characterizing and monitoring land condition at various spatial scales and levels of detail. This report documents evaluation of linear spectral demixing and spectral brightness and greenness index correlations with abundance of land-cover types as alternative methods for more detailed characterization and monitoring of land condition using coarse resolution satellite imagery. Detailed conclusions on the acceptability of various strategies and techniques are presented along with recommendations for related research.						
15. SUBJECT TERMS Ft Bliss, TX satellite imagery natural resource management land management vegetation						
16. SECURITY CLASSIFICATION OF:				17. LIMITATION OF ABSTRACT SAR	18. NUMBER OF PAGES 151	19a. NAME OF RESPONSIBLE PERSON Scott Tweddale
a. REPORT Unclassified	b. ABSTRACT Unclassified	c. THIS PAGE Unclassified	19b. TELEPHONE NUMBER (217) 352-6511, ext 7409			